Università degli Studi di Padova

Department of Agronomy, Food, Natural resources, Animals and Environment (DAFNAE)

Ph.D. COURSE IN CROP SCIENCE

XXXV cycle

Fate of glyphosate in different agroecosystems of the Veneto region and its impact on groundwater quality

Coordinator: Prof. Claudio Bonghi

Supervisor: Prof. Nicola Dal Ferro

Co-Supervisor: Prof. Francesco Morari

Ph.D. student: Marta Mencaroni

Università degli Studi di Padova

Dipartimento di Agronomia, Animali, Alimenti, Risorse naturali e Ambiente (DAFNAE)

CORSO DI DOTTORATO IN CROP SCIENCE

XXXV ciclo

Destino ambientale di glyphosate in agroecosistemi differenti della regione Veneto e il suo impatto sulle acque sotterranee

Coordinatore: Prof. Claudio Bonghi

Supervisore: Prof. Nicola Dal Ferro

Co-Supervisore: Prof. Francesco Morari

Dottoranda: Marta Mencaroni

Table of Contents

I. Summary

Glyphosate is one of the most used broad-spectrum, systemic, and post-emergence herbicides worldwide. In this context, 90% of the annual sales are used by the agricultural sector, where glyphosate-based agrochemicals are sprayed mainly before planting the crop or post-harvest during the intercropping period to control weeds' growth. Crops treated with this herbicide are both annual (cereals and oilseeds) and perennial crops (orchards and vineyards).

In Europe, glyphosate is currently approved until December 15th, 2022, and the EU Commission might decide to prolong its use in agricultural lands due to the decision of EFSA to postpone its scientific opinion on the re-approval of glyphosate. For this reason, studying glyphosate dynamics in soil and water is still necessary to outstand its role in groundwater pollution. Site-specific studies for the prevention of water contamination are highly recommended to help decision-makers to set up guidelines for identifying water protection areas for drinking waters, which are nowadays still largely undefined. The identification of unique rules is difficult because of the complex relationship between the agrochemical and the agroecosystem, due to the strongly site-specific adsorption-degradation-transport dynamic which depends on peculiar characteristics of each molecule (adsorption coefficient, solubility, half-life time, etc.), and the pedo-climatic and management variability of the site involved. For instance, in the Veneto region, particular attention must be given to the low-lying plain, where shallow water table conditions increase the risk of groundwater pollution in agricultural areas.

This thesis wants to offer new insights into the peculiar dynamic of glyphosate in soil and water under poorly studied conditions. Extensive studies of the fate in the environment of glyphosate have been carried out in two areas of the Veneto region (high foothills and the low-lying Venetian plain) comprising three different agroecosystems (vineyards, conventional and conservation agriculture) (*Chapters 2 and 3*), and the factors affecting the adsorption, dissipation, and transport dynamics of the herbicide were identified. Adsorption coefficients for glyphosate have been calculated along the soil profile for several soil layers, down to 70 and 110 cm (*Chapters 2 and 3*, respectively). In particular, the key role of SOM-chelated Fe and Al on herbicide adsorption has been largely demonstrated, suggesting that a careful analysis of the mineral composition, in addition to that of e.g. pH and soil texture, is required to determine the agroecosystem vulnerability to groundwater pollution. Moreover,

glyphosate dissipation in soil has been monitored and modeled (*Chapter 2*), as for AMPA – still poorly investigated – with a new proposed equation to predict its decay rate. The transport of glyphosate and AMPA revealed low mobility in the foothill vineyards, despite some fast vertical movement down to the deepest layer suggested that preferential movements due to likely well-structured soil conditions occurred. A fast movement down to the water table was also found in the low-lying Venetian plain. The modelling study conducted with HYDRUS-1D (*Chapter 4*) made it possible to identify the drivers leading to contamination. Here, shallow groundwater conditions greatly affected solute transport by modifying the soil structure, enhancing macropores frequency. Moreover, the flow field was modified compared to free drainage conditions, with a reduction of solute exchange between mobile and immobile soil regions that promoted non-equilibrium flows and preferential pathways.

II. Riassunto

Il glifosate è uno degli erbicidi più utilizzati a livello mondiale, ad ampio spettro, sistemico e di post-emergenza. In questo contesto, il 90% delle vendite annuali dell'erbicida è utilizzato nel settore agricolo, dove gli agrofarmaci a base di glifosate vengono distribuiti principalmente prima della semina o in post-raccolta (durante il periodo di intercolturale) per il controllo chimico delle infestanti. Le colture trattate con l'erbicida sono sia annuali (cereali e semi oleosi) che perenni (frutteti e vigneti).

In Europa, il glifosate è attualmente approvato fino al 15 dicembre 2022 e la Commissione Europea potrebbe decidere di prolungarne ulteriormente l'uso nei terreni agricoli a causa della decisione di EFSA di rinviare il suo parere scientifico sulla riapprovazione di glifosate. Per questo motivo, studiare le dinamiche di glifosate nel suolo e nell'acqua è ancora necessario per capire il suo ruolo nell'inquinamento delle acque sotterranee. Studi specifici per la prevenzione della contaminazione delle acque di falda sono altamente raccomandati per supportare i decisori politici e i professionisti del settore a identificare le aree di protezione delle acque potabili, che ancora oggi sono, in gran parte, poco definite. L'identificazione di regole univoche risulta essere particolarmente difficile a causa della complessa relazione tra agrofarmaco e agroecosistema, e quindi delle dinamiche di adsorbimento-degradazione-trasporto fortemente sito-specifiche. Ciò dipende anche dalle caratteristiche peculiari di ciascuna molecola (coefficiente di adsorbimento, solubilità, tempo di emivita, ecc.) e dalla variabilità pedo-climatica e gestionale del sito interessato. Ad esempio, nella regione Veneto, particolare attenzione va prestata alle aree di bassa pianura, dove le condizioni di falda superficiale aumentano il rischio di contaminazione delle acque sotterranee nelle aree agricole.

L'intento di questa tesi è quelli di fornire nuovi spunti di riflessione sulla peculiare dinamica nel suolo e nell'acqua di glifosate in condizioni ancora poco studiate. In particolare, gli studi sono stati condotti in due aree della regione Veneto (alta pedemontana e bassa pianura), comprendenti tre diversi agroecosistemi (vigneto, agricoltura convenzionale e conservativa) e sono stati identificati i fattori che influenzano le dinamiche di adsorbimento, dissipazione e trasporto dell'erbicida (*Capitoli 2 e 3*). I coefficienti di adsorbimento di glifosate sono stati calcolati lungo il profilo di suolo per diversi strati, fino a 70 e 110 cm (*Capitoli 2 e 3*, rispettivamente). In particolare, è stato ampiamente dimostrato il ruolo chiave

sull'adsorbimento di Fe e Al chelati alla sostanza organica, suggerendo che un'attenta analisi della composizione minerale (oltre a quella del pH e della tessitura del suolo) risulta necessaria per determinare la vulnerabilità dell'agroecosistema all'inquinamento della falda (*Capitoli 2 e 3*). Inoltre, la dissipazione di glifosate nel suolo è stata monitorata e modellata (*Capitolo 2*), così come per AMPA - ancora poco studiato nella letteratura scientifica - con una nuova equazione proposta per prevedere il suo tasso di decadimento. Lo studio del trasporto di glifosate e AMPA ha rivelato una bassa mobilità nei vigneti dell'area pedemontana, nonostante alcuni rapidi movimenti verticali fino allo strato più profondo abbiano suggerito la presenza di movimenti preferenziali dovuti a condizioni di suolo ben strutturato. Anche nella bassa pianura veneta è stato riscontrato un rapido movimento verso la falda freatica. Lo studio modellistico condotto con HYDRUS-1D (*Capitolo 4*) ha permesso di identificare i fattori che hanno portato alla contaminazione. In questo caso, le condizioni delle acque sotterranee poco profonde hanno influenzato notevolmente il trasporto dei soluti modificando la struttura del suolo e aumentando la frequenza dei macropori. Inoltre, la dinamica di flusso è stata modificata rispetto alle condizioni di drenaggio libero, con una riduzione dello scambio di soluti tra la regione mobile e quella immobile della matrice del suolo, promuovendo così la presenza di flussi preferenziali.

III. Thesis' structure

This Ph.D. thesis comprises 5 chapters. Chapter 1 is the general introduction, regarding the use and distribution of Plant Protection Products in agricultural lands, including a focus on the herbicide glyphosate and the occurrence of preferential flows in soil which can worsen the contamination of glyphosate towards the groundwater. Chapter 2 "*Glyphosate and AMPA have low mobility through different soil profiles of the Prosecco wine production area: a monitoring study in North-eastern Italy*" describes the environmental fate of glyphosate in Veneto's high foothills, specifically in the Prosecco production area of Valdobbiadene and Conegliano, which has been recently included in the UNESCO world's heritage list. Chapter 3 "*Glyphosate and AMPA dynamics during the transition towards conservation agriculture: drivers under shallow groundwater conditions*" explores glyphosate dynamic in a mesocosm scale experiment under shallow water table conditions, which is common in the low-lying Venetian plain, comparing conventional and conservation agricultural practices. Chapter 4 "*Preferential solute transport under variably saturated conditions in a silty loam soil: is the shallow water table a driving factor?*" presents the results obtained by an inverse modelling study on water flow and tracer dynamics in lysimeters under shallow groundwater conditions. The chapter confirms the occurrence of preferential flow under shallow water tables compared to free drainage conditions by modifying the soil macropore structure. Chapter 5 summarize the conclusions of all the research work.

Chapters 2 and 4 have been published in international peer-reviewed journals (Chapter 2 in Frontiers in Environmental Science, IF 4.75; Chapter 4 in Journal of Hydrology, IF 6.51). Chapter 3 has been submitted to Soil & Tillage Research journal (IF 5.37). For this reason, they are all standalone chapters and can be read independently.

Chapter 1. General Introduction

1.1 Plant Protection Products: state of art in Europe

Nowadays the use of agrochemicals (better called Plant Protection Products, PPPs) in agriculture is essential for crop protection. Plant Protection Products are formulations containing one or more active substances, used mainly in agriculture for weeds, insects, fungi, and bacteria control or to influence the life processes of plants (growth regulators). The use of PPPs in agriculture contributes to environmental pollution, biodiversity loss and can harm non-target plants, insects, birds, mammals and amphibians. The transition to a sustainable food system is the goal of the *Farm to Fork strategy*, which aims to reduce the dependency on pesticides and antimicrobials in Europe. Among the key objectives to achieve by 2030, there is (i) the reduction of the use of chemical pesticides by 50%, (ii) the decrease of fertilizer use by at least 20% by halving nutrient loss, ensuring a good soil fertility, (iii) the reduction of total sales of antimicrobials and antibiotics by 50%, and (iv) the conversion of 25% of farmland to organic (European Commission, 2020).

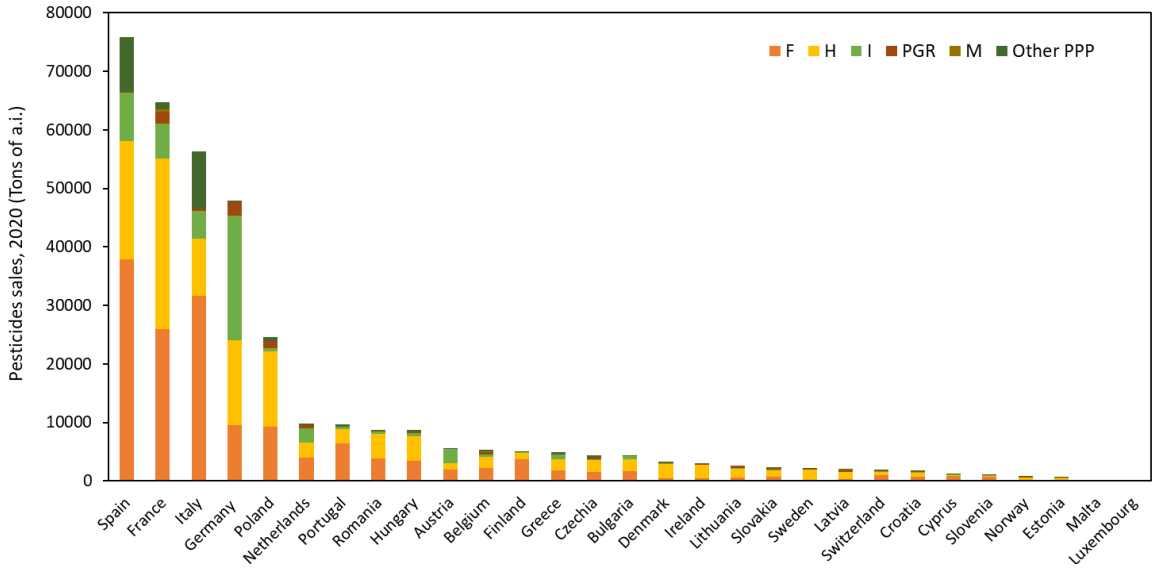

Figure 1.1. Annual pesticide sales in Europe in 2020. Different colors indicate groups of PPPs (orange, Fungicides F; yellow, Herbicides H; green, insecticides I; red, Plant Growth regulator PGR; brown, molluscicides M; dark green, other PPPs). Data source: Eurostat, 2022. Edited by the author.

In 2021 in Europe, the annual sales of PPPs fluctuate around 350 000 tons per year (Eurostat, 2022). The three major groups of substances used are fungicides, herbicides, and insecticides (orange, yellow, and green columns in **Figure 1.1**), while in a minor part are plant growth regulators, molluscicides, and other products. In this context, Spain, France, Italy, and Germany – the main European agricultural producers – are the four top countries with the highest volume of pesticides sold in 2020 (76, 65, 56, and 48 thousand tons respectively), accounting for 49 % of the total EU arable land (**Figure 1.1**).

Although a general reduction in PPPs sales (-7.3%), has been registered in Europe in 10 years (2011-2020), and so has Italy (-20%), the distribution of agrochemicals in agricultural lands is still raising questions about their sustainable use (Helepciuc and Todor, 2021). In Italy, more than half of the total volume of PPPs sold in the country in 2020 were fungicides, and herbicides accounted for 17%.

Herbicides are commonly classified based on the type of active ingredient contained in the formulation. In Europe, more than 40% of sales of herbicides in 2020 were organophosphorus herbicides (**Figure 1.2**), including glyphosate. This percentage increases up to 68% if referred to Italy.

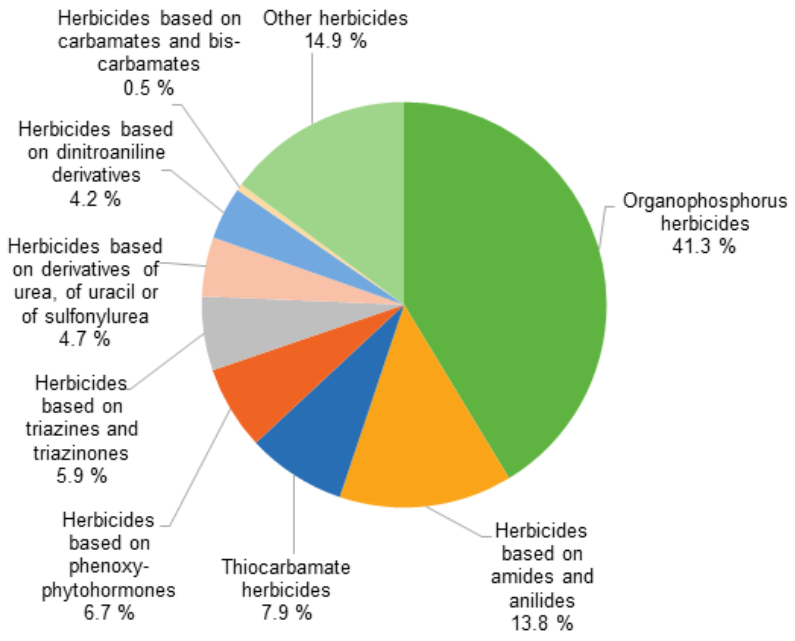

Figure 1.2. Sales of herbicides, haulm destructors, and moss killers by category of products in Europe, 2020, reported as a percentage. Source: Eurostat, 2022.

1.2 The herbicide glyphosate: toxicity and environmental fate

N-(phosphonomethyl)glycine, better known as glyphosate (GLP) is a phosphonate compound, used as an herbicide in agriculture. Discovered in 1950 by H. Martin, a Swiss chemist, GLP was first used as a chelator for its binding affinity towards Cu, Ca, Mg and Zn. Later in 1970, Monsanto, an agrochemical corporation in the USA, independently synthesized GLP as a weed killer, starting to be commercialized in 1974 with the brand name *Roundup*.

Glyphosate acts as a weed killer by inhibiting the 5-enolpyruvylshikimate-3-phosphate synthase, a plant enzyme responsible for the synthesis of three aromatic amino acids (tryptophan, tyrosine, and phenylalanine) which are fundamental for plant growing. The herbicide is commonly sprayed in pre-sowing to clean the seedbed for the main crop, and it enters on weeds through foliage absorption. Here, it is translocated through the whole plant system via phloem flow (Gougler and Geiger, 1981). GLP is a non-selective, systemic, and post-emergence herbicide, not effective in pre-emergence. For many years, GLP has been defined as a non-toxic compound for humans and animals due to its specific action which inhibits the shikimate pathway, which only occurs in plants and some microorganisms. In the last decades, several studies gave evidence of a potential negative effect of GLP on aquatic ecosystems and its genotoxic effect on non-target species, like freshwater microorganisms (e.g. bacterium, microalgae, protozoa and crustaceans), algae, fishes and amphibians (Annett et al., 2014). Recently, a review by Serra et al. (2021) reported that GLP can induce alterations in the reproductive tracts in both males and females in humans and aquatic fauna, which can be transmitted to the next generations, being cataloged as an endocrine disruptor. Other studies showed that GLP-based herbicides have worse effects on fertility than the active ingredient, due to the presence of co-formulants in the commercial product (Defarge et al., 2016).

Glyphosate is an amphoteric molecule with three chemical moieties (phosphonate, amino and carboxyl group, **Figure 1.3**) and it commonly occurs in the environment as a zwitterion. Depending on pH, the phosphonic and carboxylic moieties can be ionized and the aminic protonated, resulting in different ionic states (**Figure 1.4**). In general, GLP is highly soluble in water, polar, moderately persistent in soil with low affinity for the organic phase (low octanol-

water repartition coefficient, K_{ow}), and non-volatile (**Table 1.1**). Furthermore, it is considered a low-leachable herbicide due to its high adsorption by the mineral phase of soil (Glass, 1987).

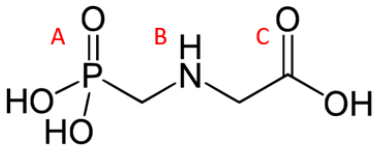

Figure 1.3. Chemical structure of the N-(phosphonomethyl)glycine. Red letters refer to the three moieties of the molecule: A, phosphonic; B, aminic; C, carboxylic.

Specifically, in soil GLP is mainly adsorbed by clay minerals, iron and aluminum oxides – goethite, hematite and ferrihydrite (Sheals et al., 2002; Gimsing and Borggaard, 2007) –, poorly ordered aluminum silicates – such as allophane and imogolite –, and very low sorption has been detected for clay silicates, as kaolinite, illite and montmorillonite (Borggaard and Gimsing, 2008). Moreover, the addition of tri- and bivalent cations in soil, such as Al^{3+}, Fe^{3+}, Cu^{2+}, Mg^{2+}, Zn^{2+}, Mn^{2+}, Ca^{2+} and Na^{+} increases the adsorption of the herbicide (Glass, 1987). On the contrary, the role of soil organic matter (SOM) towards GLP is not yet fully clarified, as it seems to play a double effect: many authors found a negative correlation between SOM content and GLP adsorption, being the organic matter competing for soil sorption sites, in turn inhibiting the adsorption of GLP (Gerritse et al., 1996; Fink et al., 2016).

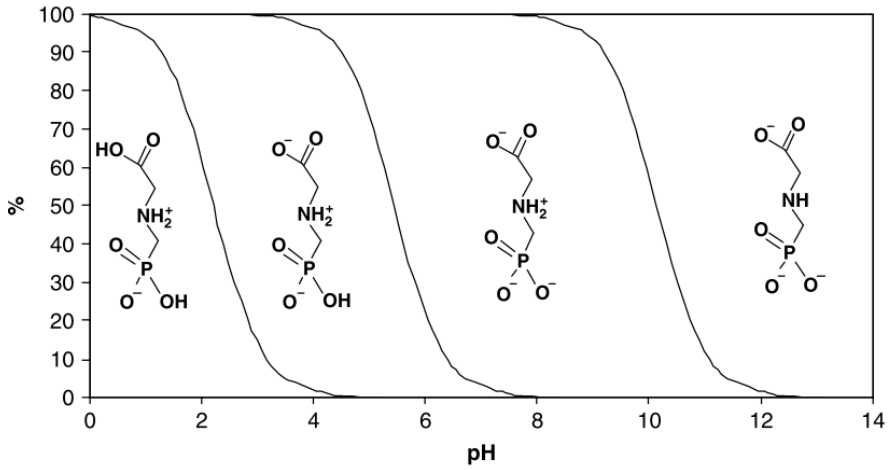

Figure 1.4. Distribution of glyphosate species as a function of pH (Bjerrum diagram). Source: Borggaard and Gimsing, (2008).

On the other hand, SOM can increase the adsorption of GLP due to the formation of SOM-cation-herbicide complexes (Sprankle et al., 1975) and because poorly ordered Al and Fe oxides can be favored at higher SOM content (Wagai et al., 2013; Kirsten et al., 2021). A key factor that can greatly determine the fate of GLP in soil is the phosphate content, as it can compete for the same sorption sites of GLP (Gimsing and Borggaard, 2002, 2007). This means that phosphate fertilizers application reduces the availability of sorption sites for the herbicide, which might leach into groundwater (Munira et al., 2016). In addition, the adsorption of GLP is strongly affected by pH conditions, as adsorption decreases under alkaline conditions (Sheals et al., 2002; Pereira et al., 2019), due to decreased interaction when sorbents and GLP became more negatively charged (McConnell and Hossner, 1985). Another factor that positively affects GLP affinity to the soil phase is the cation exchange capacity, which is related to the clay content (Padilla and Selim, 2018).

Table 1.1. Glyphosate properties. Log k_{ow} is the octanol-water repartition coefficient, DT_{50} is the time for the dissipation of 50% of the concentration of a molecule, and GUS is the Groundwater Ubiquity Score as reported by Gustafson (1989). Source: Pesticides Property Database (PPDB), IUPAC, (Lewis and Tzilivakis, 2017).

Physical-chemical properties of glyphosate	
Name	N-(phosphonomethyl)glycine
Chemical Formula	$C_3H_8NO_5P$
Molecular Weight	169.4 g mol^{-1}
Melting Point	189.5°C
Density at 20°C	1.71 g ml^{-1}
Solubility	
- in Water at 20°C	10.5 g l^{-1}
- in Organic solvents	Almost insoluble
log K_{ow}	-6.28
Vapour Pressure at 20°C	0.0131 mPa
Soil degradation	
- DT_{50} lab 20°C	0.7 - 78.9 days
- DT_{50} field	1.1 - 13.7 days
Soil Adsorption	
Linear K_d	5.0 - 510 ml g^{-1}
Freundlich K_f	18.1 - 166.4 ml g^{-1}
1/n	0.54 - 0.78
GUS leaching index	0.21 (Low Leachability)
Metabolites in soil	Aminomethylphosphonic acid Sarcosine

Once reached the soil, GLP undergoes dissipation, which is only partially affected by abiotic factors, such as soil moisture, temperature, and nutrients (Bento et al., 2016). Therefore, the main breakdown pathway is through microbial degradation, producing aminomethylphosphonic acid (AMPA) and glyoxylic acid. A minor pathway, occurring only in specialized soil bacteria species, produces inorganic phosphate and sarcosine, thus converted into glycine, an amino acid (Kishore and Jacob, 1987; Dick and Quinn, 1995). The production of sarcosine from glyphosate degradation does not have negative effects on the environment. On the contrary, AMPA is highly soluble, mobile, strongly adsorbed to soil particles, and more persistent than glyphosate, and is therefore a potential contaminant for water resources (Sidoli et al., 2016). Water resources are not the only environmental compartment that can be contaminated by herbicides. In a study across agricultural soils in Europe, Silva et al. (2018) detected high concentrations of GLP in the southern part, while AMPA here occurred with a lower proportion suggesting a slower degradation of GLP under drier conditions. The occurrence of GLP in soils is not only a risk for soil health but also a potential risk for water resources and the atmosphere. Indeed, organisms can be exposed to these substances by inhalation of contaminated dust particles, dermal contact, or ingestion by water or wind erosion. Therefore, the strong debate about the potential harmfulness of the molecule is still ongoing (Myers et al., 2016; EFSA, 2017).

To protect water quality and human health from contamination, maximum contaminant levels (MCL) allowed in drinking water have been established for many molecules. In Europe, the MCL for GLP is 0.1 μg l^{-1}, which is administratively set as the upper tolerable threshold for all pesticides[1] (European Parliament, 2020). This threshold might be seen as precautionary if the USA limit is considered, set at 700 μgL^{-1}. This discrepancy is mainly related to the decision of US to carry specific toxicity tests for GLP, resulting in higher MCL than for other pesticides (US EPA, 2003), while in Europe the precautionary principle is commonly applied to risk management (Dolan et al., 2013). About its use, the European Commission had already been asked to decide on the ban on GLP-based herbicides in 2017 and has postponed the decision for 5 years. Therefore, the use of GLP is currently approved until December 15th, 2022, and the EU Commission must decide on its ban or allow its use (European Parliament, 2022). The

[1] In Italy, MCLs for agrochemicals are reported in Table 1/B (Annex 2) of the legislative decree 152/2006, which sets out the legislative framework applicable to all matters concerning environmental protection.

potential prohibition of GLP-based herbicides in Europe has caused concerns among farmers about the economic effects, mainly related to crop management based on conservation agriculture practices. Since tillage in conservation agriculture is not allowed (no-tillage) or at least reduced (minimum-tillage), weed control largely depends on the use of herbicides to replace mechanical control used in conventional agriculture. Indeed, the three principles on which conservation agriculture is based are (i) minimum tillage and soil disturbance, (ii) permanent soil cover by using cover crops, crop residues and live mulches, and (iii) intercropping or crop rotations (Baker et al., 2006; Stanojevic, 2021). Pardo and Martínez (2019) estimated that banning GLP, which is low-cost and easily degradable, would lead to an increase in the costs of chemical weed control by 40% and 57% for herbaceous and tree crops respectively, likely favouring a reconversion of conservation-managed fields to conventional tillage, as it would be the cheapest option. Currently, no safer alternatives to GLP have been produced among herbicides, and a possible ban of this active ingredient would lead to a chemical substitute that might not have the same low-impact characteristics (e.g., rapid degradation, strong adsorption in the soil, and low mobility).

Pesticides, depending on their chemical properties, can be lost by different transport processes. The most important one for GLP is through runoff in surface waters (Lupi et al., 2019), but it can also happen by soil erosion (Yang et al., 2015) and by leaching to the groundwater (Borggaard and Gimsing, 2008). Since glyphosate is highly soluble in water but strongly adsorbed to soil particles, its prediction in the environment is still challenging. In surface and groundwater, GLP has been detected several times (Vereecken, 2005; Carles et al., 2019; Carretta et al., 2022). In Italy, GLP and AMPA were the mostly detected molecules in surface water in 2018, exceeding the MCL of 21.7 and 54.3% of the total samples respectively, while in groundwater GLP and AMPA were found only in 2 and 1.6% of the total samples (ISPRA, 2020). Although it is sporadically present in groundwater resources, when found in concentrations above the MCL, it can be considered a threat to public and environmental health. The leaching to groundwater might be due to several factors, like (i) the occurrence of heavy rainfall shortly after herbicide distribution (Székács et al., 2015), (ii) the peculiar soil structure – macroporosity and presence of preferential flow – (Kjær et al., 2011) and (iii) the applied dose (Börjesson and Torstensson, 2000). In fact, in a monitoring study conducted in Mexico by Lutri et al. (2020), authors found that groundwater samples presented higher concentration of GLP in comparison with the stream water, due to the

greater dilution capacity of the latter. Moreover, this phenomenon can be worsened when the water table level is shallow, which is a common condition in the low-lying Venetian plain, where intensive agricultural practices are conducted. Here, the leaching potential of a pesticide can be exacerbated by the reduced unsaturated soil zone, according to peculiar characteristics of the agrochemical (e.g. solubility, adsorption to soil, degradation time). Furthermore, the occurrence of a shallow groundwater might influence the number of preferential flow pathways (Haria et al., 2003) by changing the water content in the soil matrix due to drying-wetting cycles.

1.3 The occurrence of preferential flow in soils and its impact on groundwater quality

Preferential flow (PF) is the rapid transport of water and/or solutes via macropore-dominated pathways in soils, bypassing the porous matrix (Bundt et al., 2001; Hendrickx and Flury, 2001). Through PF, a contaminant can reach groundwater resources via faster transport, leading to reduced water quality. Several types of PF can occur in soil, like macropore flow (including crack flow and biopores), finger flow (non-uniform water flow due to hydraulic heterogeneity), funnel flow (lateral flow along boundaries) or film flow (water flows as a thin film along the macropore's walls) (Lin, 2010). Soil architecture is the most important factor – among the others – controlling PF pathways in soil. This includes the macropore structure, which can be characterized by imaging technologies (Zhang et al., 2015). The amount of connected macropores is a key factor under saturated conditions dominating PF, whereas under unsaturated conditions a limited fraction of macropores might be activated (Sammartino et al., 2015). When the macropore network formed by earthworms, root channels and cracks is not disrupted (e.g. under conservation tillage and no-tillage), it allows water to flow downward at higher rate than through the soil matrix (Alletto et al., 2010; Behrends Kraemer et al., 2022).

Several methods have been used in the last decades to monitor PF occurrence in soils, such as dye staining (**Figure 1.5**), breakthrough curve experiments at the soil column scale, geophysical techniques, conservative tracer tests, and X-ray computed microtomography (Larsbo et al., 2014; Guo and Lin, 2018).

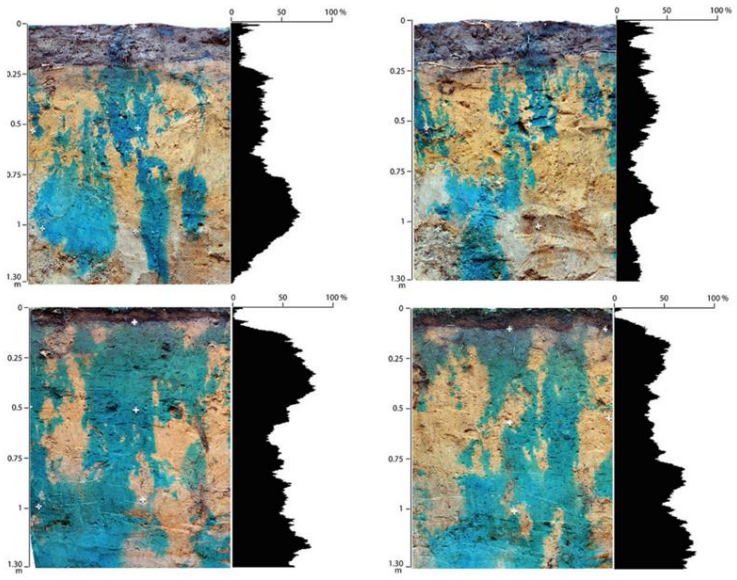

Figure 1.5. Different dye tracer stain patterns in soil profiles and plots of values of relative dye coverage vs. depth for vertical soil profiles. Modified from Schneider et al. (2018).

Observed data might be then used to feed a hydrological model which can account for PF. Many hydrogeological models have been commonly applied to study water flow and solute transport, like MACRO (Beulke et al., 2001), RZWQM (Hanson et al., 1998), CRACK-NP (Armstrong et al., 2000), and HYDRUS 1D (Šimůneket al., 2009). Research on preferential flow modelling goes back to the 1970s thanks to the work of Germann and Beven (1981). Currently, models accounting for PF usually apply a dual-porosity or dual-permeability approach (Jarvis, 2007). These models divide the domain into two interacting regions (the matrix and the macropores) where water flow is described by different governing equations (Holbak et al., 2021). In the dual-porosity approach, water is considered immobile in the matrix domain, while in the macropores water flow is described by the Richards equation (Haws et al., 2005). In the dual-permeability model, water flow in both the matrix and macropores is described by two separately parameterized Richards equations (Gerke and Köhne, 2004).

Among numerical models, HYDRUS 1D is a process-based model that solves Richards' equation for unsaturated water flow and the advection-dispersion equation (ADE) or several physical and/or chemical non-equilibrium equations for solute transport. Physical non-equilibrium models comprise Mobile-Immobile water (MIM) – which is only applied to solute transport maintaining uniform water flow –, Dual-Porosity, Dual-Permeability and Dual-Permeability with MIM (**Figure 1.6**). It has to be noted that, for some soils the behavior of the solute may not necessarily be the same as that of water, since the water flow rate might have negligible

or no effect on the shape of solute breakthrough curves, as this is the case when MIM is applied (Jacques et al., 2002; Larsbo et al., 2014).

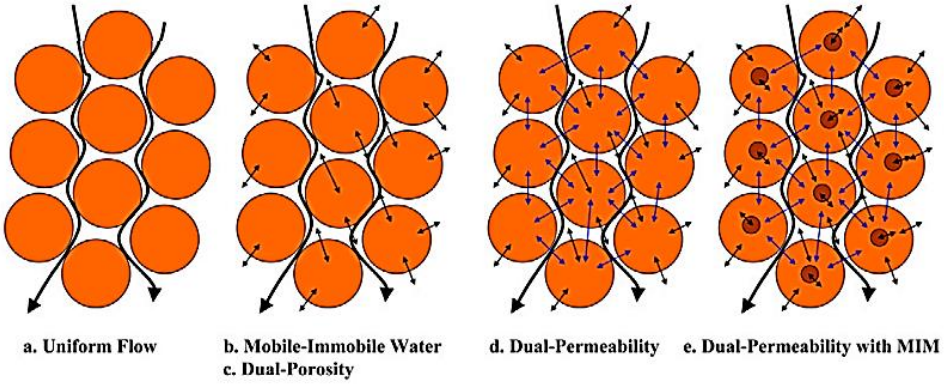

Figure 1.6. Conceptual physical nonequilibrium models for water flow and solute transport. From: Šimůnek and van Genuchten, 2008.

Moreover, Different sorption models are integrated in HYDRUS 1D to consider linear or non-linear adsorption isotherms (Freundlich or Langmuir), and metabolites formed by first-order degradation reactions can also be simulated (Šimůnek and Genuchten, 2008). Moreover, the inverse modeling approach can be used to estimate soil hydraulic and solute properties from observed data measured in the field (e.g. water content, matric head, and solute concentration). For this purpose, appropriate algorithms are applied to minimize the objective function starting from soil water and solute data, resulting in the best set of values of the optimized parameters (Ritter et al., 2003).

1.4 Thesis objectives

The main objective of this Ph.D. thesis was to evaluate the environmental fate of glyphosate under contrasting conditions in the Veneto region, Northeastern Italy. The research was performed in two areas and contrasting agroecosystems: the high foothills and the low-lying Venetian plain, on one hand, vineyards, conventional and conservation agriculture on the other hand (**Figure 1.7**). Two sites (which correspond to different soils) were chosen in the high foothills of the Treviso province – Conegliano and Valdobbiadene – which is a widely extensive vineyard area for the production of the Prosecco wine and has been recently included in the UNESCO's World Heritage List. In the low-lying Venetian plain, the study was conducted on a set of lysimeters of the Experimental Farm of the University of Padova (Legnaro). Here, conventional and short-term conservation agricultural practices, as the effect of shallow groundwater, have been investigated to identify factors affecting the adsorption, dissipation, and transport dynamics of glyphosate. Furthermore, the influence of shallow water table – which is a common condition in the low-lying Venetian plain – has been investigated on soil structure and solute transport. Specifically, preferential flow occurrence was evaluated to understand if different groundwater levels can enhance the risk of solute bypass and groundwater pollution.

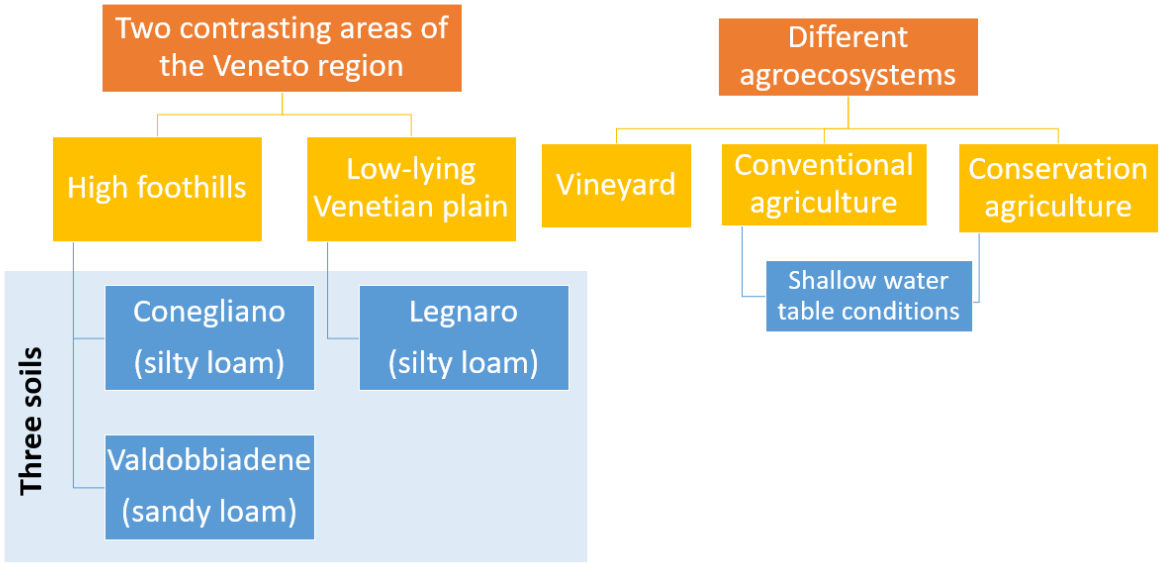

Figure 1.7. The fate of glyphosate has been evaluated in contrasting areas and agroecosystems of the Veneto region.

In this thesis, several questions have been raised that can be summarized as the followings:

i. What are the main soil properties that influence the adsorption capacity of glyphosate and how does it change for different soils?
ii. How do dissipation rates and herbicide residues in soil change under different agroecosystems and soil management?
iii. Can short-term conservation practices influence glyphosate dynamics in soil and water and how?
iv. Can a shallow water table be a driver able to affect the transport of solutes in water through the soil profile and how?

These aspects are deeply explored in the following chapters, which seek to provide answers and comments to the above questions. In some cases, it has not been possible to give an unequivocal and certain answer to a specific question, but several new insights have emerged that could be further investigated to better understand the fate of glyphosate under particular soil conditions.

References

Alletto, L., Coquet, Y., Benoit, P., Heddadj, D., and Barriuso, E. (2010). Tillage management e ff ects on pesticide fate in soils . A review. *Agron. Sustain. Dev.* 30, 367–400.

Annett, R., Habibi, H. R., and Hontela, A. (2014). Impact of glyphosate and glyphosate-based herbicides on the freshwater environment. *J. Appl. Toxicol.* 34, 458–479. doi:10.1002/jat.2997.

Armstrong, A. C., Matthews, A. M., Portwood, A. M., Leeds-Harrison, P. B., and Jarvis, N. J. (2000). CRACK-NP: A pesticide leaching model for cracking clay soils. *Agric. Water Manag.* 44, 183–199. doi:10.1016/S0378-3774(99)00091-8.

Baker, C. J., Saxton, K. E., Ritchie, W. R., Chamen, W. C. T., Reicosky, D. C., Ribeiro, M. F. S., et al. (2006). No-tillage seeding in conservation agriculture: Second edition. *No-Tillage Seeding Conserv. Agric. Second Ed.*, 1–326.

Behrends Kraemer, F., Castiglioni, M. G., Chagas, C. I., De Paula, R., Sainz, D. S., De Gerónimo, E., et al. (2022). Pesticide dynamics in agroecosystems: Assessing climatic and hydro-physical effects in a soybean cycle under no-tillage. *Soil Tillage Res.* 223. doi:10.1016/j.still.2022.105489.

Bento, C. P. M., Yang, X., Gort, G., Xue, S., van Dam, R., Zomer, P., et al. (2016). Persistence of glyphosate and aminomethylphosphonic acid in loess soil under different combinations of temperature, soil moisture and light/darkness. *Sci. Total Environ.* 572, 301–311. doi:10.1016/j.scitotenv.2016.07.215.

Beulke, S., Brown, C. D., and Jarvis, N. J. (2001). Macro: A Preferential Flow Model to Simulate Pesticide Leaching and Movement to Drains. *Model. Environ. Chem. Expo. Risk*, 117–132. doi:10.1007/978-94-010-0884-6_12.

Borggaard, O. K., and Gimsing, A. L. (2008). Fate of glyphosate in soil and the possibility of leaching to ground and surface waters : a review. *Pest Manag. Sci.* 456, 441–456. doi:10.1002/ps.

Börjesson, E., and Torstensson, L. (2000). New methods for determination of glyphosate and (aminomethyl)phosphonic acid in water and soil. *J. Chromatogr. A* 886, 207–216. doi:10.1016/S0021-9673(00)00514-8.

Bundt, M., Zimmermann, S., Blaser, P., and Hagedorn, F. (2001). Sorption and transport of metals in preferential flow paths and soil matrix after the addition of wood ash. *Eur. J. Soil Sci.* 52, 423–431. doi:10.1046/j.1365-2389.2001.00405.x.

Carles, L., Gardon, H., Joseph, L., Sanchís, J., Farré, M., and Artigas, J. (2019). Meta-analysis of glyphosate contamination in surface waters and dissipation by biofilms. *Environ. Int.* 124, 284–293. doi:10.1016/j.envint.2018.12.064.

Carretta, L., Masin, R., and Zanin, G. (2022). Review of studies analysing glyphosate and aminomethylphosphonic acid (AMPA) occurrence in groundwater. *Environ. Rev.* 30, 88–109. doi:10.1139/er-2020-0106.

Defarge, N., Takács, E., Lozano, V. L., Mesnage, R., de Vendômois, J. S., Séralini, G. E., et al.

(2016). Co-formulants in glyphosate-based herbicides disrupt aromatase activity in human cells below toxic levels. *Int. J. Environ. Res. Public Health* 13. doi:10.3390/ijerph13030264.

Dick, R. E., and Quinn, J. P. (1995). Glyphosate-degrading isolates from environmental samples: occurrence and pathways of degradation. *Appl. Microbiol. Biotechnol.* 43, 545–550. doi:10.1007/BF00218464.

Dolan, T., Howsam, P., Parsons, D. J., and Whelan, M. J. (2013). Is the EU drinking water directive standard for pesticides in drinking water consistent with the precautionary principle? *Environ. Sci. Technol.* 47, 4999–5006. doi:10.1021/es304955g.

EFSA (2017). Peer review of the pesticide risk assessment of the potential endocrine disrupting properties of glyphosate. *EFSA J.* 15. doi:10.2903/j.efsa.2017.4979.

European Commission (2020). Farm to Fork Strategy. *DG SANTE/Unit 'Food Inf. Compos. food waste'','* 23. Available at: https://ec.europa.eu/food/sites/food/files/safety/docs/f2f_action-plan_2020_strategy-info_en.pdf.

European Parliament (2020). Directive (EU) 2020/2184 of the European Parliament and of the Council. *Off. J. Eur. Union* 2019, 1–62.

European Parliament (2022). Plenary – June I 2022 Question time : Reducing the use of pesticides and strengthening consumer protection.

Eurostat (2022). Agri-environmental indicator — consumption of pesticides — Statistics Explained. Available at: http://epp.eurostat.ec.europa.eu/statistics_explained/index.php/Agri-environmental_indicator_-_consumption_of_pesticides.

Fink, J. R., Inda, A. V., Tiecher, T., and Barrón, V. (2016). Iron oxides and organic matter on soil phosphorus availability. *Cienc. e Agrotecnologia* 40, 369–379. doi:10.1590/1413-70542016404023016.

Gerke, H. H., and Köhne, J. M. (2004). Dual-permeability modeling of preferential bromide leaching from a tile-drained glacial till agricultural field. *J. Hydrol.* 289, 239–257. doi:10.1016/j.jhydrol.2003.11.019.

Germann, P., and Beven, K. (1981). Water Flow in Soil Macropores I. an Experimental Approach. *J. Soil Sci.* 32, 1–13. doi:10.1111/j.1365-2389.1981.tb01681.x.

Gerritse, R. G., Beltran, J., and Hernandez, F. (1996). Adsorption of atrazine, simazine, and glyphosate in soils of the Gnangara Mound, Western Australia. *Aust. J. Soil Res.* 34, 599–607. doi:10.1071/SR9960599.

Gimsing, A. L., and Borggaard, O. K. (2002). Effect of phosphate on the adsorption of glyphosate on soils, clay minerals and oxides. *Int. J. Environ. Anal. Chem.* 82, 545–552. doi:10.1080/0306731021000062964.

Gimsing, A. L., and Borggaard, O. K. (2007). Phosphate and glyphosate adsorption by

hematite and ferrihydrite and comparison with other variable-charge minerals. *Clays Clay Miner.* 55, 108–114. doi:10.1346/CCMN.2007.0550109.

Glass, R. L. (1987). Adsorption of Glyphosate by Soils and Clay Minerals. *J. Agric. Food Chem.* 35, 497–500. doi:10.1021/jf00076a013.

Gougler, J., and Geiger, D. R. (1981). Uptake and Distribution of N-Phosphonomethylglycine in. *Plant Phisiology* 68, 668–672.

Guo, L., and Lin, H. (2018). Addressing Two Bottlenecks to Advance the Understanding of Preferential Flow in Soils. *Adv. Agron.* 147.

Gustafson, D. I. (1989). Groundwater ubiquity score: A simple method for assessing pesticide leachability. *Environ. Toxicol. Chem.* 8, 339–357. doi:10.1002/etc.5620080411.

Hanson, J. D., Ahuja, L. R., Shaffer, M. D., Rojas, K. W., DeCoursey, D. G., Farahani, H., et al. (1998). RZWQM: Simulating the effects of management on water quality and crop production. *Agric. Syst.* 57, 161–195. doi:10.1016/S0308-521X(98)00002-X.

Haria, A. H., Hodnett, M. G., and Johnson, A. C. (2003). Mechanisms of groundwater recharge and pesticide penetration to a chalk aquifer in southern England. *J. Hydrol.* 275, 122–137. doi:10.1016/S0022-1694(03)00017-9.

Haws, N. W., Rao, P. S. C., Šimůnek, J., and Poyer, I. C. (2005). Single-porosity and dual-porosity modeling of water flow and solute transport in subsurface-drained fields using effective field-scale parameters. *J. Hydrol.* 313, 257–273. doi:10.1016/j.jhydrol.2005.03.035.

Helepciuc, F. E., and Todor, A. (2021). Evaluating the effectiveness of the EU's approach to the sustainable use of pesticides. *PLoS One* 16, 1–18. doi:10.1371/journal.pone.0256719.

Hendrickx, J. M. H., and Flury, M. (2001). Uniform and preferential flow mechanisms in the vadose zone. *Concept. Model. flow Transp. Fract. vadose Zo. Washington, DC*, 149–187.

Holbak, M., Abrahamsen, P., Hansen, S., and Diamantopoulos, E. (2021). A Physically Based Model for Preferential Water Flow and Solute Transport in Drained Agricultural Fields. *Water Resour. Res.* 57, 1–19. doi:10.1029/2020WR027954.

ISPRA (2020). *National report on pesticides in water (in Italian)*.

J. Šimůnek, M. Šejna, H. Saito, M. Sakai, M. T. van G. (2009). The HYDRUS-1D Software Package for Simulating the One-Dimensional Movement of Water, Heat, and Multiple Solutes in Variably-Saturated Media.

Jacques, D., Šimůnek, J., Timmerman, A., and Feyen, J. (2002). Calibration of Richards' and convection-dispersion equations to field-scale water flow and solute transport under rainfall conditions. *J. Hydrol.* 259, 15–31. doi:10.1016/S0022-1694(01)00591-1.

Jarvis, N. J. (2007). A review of non-equilibrium water flow and solute transport in soil macropores: principles, controlling factors and consequences for water quality. *Eur. J. Soil Sci.* 71, 279–302. doi:10.1111/ejss.12973.

Kirsten, M., Mikutta, R., Vogel, C., Thompson, A., Mueller, C. W., Kimaro, D. N., et al. (2021). Iron oxides and aluminous clays selectively control soil carbon storage and stability in the humid tropics. *Sci. Rep.* 11, 1–12. doi:10.1038/s41598-021-84777-7.

Kishore, G. M., and Jacob, G. S. (1987). Degradation of glyphosate by Pseudomonas sp. PG2982 via a sarcosine intermediate. *J. Biol. Chem.* 262, 12164–12168. doi:10.1016/s0021-9258(18)45331-8.

Kjær, J., Ernsten, V., Jacobsen, O. H., Hansen, N., de Jonge, L. W., and Olsen, P. (2011). Transport modes and pathways of the strongly sorbing pesticides glyphosate and pendimethalin through structured drained soils. *Chemosphere* 84, 471–479. doi:10.1016/j.chemosphere.2011.03.029.

Kjær, J., Olsen, P., Ullum, M., and Grant, R. (2005). Leaching of Glyphosate and Amino-Methylphosphonic Acid from Danish Agricultural Field Sites. *J. Environ. Qual.*, 608–620.

Larsbo, M., Koestel, J., and Jarvis, N. (2014). Relations between macropore network characteristics and the degree of preferential solute transport. *Hydrol. Earth Syst. Sci.* 18, 5255–5269. doi:10.5194/hess-18-5255-2014.

Lewis, K., and Tzilivakis, J. (2017). Development of a data set of pesticide dissipation rates in/on various plant matrices for the pesticide properties database (PPDB). *Data* 2. doi:10.3390/data2030028.

Lin, H. (2010). Linking principles of soil formation and flow regimes. *J. Hydrol.* 393, 3–19. doi:10.1016/j.jhydrol.2010.02.013.

Lupi, L., Bedmar, F., Puricelli, M., Marino, D., Aparicio, V. C., Wunderlin, D., et al. (2019). Glyphosate runoff and its occurrence in rainwater and subsurface soil in the nearby area of agricultural fields in Argentina. *Chemosphere* 225, 906–914. doi:10.1016/j.chemosphere.2019.03.090.

Lutri, V. F., Matteoda, E., Blarasin, M., Aparicio, V., Giacobone, D., Maldonado, L., et al. (2020). Hydrogeological features affecting spatial distribution of glyphosate and AMPA in groundwater and surface water in an agroecosystem. Córdoba, Argentina. *Sci. Total Environ.* 711, 134557. doi:10.1016/j.scitotenv.2019.134557.

McConnell, J. S., and Hossner, L. R. (1985). pH-Dependent Adsorption Isotherms of Glyphosate. *J. Agric. Food Chem.* 33, 1075–1078. doi:10.1021/jf00066a014.

Morrás, H., Behrends Kraemer, F., Sainz, D., Fernández, P., and Chagas, C. (2022). Soil structure and glyphosate fate under no-till management in the Pampa region. II. Glyphosate and AMPA persistence and spatial distribution in the long-term. A conceptual model. *Soil Tillage Res.* 223. doi:10.1016/j.still.2022.105471.

Munira, S., Farenhorst, A., Flaten, D., and Grant, C. (2016). Phosphate fertilizer impacts on glyphosate sorption by soil. *Chemosphere* 153, 471–477. doi:10.1016/j.chemosphere.2016.03.028.

Myers, J. P., Antoniou, M. N., Blumberg, B., Carroll, L., Colborn, T., Everett, L. G., et al. (2016). Concerns over use of glyphosate-based herbicides and risks associated with exposures:

A consensus statement. *Environ. Heal. A Glob. Access Sci. Source* 15, 1–13. doi:10.1186/s12940-016-0117-0.

Padilla, J. T., and Selim, H. M. (2018). Glyphosate transport in two louisiana agricultural soils: Miscible displacement studies and numerical modeling. *Soil Syst.* 2, 1–18. doi:10.3390/soilsystems2030053.

Pardo, G., and Martínez, Y. (2019). Conservation agriculture in trouble? Estimating the economic impact of an eventual glyphosate prohibition in Spain. *Planta Daninha* 37. doi:10.1590/s0100-83582019370100138.

Pereira, R. C., Anizelli, P. R., Di Mauro, E., Valezi, D. F., Da Costa, A. C. S., Zaia, C. T. B. V., et al. (2019). The effect of pH and ionic strength on the adsorption of glyphosate onto ferrihydrite. *Geochem. Trans.* 20, 1–14. doi:10.1186/s12932-019-0063-1.

Ritter, A., Hupet, F., Muñoz-Carpena, R., Lambot, S., and Vanclooster, M. (2003). Using inverse methods for estimating soil hydraulic properties from field data as an alternative to direct methods. *Agric. Water Manag.* 59, 77–96. doi:10.1016/S0378-3774(02)00160-9.

Sammartino, S., Lissy, A.-S., Bogner, C., Van Den Bogaert, R., Capowiez, Y., Ruy, S., et al. (2015). Identifying the Functional Macropore Network Related to Preferential Flow in Structured Soils. *Vadose Zo. J.* 14, vzj2015.05.0070. doi:10.2136/vzj2015.05.0070.

Schneider, A., Hirsch, F., Raab, A., and Raab, T. (2018). Dye tracer visualization of infiltration patterns in soils on relict charcoal hearths. *Front. Environ. Sci.* 6, 1–14. doi:10.3389/fenvs.2018.00143.

Serra, L., Estienne, A., Vasseur, C., Froment, P., and Dupont, J. (2021). Review: Mechanisms of glyphosate and glyphosate-based herbicides action in female and male fertility in humans and animal models. *Cells* 10. doi:10.3390/cells10113079.

Sheals, J., Sjöberg, S., and Persson, P. (2002). Adsorption of glyphosate on goethite: Molecular characterization of surface complexes. *Environ. Sci. Technol.* 36, 3090–3095. doi:10.1021/es010295w.

Sidoli, P., Baran, N., and Angulo-Jaramillo, R. (2016). Glyphosate and AMPA adsorption in soils: laboratory experiments and pedotransfer rules. *Environ. Sci. Pollut. Res.* 23, 5733–5742. doi:10.1007/s11356-015-5796-5.

Silva, V., Montanarella, L., Jones, A., Fernández-Ugalde, O., Mol, H. G. J., Ritsema, C. J., et al. (2018). Distribution of glyphosate and aminomethylphosphonic acid (AMPA) in agricultural topsoils of the European Union. *Sci. Total Environ.* 621, 1352–1359. doi:10.1016/j.scitotenv.2017.10.093.

Šimůnek, J., and Genuchten, M. T. (2008). Modeling Nonequilibrium Flow and Transport Processes Using HYDRUS. *Vadose Zo. J.* 7, 782–797. doi:10.2136/vzj2007.0074.

Sprankle, P., Meggitt, W. F., and Penner, D. (1975). Adsorption, mobility and microbial degradation of glyphosate in soil. *Weed Sci.* 23, 229–234.

Stanojevic, A. B. (2021). Conservation agriculture and its principles. *Ann. Environ. Sci. Toxicol.* 5, 018–022. doi:10.17352/aest.000031.

Székács, A., Mörtl, M., and Darvas, B. (2015). Monitoring Pesticide Residues in Surface and Ground Water in Hungary: Surveys in 1990–2015. *J. Chem.* 2015. doi:http://dx.doi.org/10.1155/2015/717948 Research.

US EPA (2003). Six-Year Review Chemical Contaminants Health Effects Technical Support Document.

Vereecken, H. (2005). Mobility and leaching of glyphosate: A review. *Pest Manag. Sci.* 61, 1139–1151. doi:10.1002/ps.1122.

Wagai, R., Mayer, L. M., Kitayama, K., and Shirato, Y. (2013). Association of organic matter with iron and aluminum across a range of soils determined via selective dissolution techniques coupled with dissolved nitrogen analysis. *Biogeochemistry* 112, 95–109. doi:10.1007/s.

Yang, X., Wang, F., Bento, C. P. M., Xue, S., Gai, L., van Dam, R., et al. (2015). Short-term transport of glyphosate with erosion in Chinese loess soil - A flume experiment. *Sci. Total Environ.* 512–513, 406–414. doi:10.1016/j.scitotenv.2015.01.071.

Zhang, Z. B., Peng, X., Zhou, H., Lin, H., and Sun, H. (2015). Characterizing preferential flow in cracked paddy soils using computed tomography and breakthrough curve. *Soil Tillage Res.* 146, 53–65. doi:10.1016/j.still.2014.05.016.

Chapter 2. Glyphosate and AMPA have low mobility through different soil profiles of the Prosecco wine production area: a monitoring study in North-eastern Italy*

*Mencaroni M., Cardinali A., Costa L., Morari F., Salandin P., Zanin G. and Dal Ferro N. (2022), Glyphosate and AMPA have low mobility through different soil profiles of the prosecco wine production area: A monitoring study in north-eastern Italy. Front. Environ. Sci. 10:971931. doi: 10.3389/fenvs.2022.97193

Abstract

Contamination of the environment by glyphosate (GLP) and its metabolite aminomethylphosphonic acid (AMPA) is still of major concern worldwide due to specific interactions among these molecules and soil and water. Two monitoring sites were established in the Prosecco wine production area (Conegliano and Valdobbiadene) in northeastern Italy, which has been included in the UNESCO's World Heritage List since 2019. The study aims to increase the knowledge about GLP dynamics in this area where it has been intensively used by farmers and the potential risk for groundwater pollution is still debated. Each site was equipped with two soil-water monitoring stations consisting of multi-sensor soil probes and suction cups at three soil depths (10, 30 and 70 cm). Soil and water were sampled for 10 and 6 months respectively and analyzed for GLP and AMPA concentrations, for a total of 242 samples to describe their vertical movement and dissipation dynamics. Soil properties, in particular the different forms of Fe and Al oxides contents, and Freundlich adsorption coefficients were quantified along the soil profile. First attempts showed that glyphosate dissipation time was 36±8 days in Conegliano and Valdobbiadene soil and fully completed in both after 6 months. In contrast, AMPA dissipation dynamics -first described by an original equation- was longer than GLP and fully dissipated after almost 300 days. GLP showed a strong binding affinity with clay and Fe and Al chelated to soil organic matter, which likely acted as cation bridges and in turn led to low GLP mobility. GLP and AMPA were mostly detected after heavy rainfall events at 70 cm depth, likely bypassing the porous matrix of the intermediate layers.

2.1 Introduction

Glyphosate (GLP) is one of the most-used broad-spectrum, systemic and post-emergence herbicides worldwide, with sales estimates of about 825804 tons in 2014 – of which 90% was used by the agricultural sector (Antier et al., 2020) – and expected 6.5% annual sales growth between 2016 and 2024 (Ahuja and Raeat, 2017). In agricultural lands, GLP-based agrochemicals are sprayed mainly before planting the crop or post-harvest during the intercropping period to control weeds growth. Glyphosate may also be used in pre-harvest on cereal, oilseed and pulse crops to aid harvesting and protect grain quality. Crops treated annually with GLP are annual (e.g. cereals and oilseeds) and perennial crops, like orchards and vineyards (Antier et al., 2020). GLP is usually considered of reduced mobility in soil due to its high affinity with clay minerals, soil oxides and hydroxides (Vereecken, 2005). As a polyprotic acid, its charge depends on soil pH resulting in complex sorption equilibrium dynamics. GLP commonly occurs as an anion and for this reason, it can only be sorbed onto variable-charge sites (e.g. Al and Fe oxides and 1:1 layer silicate clays in acidic soils). Moreover, its molecular structure makes interaction with soil organic matter (SOM) controversial compared to most non-polar pesticides due to: (i) dominating repulsive forces between negatively charged molecules – GLP and SOM components; (ii) blocking effect of SOM on other sorption sites that can lead to low GLP adsorption (Ololade et al., 2014). Conversely, the SOM propensity to promote poorly ordered Al and Fe might increase the soil sorption capacity of GLP (Okada et al., 2016), although this has been little studied so far and deserves attention, especially because it is strongly influenced by site-specific conditions. Furthermore, the presence of phosphate in soil might worsen the sorption capacity of the molecule by competing with bonding sites on Al-OH and Fe-OH surfaces (Borggaard and Gimsing, 2008). At the same time, GLP could be sorbed on phosphates through a metal cation bond (Al^{3+} and Fe^{3+}, or $Ca^{2+}$and Mg^{2+}) as suggested by some authors (Morillo et al., 1997; Nowack and Stone, 2006). Glyphosate adsorption in soil is usually described by a nonlinear Freundlich sorption isotherm, where the sorption coefficient (K_f) values can range from 0.6 to 700 (Vereecken, 2005; EFSA, 2015), depending on soil-specific characteristics. The main metabolite of GLP, aminomethylphosphonic acid (AMPA), is also characterized by high adsorption, depending on soil pH, Al and Fe oxide contents, available phosphorus and carbonates content. The low mobility of GLP and AMPA should exclude the potential risk of leaching to groundwater

(Borggaard and Gimsing, 2008). However, large discrepancies exist in the literature about their transfer towards water. Indeed, GLP and AMPA are frequently detected not only in surface waters, e.g. transported in runoff or by erosion processes, but also in groundwater increasing concerns about the GLP use in agriculture as in urban areas or railways and raising questions on the driving factors that lead to contamination of the surface and below-ground aquatic environment (Blake and Pallett, 2018). Furthermore, the high GLP and AMPA solubility in water (11.6 and 1466.5 g l^{-1}, respectively) (Pesticide Property DataBase by IUPAC, Lewis and Tzilivakis, 2017) increases the risk of being transported in the aqueous phase. Studies investigating GLP mobility reported that leaching may occur (Kjær et al., 2003; Stone and Wilson, 2006) under specific conditions, e.g. through macropore- or crack-mediated preferential flow pathways. The leachability of GLP could also be aggravated in soils that are phosphate-saturated or after phosphate addition to soil (De Jonge et al., 2001). Moreover, some studies emphasized that GLP could be released by root exudation when target plants start to decompose, bypassing the rootzone (Laitinen et al., 2007; Neumann et al., 2006; Viti et al., 2019). The persistence of GLP in the soil environment is mainly influenced by the microbiota (Sprankle et al., 1975), as well as by different soil conditions – such as water content, temperature and particle size distribution (Bento et al., 2016). It follows that site-specific conditions can strongly affect GLP persistence, the dissipation half-life in soils (DT_{50}) being in the order of 1.5-50 days (Okada et al., 2019; Bento et al., 2016), up to 8 months (Laitinen et al., 2006). The persistence, in addition to mobility and leaching, is particularly important for areas where GLP is broadly used, as recently reported by Gairhe et al. (2021). Its use in vineyards is one of the major concerns in the Prosecco wine production area in northeastern Italy, which has been included (since July 2019) in the UNESCO's World Heritage List. Here, GLP has been used for decades and its application is still debated, mainly by the local population and authorities due to sporadic GLP findings in groundwaters (De Polo et al., 2019). Therefore, in 2019 the Prosecco Conegliano Valdobbiadene DOCG consortium decided to ban the use of GLP by encouraging alternative vineyard management, such as the use of mechanical mowing (Consorzio di Tutela DOCG Conegliano Valdobbiadene, 2019). However, scarce information is available on GLP and AMPA behavior in these soils. It is therefore imperative to understand how these molecules move, bind, and degrade in the Prosecco area to improve its utilization for weed control.

The aims of this study were therefore: (i) to understand the site-specific GLP adsorption, dissipation and propensity to leaching in two different agricultural soils; (ii) to identify the driving factors leading to specific soil-water-contaminant interactions in the winegrowing *terroir* of the Prosecco wine production.

2.2 Materials and Methods

2.2.1 Experimental sites description and field set-up

The study was conducted in two experimental sites located in Conegliano and Valdobbiadene municipalities (NE Italy, **Figure 2.1**), 35 km apart, which are included in a vast foothill and hilly agricultural area of extensive vineyard cultivations. The study area is part of the winegrowing *terroir* of the DOCG Prosecco wine, which includes 15 municipalities (about 18,000 hectares). The experimental sites, already included in a wider network of monitored sites within a project on drinking groundwater quality monitoring and protection (Perri et al., 2012; Zovi et al., 2017), were selected due to their location near catchment wells used for drinking water purposes. It should be noted that no GLP-based herbicides were used in the two experimental sites at least three years prior to our study.

The Conegliano site (45° 53.999'N, 12° 17.732'E) (**Figure 2.1**, 66 m a.s.l.) falls within a flat grassed vineyard, 1.8 ha in size, close to the Monticano river. The climate is sub-humid, with a mean annual temperature of 14.2 °C, ranging between a mean minimum of 1.2 °C and mean maximum of 29.5 °C in January and July respectively, and annual rainfall of 1200 mm distributed uniformly throughout the year (1994-2019 data time series; ARPAV, 2020). According to the regional soil map (scale 1:50,000), the soil of the area is homogeneous (**Figure 2.1**), and geomorphologically originated from recent gravelly and calcareous high plains and terraces (ARPAV, 2008). The soil is classified as a Fluvic Cambisol (WRB, 2014; ARPAV, 2019) with a silty loam texture, pH of 8.4, 1.01% of organic carbon, cation exchange capacity (CEC) of 15.7 meq 100 g^{-1} as average values through the soil profile (**Table 2.1**). The Conegliano site has two aquifer levels: the shallow one, consisting mainly of gravel in a silty or sandy matrix, fluctuates during the year between 1.5 and 6.3 m in depth depending on the season, while the deep one develops below 10 m depth.

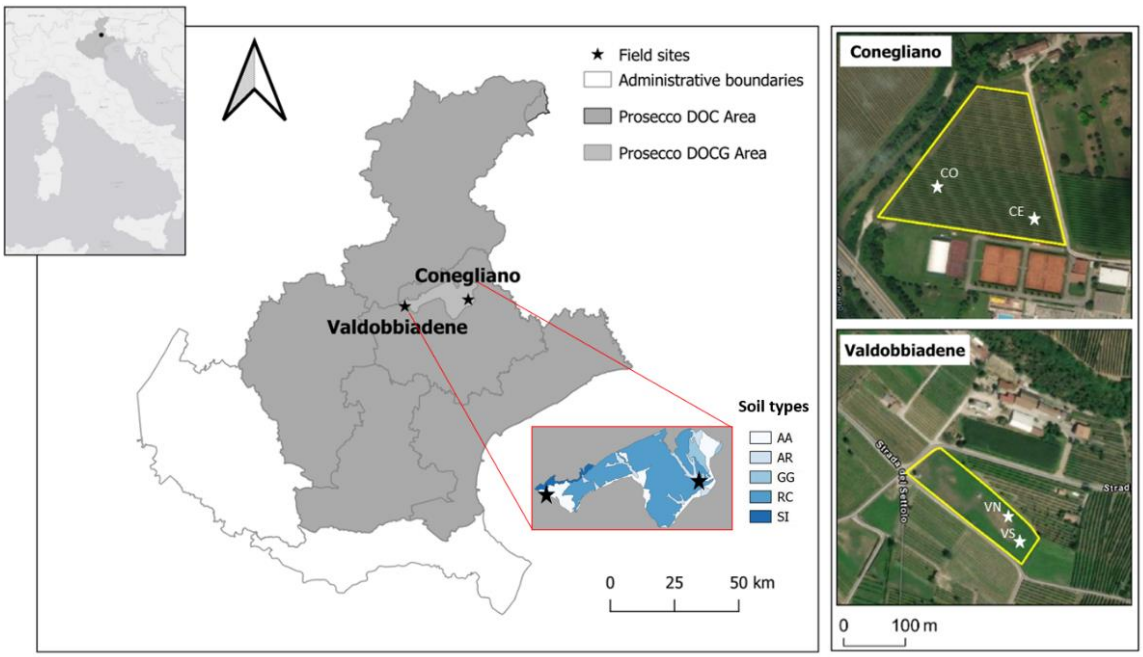

Figure 2.1. Location of the experimental area in the Veneto region and of the two monitored sites (black stars) within the Prosecco DOCG area, Conegliano and Valdobbiadene (satellite images on the right). Soil types within the DOCG area - and the corresponding geomorphological origin - are also reported (AA: ancient, gravelly, calcareous high plain; AR: recent high plains and terraces, gravelly and calcareous; GG: Pleistocene moraine amphitheaters consisting of long, arcuate hills; RC: Pre-Alpine hilly reliefs placed at the foot of massifs; SI: long and articulated pre-Alpine mountain ridges, consisting of hard and marly limestone) (ARPAV, 2008). The white stars indicate the two monitoring stations identified in each site with the corresponding names.

The Valdobbiadene site (45° 53.148'N 11° 58.658'E) (**Figure 2.1**, 176 m a.s.l.) is a 0.7 ha flat meadow surrounded by vineyards, about 1 km north of the Piave river. The site has a similar climate to the Conegliano one, with a mean annual temperature of 13.2 °C, registering the mean minimum temperature of 0.5 °C in January and mean maximum of 28.7 °C in July, and annual rainfall of 1470 mm with November being the wettest month – 195 mm (1994-2019 data time series; ARPAV, 2020). The soil of the Valdobbiadene area is homogeneous (**Figure 2.1**), gravelly and calcareous. The soil of this area is originated by ancient high plain soils consisting of locally terraced fluvioglacial deposits and secondarily alluvial plains of pre-Alpine streams (ARPAV, 2008). It is a thin Haplic Regosol (WRB, 2014; ARPAV, 2019), sandy loam, which quickly turns into a gravel layer roughly below 50 cm depth, delimiting the top boundary of the ancient Piave riverbed. The soil has a pH of 8.4, 0.86% of organic carbon, CEC of 10.6 meq 100 g^{-1} as average values through the soil profile (**Table 2.1**). The groundwater level fluctuates yearly between 4 and 8 m depth and is strongly affected by the Piave river water levels.

Table 2.1. Soil chemical properties at the four monitoring stations as a function of depth. SOC is soil organic carbon (g kg^{-1}); Total N is total nitrogen (g kg^{-1}); P Olsen is available phosphorus (mg kg^{-1}); EC is electrical conductivity (mS cm^{-1}); CEC is cation exchange capacity (meq 100 g^{-1}).

Monitoring	Layer	Particle size distribution %			SOC	Total N	P Olsen	pH	EC	CEC
station	cm	Sand	Silt	Clay	g kg^{-1}	g kg^{-1}	mg kg^{-1}		mS cm^{-1}	meq 100g^{-1}
CE	0-15	32.2	52.2	15.6	16.4	2.1	12.5	8.51	0.30	19.9
	15-40	33.2	49.5	17.2	9.5	1.3	11.7	8.38	0.21	15.7
	40-70	31.9	47.3	20.8	7.2	0.9	6.8	8.24	0.23	17.7
CO	0-15	37.2	47.8	15.0	12.5	1.6	10.7	8.29	0.24	15.3
	15-40	38.5	44.7	16.8	9.6	1.2	6.6	8.43	0.21	15.0
	40-70	43.5	38.0	18.5	6.3	0.5	2.6	8.71	0.16	11.1
VS	0-15	46.6	41.2	12.2	16.3	1.9	22.0	8.45	0.21	14.6
	15-40	48.3	36.7	14.9	8.0	0.8	18.6	8.49	0.15	10.4
	40-50	51.5	33.3	15.2	5.8	0.5	2.9	8.50	0.14	9.7
VN	0-15	53.7	34.1	12.2	12.4	1.4	15.9	8.34	0.22	11.7
	15-40	48.4	36.6	15.0	6.1	0.7	17.6	8.41	0.14	8.8
	40-50	46.0	37.6	16.4	6.4	0.4	6.5	8.36	0.13	9.4

Two soil-water monitoring stations of 25 m^2 size each were set up on each site during September 2018, hereafter referred to as CE and CO for Conegliano (inter-row grass vineyard), VS and VN for Valdobbiadene (grassland) (**Figure 2.1**). Each experimental site was equipped with a weather station that recorded air temperature, relative humidity, solar irradiance, wind speed and rainfall every 5 minutes (HD35EDLM.E, DeltaOhm, Padova, Italy). Multi-sensor probes – soil temperature (T, °C) and soil water content (SWC, m^3 m^{-3}) (HD3910.1, DeltaOhm, Padova, Italy) – and suction cups (SPE20 pore water sampler, METER Group AG München) were installed at 10, 30 and 70 cm depth in the four monitoring stations. The multi-sensor probes were set to collect data at hourly intervals. Prior to field installation, the soil moisture sensors, operating with frequency domain reflectometry technology, were calibrated in the laboratory to an accuracy of ±3%. The pore water samplers had a porous polyethylene-nylon cup whose interaction with GLP (i.e. adsorption), tested in the laboratory before field installation (**Figure 2.2**), was not significant. Due to the presence of the gravel bed below 50 cm depth in Valdobbiadene and the consequent poor functioning of the suction cups, two pan lysimeters were installed at 70 cm depth to collect the leachate.

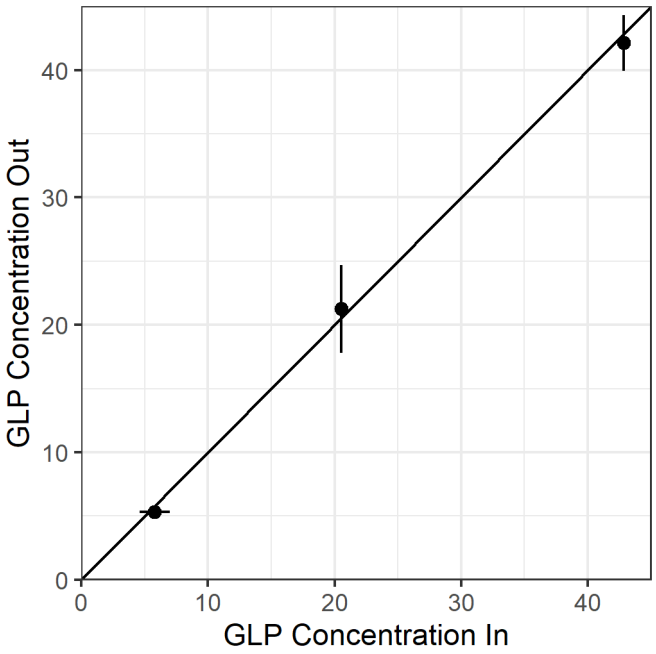

Figure 2.2. GLP concentration in µg L^{-1} in and out of the pore water samplers with the identity line 1:1 as reference.

2.2.2 Characterization of soil profiles

A hydraulic sampler was used to collect undisturbed soil cores in two random positions in each monitoring station down to 70 cm at Conegliano and 50 cm at Valdobbiadene before the experiment. A tractor-mounted double-cylinder core sampler (5 cm diameter) was used for sampling, to reduce soil compaction by slowly drilling soil layers with parallel cutting edges (Dal Ferro et al., 2020). Each soil core was measured to confirm it matched the full length of the hole (Grossman and Reinsch, 2002). After that, soil columns in each monitoring station were separated into distinct layers (0-15, 15-40 cm and 40-70 in CE and CO; 0-15, 15-40 cm and 40-50 cm in VS, VN), bulked, and later analyzed for chemical and physical properties (**Table 2.1**). Soil texture was determined by using a particle size analyzer (Mastersizer 2000, Malvern Panalytical Ltd, Spectris Company) according to Bittelli et al. (2019); soil organic carbon (SOC) and total nitrogen (Total N) content were determined by the flash combustion method with a CNS-analyzer (vario MACRO cube, Elementar Analysensysteme GmbH); pH and electrical conductivity (EC) were measured by an electrode in soil suspensions with a soil to water ratio of 1:2.5 (w/v); the cation exchange capacity (CEC) was measured using the $BaCl_2$-

triethanolamine method; the assimilable phosphate (P Olsen) was determined using the Olsen method.

2.2.3 Determination of Al and Fe oxides in soil

Mineralogical iron (Fe) and aluminum (Al) oxides were measured along the soil profiles at 0-15, 15-40 and 40-70 cm for Conegliano, and 0-15, 15-40 and 40-50 cm for Valdobbiadene. Two methods were applied to determine (i) poorly ordered Al and Fe oxides (oxalate-extractable, hereafter labeled as Fe_{Ox} and Al_{Ox}) and (ii) soil organic matter-chelated Al and Fe (sodium pyrophosphate-extractable, hereafter labeled as Fe_{Som} and Al_{Som}).

Poorly ordered Al and Fe oxides, also called "amorphous", were determined using the ammonium oxalate in darkness extraction method as reported by McKeague et al. (1971). The soils were air-dried and sieved at 0.1 mm. Due to high calcium carbonates content, soil samples were pretreated with a solution of ammonium acetate (pH = 5.5) prior to the extraction. For the extraction procedure, 0.5 g of pretreated air-dried soil was weighed in a polypropylene tube and spiked with a 30 mL of ammonium oxalate-oxalic acid solution at pH = 3. The samples were shaken for 3 h in darkness and centrifuged. The solution was then separated from the soil and collected in a polyethylene tube. Soil organic matter-chelated metals were extracted using a solution of sodium pyrophosphate at pH = 10. In this case, the alkaline environment is preferred since the extraction of crystalline and amorphous forms is slight (Bascomb, 1968). A volume of 40 mL solution was added to 0.4 g of air-dried, 0.1 mm sieved soil and the samples were shaken for 16 h at 20 °C. The samples were then centrifuged and filtered using mixed cellulose esters (MCE) membrane filters with pore diameter of 0.45 µm. All the solutions were analyzed by ICP-OES for Al and Fe content, expressed as mg kg^{-1}.

2.2.4 Adsorption isotherms of glyphosate

A batch adsorption experiment was performed following the OECD Guideline using the Batch Equilibrium Method (OECD, 2000). Chemical standard of glyphosate acid (98.6% purity) was purchased from Dr. Ehrenstorfer (LGC Labor GmbH, Augsburg, Germany). Five different concentrations of GLP in the range of 0.1-25 µg g^{-1} of dry soil were tested, three replicates each. The adsorption study was performed for three different soil layers covering the whole

soil profile (0-15, 15-40 and 40-70 cm for CE and CO, and 0-15, 15-40 and 40-50 cm for VS and VN), with the exclusion of the gravel layer. Uncontaminated soils obtained from the initial sampling –lack of glyphosate in the soil was checked in the laboratory– were air-dried, sieved at 2 mm, and stored at room temperature before the experiment. Firstly, 39 mL of 0.01 M $CaCl_2$ were added to 1 g of dry weight soil in 50-mL polypropylene tubes and shaken at 200 rpm for 24 h at 20 °C. The soil slurry was then spiked with 1 mL of the corresponding GLP solution, with three replicates for each concentration. After shaking for 24 h, the tubes were centrifuged at 3000 rpm for 20 min and an aliquot of supernatant (~1 mL) was taken and stored in the fridge at +4 °C before UHPLC-MS analysis. The amount of GLP adsorbed on the soil was calculated as the difference between the amount initially present in solution and the amount remaining at the end of the experiment.

Adsorption data were fitted to the Freundlich adsorption isotherm model by nonlinear optimization:

$$C_s = K_f C_w^{(\frac{1}{n})} \quad [1]$$

where, C_s (µg g^{-1}) is the amount of GLP adsorbed into the soil, C_w (µg ml^{-1}) is the concentration of GLP in the aqueous phase, K_f [$\mu g^{1-1/n}$ $(ml)^{1/n}$ g^{-1}] is the Freundlich adsorption coefficient and 1/*n* is the regression constant or measure of nonlinearity. To compute the unknown empirical coefficient, the least square method was applied. Moreover, to compare the K_f among sites and depths, the depth-averaged 1/n coefficient was calculated and used as a fixed value to fit experimental data using the Freundlich equation as already proposed in other studies (Kodešová et al., 2011; Sidoli et al., 2016). The closer 1/n is to 1, the more linear is the adsorption curve.

2.2.5 Glyphosate application in the field

Glyphosate was distributed on the four 25 m^2 vegetated monitoring stations during autumn 2018, on November 14 in VS and VN, and on November 21 in CO and CE. A solution of Chikara Duo (BELCHIM Crop Protection, Milan, Italy), containing 28.8% of glyphosate acid and 0.67% of flazasulfuron, was sprayed on grassy soil at pressure 2.5 atm using a multiple nozzles system at an average rate of 1.88 kg a.i. ha^{-1} (water volume = 380 L ha^{-1}), which represents the ordinary dose applied in Europe (EFSA, 2017).

2.2.6 Soil water samples collection and quantification of glyphosate and AMPA in water

Soil water samples were collected with suction cups and pan lysimeters the day after GLP distribution and at every rainfall event for six months (November 2018 – May 2019). Pore-water samples, extracted by applying a negative pressure (-0.55 bar) overnight with a portable vacuum pump (Vacuporter, Vacuum Case, UMS GmbH München), were collected on 1000 mL high-density polyethylene bottles (Nalgene™, Thermo Scientific, Waltham, Massachusetts, USA), transported to the laboratory where they were stored for a maximum of one week in a refrigerator (+4 °C) (Noori et al., 2018; Carles et al., 2019), and then analyzed by UHPLC-MS for GLP and AMPA concentrations using the procedure reported by Carretta et al. (2019) (limit of detection – LOD – and limits of quantification – LOQ –, were 0.2 and 0.5 µg l^{-1}, respectively for glyphosate and 0.05 and 0.1 µg l^{-1} respectively for AMPA). Before GLP field treatment, the soil water in all monitoring stations was sampled at each depth to measure any possible GLP and AMPA background concentration. All water samples resulted under the LOD for both analytes.

2.2.7 Soil samples collection and quantification of glyphosate and AMPA in soil

Soil samples were collected within 12 hours from GLP application, then after one month and afterwards at increasing time intervals, until September 2019 for a total of ten months. Average sampling frequency was one per month. Sampling was performed on two randomly selected points within each treated plot at four different depths: in both sites at 0-5, 5-20, 20-40 cm, plus 40-70 cm in CE and CO, and 40-50 cm in VS and VN. The two subsamples were then bulked at each depth to obtain a sample of about 0.4 kg. Once collected in plastic bags and placed in a refrigerated box, the soils were carried within an hour to the laboratory where they were air-dried (20 °C) and sieved within one day. The samples were then stored in the dark before analysis (Carretta et al., 2021a). This approach limited the loss of GLP concentration due to degradation processes that might occur in wet soils. After that, 2 g of 2 mm sieved soils were taken to analyze GLP and AMPA concentrations (three pseudoreplicates each). The extraction procedure was performed adding 10 ml of KOH 0.6 M to each sample,

shaken for one hour (280 rpm) and then centrifuged (6000 rpm for 10 min, 6 °C). An aliquot of supernatant (4 ml) was then filtered using a cellulose filter (pore diameter 0.2 µm) and purified using Oasis® HLB Plus light cartridge (pore diameter 30 µm) (Waters Corporation - Milford, MA, USA) to extract aminic components that could interfere with the analytes during the analysis. In addition, the pH was regulated to 9 by adding 85 µl of HCl 6M to1 ml of the sample. The derivatization process was performed on 200 µl as reported by Carretta et al., (2019) using the derivatization kit AccQ•Tag™ (Waters Corporation - Milford, MA, USA). The sample was then analyzed by UHPLC-MS. Recoveries were 94 and 88% for GLP and AMPA respectively. The LOD and LOQ for GLP were 15 and 50 µg kg^{-1} respectively, and 6 and 20 µg kg^{-1} for AMPA. As for water samples, soils were also analyzed before GLP application resulting in GLP and AMPA background concentrations < LOD.

2.2.8 Glyphosate dissipation and AMPA formation dynamics

Residual soil glyphosate concentrations over time were used to fit a single first order (SFO) exponential decay equation through a least square fitting procedure as follows:

$$C_t = C_0\, e^{(-kt)} \quad [2]$$

where C_t (µg kg^{-1}) is the residual concentration of GLP at time t (day), C_0 (µg kg^{-1}) is the initial concentration of GLP in the first sampling, k is the first-order rate coefficient (day^{-1}).

The formation-dissipation AMPA dynamics was described using the following modified equation based on that proposed by Otto et al. (1997):

$$A_{\mathrm{t}} = \{[C_M - (C_0 \cdot\ e^{-kt})] \cdot 0.66\} \cdot (e^{-\alpha t}) \quad [3]$$

where A_{t} is the concentration of AMPA at time t, C_M is the concentration of the parent molecule that is transformable into the metabolite (µg kg^{-1}) at the time of distribution (t_0), C_0 is the observed (Carretta et al., 2021a) initial concentration of the parent molecule (µg kg^{-1}) at the first sampling time, k is the first-order rate coefficient for the degradation of GLP (d^{-1}) and α is the coefficient that regulates AMPA dissipation (d^{-1}). The stoichiometric factor 0.66, which is the ratio of the molecular weights of GLP and AMPA, was used to convert the mass of parent into metabolite. The time of maximum occurrence of AMPA in soil (t_{max}, days) was calculated using the equation (4) reported by Otto et al. (1997):

$t_{max} = -\frac{1}{k} \cdot [\ln\left(\frac{1}{k+\alpha}\right) - \ln\left(\frac{1}{k}\right)]$. [4]

To estimate the dissipation time (DT_{50}), soils from the two monitoring stations within each site (Conegliano and Valdobbiadene) were used as replicates.

2.2.9 Relationship between soil properties and sorption parameters and data analysis

To study the possible relationship between GLP sorption coefficient and soil properties, a correlation matrix was performed to obtain Pearson correlation coefficients between parameters (N=13). Moreover, a backward stepwise multiple linear regression analysis ($Y = b + b_1X_1 + b_2X_2 + ... + b_kX_k$) was performed to identify the soil physical and chemical properties (clay, SOC, CEC, Fe_{Ox}+Al_{Ox} and Fe_{Som}+Al_{Som}) which most affected GLP adsorption. Statistical analyses were performed using R software (R Core Team, 2020).

2.2.10 Groundwater Leachability Index: the Attenuation Factor

The Attenuation Factor (AF), as proposed by Rao et al. (1985), is an index used to estimate the fraction of a molecule that could reach the groundwater table. The AF was calculated as follows:

$$AF = \exp\left(\frac{-\ln(2) \cdot D \cdot RF \cdot \vartheta fc}{q \cdot DT50}\right) \quad [5]$$

where D is the minimum groundwater depth (m) set as the maximum monitored soil depth (70 cm), RF is the retardation factor, ϑfc is the volumetric water content at field capacity (%), q is the groundwater net recharge rate (m $year^{-1}$) and DT_{50} is the dissipation time (year), calculated as follows:

$$DT_{50} = \frac{\ln(2)}{k} \quad [6]$$

where k is the rate dissipation constant calculated applying Eq. 2.

The simplified RF, which does not account for GLP volatilization (due to its low vapor pressure), is defined by Eq. 7:

$$RF = 1 + \frac{BD \cdot SOC \cdot K_{OC}}{\vartheta fc} \quad [7]$$

where BD (soil bulk density) is expressed as kg m^{-3}, K_{oc} as m^3 kg^{-1} – which is calculated as the ratio between K_f and SOC – and the SOC as percentage value.

The net recharge rate (q) during the 12-month period November 2018-October 2019 was calculated as:

$$q = P - ET \quad [8]$$

where P is the rainfall (m $year^{-1}$) and ET is the reference evapotranspiration (m $year^{-1}$) calculated using the Penman-Monteith equation. The runoff was not quantified and set to zero. During the experiment, irrigation was not performed. AF ranges between 0 and 1, where AF between 0 and 10^{-2} classifies areas at low risk of groundwater leaching (e.g. strongly adsorbed chemicals); AF between 10^{-2} and 10^{-1} classifies areas at moderate risk, and AF between 10^{-1} and 1 classifies areas at high risk (e.g. non-adsorbed chemicals) (de Paz and Rubio, 2006; Ibrahim and Ali, 2020).

2.3 Results

2.3.1 Weather conditions and soil monitoring

From November 2018 until September 2019, Conegliano and Valdobiadene showed a cumulative rainfall of 1008 and 1331 mm respectively, with the lowest monthy rainfall observed in December 2018 and the highest in April 2019, in both sites (**Table 2.2**).

Table 2.2. Monthly weather data of the two sites during the experiment. T_{Mean} is mean air temperature (°C); T_{Max} is maximum air temperature (°C); T_{Min} is minimum air temperature (°C); Rainfall is the monthly cumulated precipitation (mm).

		Conegliano				Valdobbiadene			
Year	**Month**	**T_{Mean} °C**	**T_{Max} °C**	**T_{Min} °C**	**Rainfall mm**	**T_{Mean} °C**	**T_{Max} °C**	**T_{Min} °C**	**Rainfall mm**
2018	November	9.4	23.3	-4	126.8	9.6	20.9	-2.4	146.2
	December	2.3	15.2	-7.2	10.6	3.6	14.1	-4.2	8.6
2019	January	0.6	12.6	-8.5	12.0	1.7	15.8	-6.2	14.2
	February	4.8	23.3	-6.5	102.8	6.6	22.2	-4.9	139.8
	March	8.5	24.2	-3	20.2	9.6	23.9	-1	26.8
	April	12.6	25.1	2.9	254	12.7	24.6	3.9	371.4
	May	14.5	26.4	5.4	226.4	14	26.2	4.4	271.2
	June	23.9	37.7	10	13.4	24.1	37.5	14	34.6
	July	23.6	36.1	11.9	98.2	24	36.6	13.6	130.4
	August	23.7	33.2	13.7	89	24	33.1	15.6	105.8
	September	18.3	33.8	5.4	54.6	18.6	33.2	8.9	82.4
Whole period		12.9	26.4	1.8	1008	13.5	26.2	3.8	1331.4

The soil water content dynamics is shown in **Figure 2.3B**. CE and CO were both particularly reactive to additional precipitation inputs, registering frequent peaks at each occurrence, most pronounced at shallower depths. VN and VS showed higher peaks following intense rainfall events, that sharply decreased the following day. Values of soil moisture were generally lower in VS compared to VN. As observed for the temperature dynamics, smoother responses were observed at 70 cm depth in all monitoring stations regardless of site.

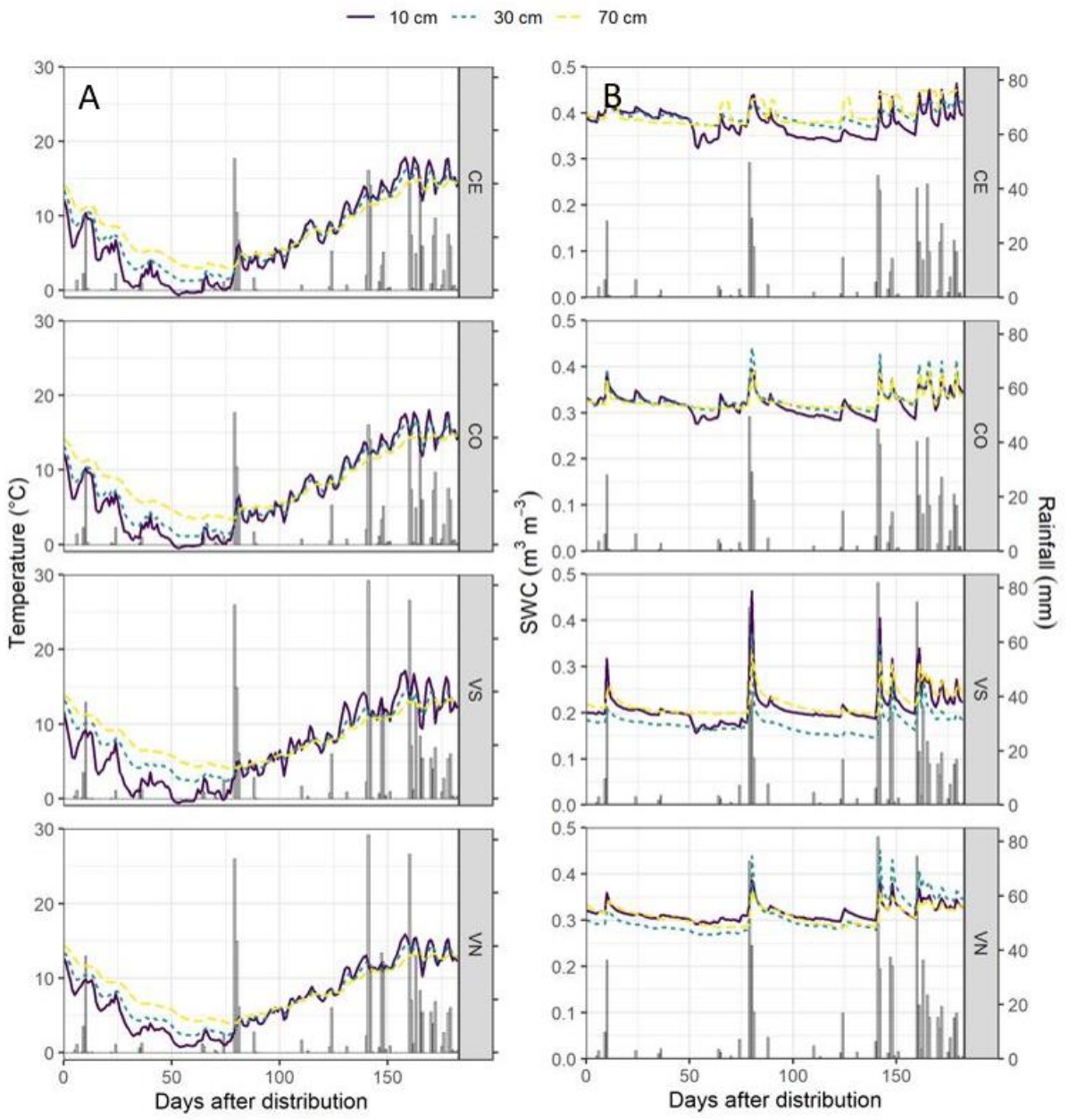

Figure 2.3. Soil temperature (°C) (A) and soil water content (SWC, $m^3\ m^{-3}$) (B) dynamics for the four monitoring stations at the three monitoring depths (10 cm – solid purple line; 30 cm – dotted green line; 70 cm – dotted yellow line) with rainfall events (mm).

2.3.2 Glyphosate and AMPA concentrations in water

A total of 146 water samples were collected during the 6-month field experiment at the different depths in the four monitoring stations. In both experimental sites, discontinuous GLP and AMPA findings were observed in soil water as highlighted by the high variability between monitoring stations and depths in **Figure 2.4**. GLP in Conegliano was hardly detectable compared to Valdobbiadene: in Conegliano GLP and AMPA concentrations were > LOQ only 7 and 3 out of 32 and 36 water samples (21.9% and 8.3%, in CE and CO respectively), compared to 14 and 12 times out of 38 and 37 in Valdobbiadene (36.8% and 32.4%, in VS and VN respectively).

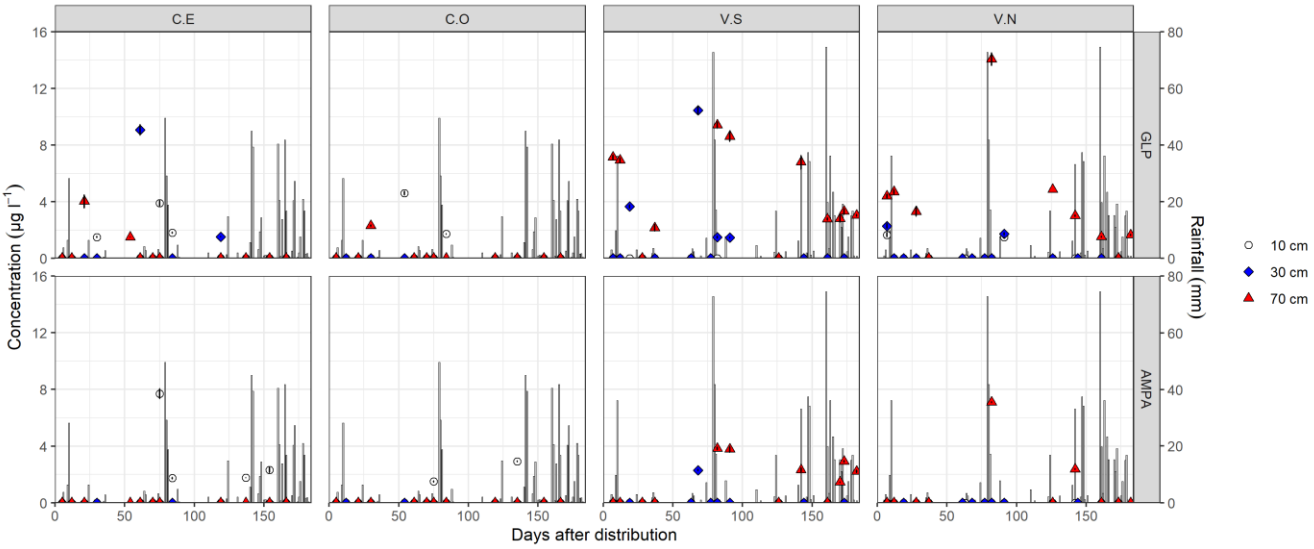

Figure 2.4. Glyphosate and AMPA detection in soil pore-water samples in different monitoring stations and depths. Bars identify daily rainfall events. Data < LOQ were reported in the graphs equal to zero.

In CE station (**Figure 2.4**), GLP was detected first at 70 cm depth (4.26 µg l^{-1}), 21 days after application, remaining below LOQ at 10 and 30 cm during the same period. At 30 days, GLP was detected only in the top layer (1.5 µg l^{-1}), followed by a maximum peak of 9.2 µg l^{-1} 61 days at 30 cm depth. Afterwards, GLP decreased to 1.5 µg l^{-1} (119 days after contamination) at 30 cm depth and was no longer detected along the soil profile. Similarly to CE, GLP in CO was detected first at 70 cm depth after some rain events (2.3 µg l^{-1}, 30 days after the distribution), then it was detected only in the surface layer until 54 (4.6 µg l^{-1}) and 84 (1.7 µg l^{-1}) days after herbicides spraying (**Figure 2.4**), and never at 30 cm. It should be noted that in both CE and CO, AMPA was found only at 15 cm from day 75.

Different GLP and AMPA dynamics were observed in Valdobbiadene, being mostly found at 70 cm depth since the beginning of the monitoring activities (**Figure 2.4**). In both VS and VN GLP was found following the first rain events. In VN, GLP was found at 10 cm (1.8 µg l^{-1}), 30 cm (2.1 µg l^{-1}) and 70 cm depth (4.4 µg l^{-1}) 7 days after spraying, which increased up to 4.8 µg l^{-1} at day 12. On the same days, GLP was 7.2 and 7.0 µg l^{-1} at 70 cm depth in VS, and never detected at 10 cm. After a 3-day heavy rainfall event (February 1 – 3, 131.8 mm in total), GLP was found in VS and VN at 70 cm (**Figure 2.4**) at very high concentrations (9.4 and 14.1 µg l^{-1}, respectively) followed by a gradual reduction until 2.7 and 1.5 µg l^{-1} at day 161. In VS, GLP in the intermediate layer increased up to 10.3 µg l^{-1} 68 days after the distribution, followed by a reduction down to 1.5 µg l^{-1} (day 91) and its subsequent disappearance (< LOQ). Notably AMPA was often found in VS since day 68 (30 cm) compared to VN where it was hardly detected, but always in conjunction with GLP. Values used for the calculation of AF are reported in **Table 2.3**. The risk of herbicide mobility to the groundwater was estimated according to the AF index: values were always zero regardless of the experimental sites, suggesting a low susceptibility to water contamination.

Table 2.3. Values and parameters used to calculate the AF. BD is bulk density, SOC is soil organic carbon, K_{oc} is the repartition coefficient between water and organic carbon, Θ_{fc} is the water content at field capacity, P is annual precipitation and ET is annual evapotranspiration calculated from data recorded by the weather station from October 2018 to September 2019.

Monitoring station	BD (kg m^{-3})	SOC (%)	K_{oc} (m^3 kg^{-1})	Θ_{fc} (%)	P (m $year^{-1}$)	ET (m $year^{-1}$)
CE	1410	1.00	12.69	30	1.036	1.042
CO	1450	0.88	9.63	26	1.036	1.042
VS	1390	1.01	4.13	24	1.401	0.953
VN	1410	0.81	4.34	24	1.401	0.953

2.3.3 Concentration of glyphosate and AMPA formation in soil

Glyphosate and AMPA in soil were always detected in the surface layer (0-5 cm), while from 5 to 70 cm, they were found occasionally and randomly (**Table 2.4**). It follows that Eq. 2 and 3 were only applied for the topsoil layer in both sites. Maximum GLP values were found one day after the application, with topsoil concentration that ranged between 1018.9 µg kg^{-1} in VN and

1279.6 µg kg^{-1} in CO. After that, GLP concentrations sharply reduced until complete dissipation in all plots between day 133 and 182, while in VN it was still detected at 182 days.

Table 2.4. GLP and AMPA (µg kg^{-1}) detection in soil layers at different times and depths after the distribution.

Days after distribution	Layer	CE		CO		VS		VN	
	cm	GLP	AMPA	GLP	AMPA	GLP	AMPA	GLP	AMPA
1	0-5	940.3	329.4	1279.6	636.0	903.2	187.5	1018.9	324.8
	5-20	80.43	<LOQ	308.8	72.0	<LOQ	<LOQ	<LOQ	<LOQ
	20-40	-[b]	-	-	-	-	-	-	-
	40-70[a]	-	-	-	-	-	-	-	-
28	0-5	415.7	425.2	631.0	661.1	435.3	212.5	549.6	377.6
	5-20	<LOQ	<LOQ	<LOQ	<LOQ	<LOQ	<LOQ	<LOQ	<LOQ
	20-40	<LOQ	<LOQ	<LOQ	<LOQ	<LOQ	<LOQ	<LOQ	<LOQ
	40-70[a]	-	-	-	-	-	-	-	-
61	0-5	156.8	199.7	292.6	442.7	189.6	153.8	167.3	150.1
	5-20	<LOQ	<LOQ	<LOQ	<LOQ	<LOQ	<LOQ	<LOQ	<LOQ
	20-40	<LOQ	<LOQ	<LOQ	<LOQ	<LOQ	<LOQ	<LOQ	<LOQ
	40-70[a]	-	-	-	-	-	-	-	-
91	0-5	123.5	200.5	113.7	281.9	229.8	271.0	244.6	322.7
	5-20	45.6	<LOQ	<LOQ	<LOQ	<LOQ	<LOQ	<LOQ	<LOQ
	20-40	<LOQ	<LOQ	<LOQ	<LOQ	<LOQ	<LOQ	<LOQ	<LOQ
	40-70[a]	53.8	<LOQ	<LOQ	<LOQ	<LOQ	<LOQ	80.7	64.6
133	0-5	56.9	144.7	58.5	218.2	110.2	311.6	129.2	420.4
	5-20	<LOQ	<LOQ	<LOQ	<LOQ	<LOQ	<LOQ	<LOQ	<LOQ
	20-40	<LOQ	<LOQ	<LOQ	<LOQ	<LOQ	<LOQ	<LOQ	<LOQ
	40-70[a]	<LOQ	<LOQ	<LOQ	<LOQ	63.1	<LOQ	<LOQ	<LOQ
182	0-5	<LOQ	68.3	<LOQ	128.2	<LOQ	132.6	87.6	349.3
	5-20	<LOQ	<LOQ	<LOQ	<LOQ	<LOQ	<LOQ	<LOQ	<LOQ
	20-40	<LOQ	<LOQ	<LOQ	<LOQ	<LOQ	<LOQ	<LOQ	<LOQ
	40-70[a]	<LOQ	<LOQ	<LOQ	<LOQ	<LOQ	<LOQ	<LOQ	<LOQ
302	0-5	<LOQ	<LOQ	<LOQ	<LOQ	<LOQ	<LOQ	<LOQ	<LOQ
	5-20	<LOQ	<LOQ	<LOQ	<LOQ	<LOQ	<LOQ	<LOQ	<LOQ
	20-40	<LOQ	<LOQ	<LOQ	<LOQ	<LOQ	<LOQ	<LOQ	<LOQ
	40-70[a]	<LOQ	<LOQ	<LOQ	<LOQ	<LOQ	<LOQ	<LOQ	<LOQ

[a] For VS and VN is 40-50 cm.

[b] No data were available where "–" is reported.

GLP residue in topsoil was well fitted by first order exponential decay (Eq. 2), with $R^2 > 0.94$. In particular, the rate constants *k* varied between 0.016 and 0.025 d^{-1} in Valdobbiadene and Conegliano, respectively (**Table 2.5**). The lower *k* estimated in Valdobbiadene highlighted slower dissipation dynamics than in Conegliano (**Figure 2.5** left, and **Table 2.5**), which had a constant rate 36% higher than the other one. The formation-dissipation AMPA kinetics (**Figure 2.5** right) were slightly different between Conegliano and Valdobbiadene.

Table 2.5. Rate constants (*k* and *α*), coefficient of determination (R^2) and root mean square error (RMSE) as indicators of the goodness of fit of glyphosate and AMPA with dissipation times (DT_{50} in days) in the topsoil layer (0-5 cm) of the four monitoring stations. C_M (μg kg^{-1}) is the concentration of the parent molecule that is transformed to AMPA at the initial time and t_{max} (days) is the time at maximum AMPA occurrence.

Monitoring station	GLP				AMPA					
	Fitting model parameter	Goodness of fit			Fitting model parameter		Goodness of fit			
	k (d^{-1})	R^2	RMSE	DT_{50} (d)	C_M (μg kg^{-1})	α (d^{-1})	R^2	RMSE	DT_{50} (d)	t_{max} (d)
Conegliano	0.025	0.99	22.7	28.2	1826.2	0.017	0.85	130.2	42.0	20.3
Valdobbiadene	0.016	0.94	85.7	43.3	1273.6	0.008	0.80	93.6	92.0	24.1

In the first case, the formation of AMPA was faster than its dissipation until day 30 in both CE and CO, when a peak in soil concentration reached 425.2 and 661.1 μg kg^{-1} respectively. After day 30, the formation was slower and AMPA in soils declined. In Valdobbiadene, maximum soil AMPA concentrations (**Table 2.4**) were observed at day 133 for both VS (311.6 μg kg^{-1}) and VN (420.4 μg kg^{-1}). The fitting model described the observed AMPA dynamics in Conegliano better (R^2 = 0.85) than in Valdobbiadene (R^2 = 0.80): the alpha (*α*) value and maximum occurrence time (t_{max}) in Conegliano were 0.017 and 21.2 d respectively (**Table 2.5**), while a slower (*α* = 0.008 d^{-1}) and delayed (t_{max} = 28.8 ±0.2 d, on average) AMPA dissipation was found in Valdobbiadene. Related to the deeper soil layers, GLP was found only six out of 68 times, e.g. at 5-20 cm in CE and CO the day after the distribution (**Table 2.4**). After 91 days it was found at 40-70 cm in CE and at 40-50 cm in VN. At the same depth in the latter, AMPA was also detected (64.6 μg kg^{-1}). At day 133, GLP was found at 40-50 cm only in VS, while more than 300 days after the herbicide distribution, GLP and AMPA were not detected. Related to the deeper soil layers, GLP was found only six out of 68 times, e.g. at 5-20 cm in CE and CO the day after the distribution (**Table 2.4**). After 91 days it was found at 40-70 cm in CE and at 40-50 cm in VN. At the same depth in the latter, AMPA was also detected (64.6 μg kg^{-1}). At day 133, GLP was found at 40-50 cm only in VS, while more than 300 days after the herbicide distribution, GLP and AMPA were not detected.

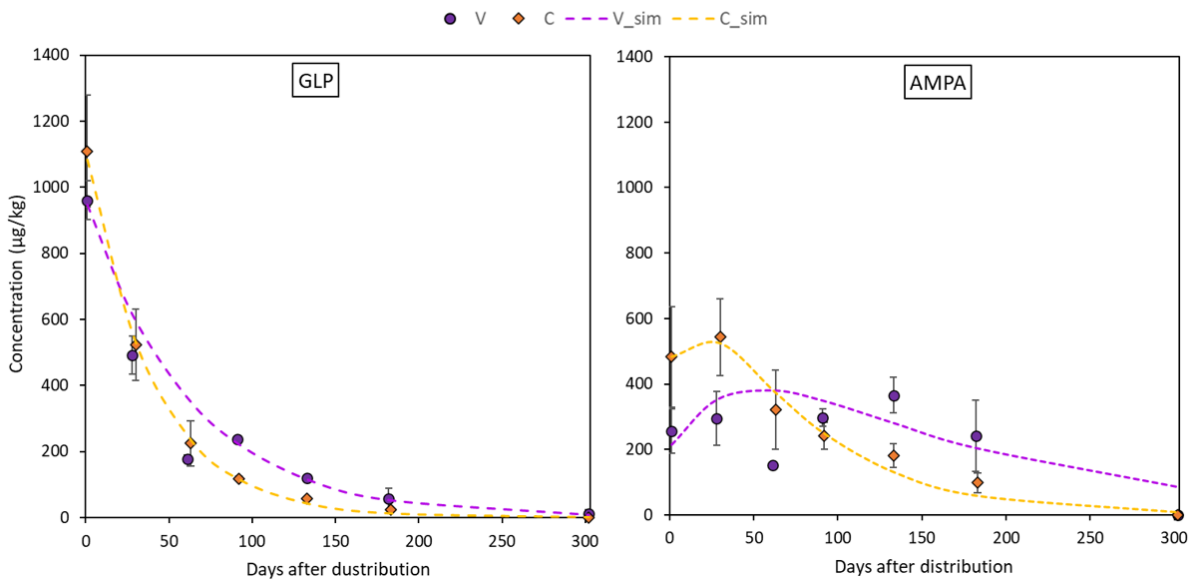

Figure 2.5. Dissipation dynamics of GLP in the topsoil layer (0-5 cm) for the two sites fitted with the SFO equation (on the left) and formation/dissipation dynamics of AMPA in the topsoil layer for the two sites fitted with Equation 5 (on the right). Dots are experimental concentrations (yellow rhombus for Conegliano – C –; purple circles for Valdobbiadene – V –) and dotted lines refer to fitted dynamics.

2.3.4 Adsorption of glyphosate

Regarding the analysis of GLP adsorption, a good accuracy of the Freundlich equation (**Table 2.6**) was found at all depths and in the different experimental sites (R^2 always ≥ 0.95). The estimated 1/n were always < 1 indicating that non-linear adsorption occurred. The averaged 1/n was fixed at 0.76 ±0.03 to calculate the averaged adsorption coefficient ($K_{f\text{-}mean}$). In general, $K_{f\text{-}mean}$ varied between sites and depths showing a weaker GLP adsorption in Valdobbiadene than in Conegliano soils, the average being $K_{f\text{-}mean}$= 35.6 ±3.4 and 140.7 ±25.2, respectively. According to soil depth, the lowest $K_{f\text{-}mean}$ was always observed in the topsoil layer (on average, 25.4 ± 3.2 and 112.9 ± 34.2 in Valdobbiadene and Conegliano), which gradually increased with depth until average values of 42.8 ±1.8 and 174.7 ± 68.0 below 40 cm. Within Conegliano, the adsorption was broadly variable between monitoring stations, with $K_{f\text{-}mean}$ that ranged between 147.0 and 242.7 in CE, and between 78.7 and 106.7 in CO. Lower variability was observed in Valdobbiadene, $K_{f\text{-}mean}$ being in the 28.7-44.6 range in VS and 22.2-41.0 in VN.

Table 2.6. Freundlich equation parameters for GLP (K_f, n and $K_{f\text{-}mean}$) and coefficients of determination (R^2) for different monitoring stations and soil layers. K_f and $K_{f\text{-}mean}$ are reported in $\mu g^{1-1/n} (ml)^{1/n} g^{-1}$.

Monitoring Station	Layer (cm)	K_f	1/n	R^2	$K_{f\text{-}mean}$[a]	R^2 [b]
CE	0-15	176.4	0.82	0.995	147.0	0.998
	15-40	193.6	0.78	0.960	176.2	0.964
	40-70	229.4	0.73	0.986	242.7	0.993
CO	0-15	96.3	0.84	0.978	78.7	0.982
	15-40	63.8	0.58	0.970	92.7	0.945
	40-70	96.4	0.71	0.999	106.7	0.998
VS	0-15	29.0	0.79	0.998	28.7	0.999
	15-40	44.1	0.84	0.995	38.5	0.998
	40-50	53.5	0.86	0.988	44.6	0.995
VN	0-15	18.7	0.61	0.975	22.2	0.955
	15-40	40.4	0.78	0.989	38.7	0.991
	40-50	45.9	0.82	0.986	41.0	0.991

[a] Adjusted with fixed $1/n_{mean} = 0.76 \pm 0.03$

[b] Using adjusted $K_{f\text{-}mean}$

2.3.5 Al and Fe content in soil

Poorly ordered Fe and Al oxides (Fe_{Ox} and Al_{Ox}, mg kg^{-1}) generally decreased with depth in Conegliano (**Table 2.7**). Lower values were observed in the topsoil layer than deeper ones for Al_{Ox} in both VS and VN, and for Fe_{Ox} in VS. Conegliano had Fe_{Ox} always below 2000 mg kg^{-1}, with the lowest values being found in CO along the whole soil profile (761.9 ± 201.8 mg kg^{-1}). In contrast Valdobbiadene had relatively higher Fe_{Ox} content, being 2538.3 ± 310.0 mg kg^{-1} in VS and 2648.1 ± 86.6 mg kg^{-1} in VN. Differently, Al_{Ox} was always found at lower concentrations than Fe_{Ox}, and with similar concentrations between experimental sites. The Al_{Ox} concentration was on average 279.7 ± 13.4 and 293.6 ± 15.6 mg kg^{-1} in Conegliano and Valdobbiadene, respectively, and ranged between a minimum of 217.7 mg kg^{-1} at the 40-70 cm layer in CO and a maximum of 354.6 mg kg^{-1} at the 15-40 cm layer in VS. Iron and aluminum chelated to soil organic matter (Fe_{Som} and Al_{Som}) were at similar average concentrations between the two sites, although some different composition was found with variation of depth. Both SOM-chelated metals in Conegliano site increased with depth (+26% and +65% on average in the deepest layer compared to the shallower for Fe_{Som} and Al_{Som} respectively), while in Valdobbiadene they decreased at deeper soil depths (-47% and -20% for Fe_{Som} and Al_{Som}

respectively). In Conegliano, CE had the highest amount of Fe_{Som} and Al_{Som} (on average 606.37 ± 44.32 and 648.03 ± 91.99 mg kg^{-1}, respectively). Furthermore, in Conegliano at 40-70 cm, Al_{Som} was predominant with respect to Fe_{Som} (+26% as average between the two stations). An inverse trend was found in Valdobbiadene. Here, both monitoring stations had similar Fe_{Som} content in the 0-15 cm layer (359 ± 16.80 mg kg^{-1}), decreasing down to 224.1 in VS and 148.7 mg kg^{-1} in VN at 40-70 cm depth. Furthermore, Al_{Som} had about half the concentration related to Fe_{Som}. The ratio between Fe_{Som} and Al_{Som} and SOC content is also reported in **Table 2.7**.

Table 2.7. Oxalate-extractable (Fe_{Ox} and Al_{Ox}) and SOM-chelated (Fe_{Som} and Al_{Som}) Al and Fe content (mg kg^{-1}) in the four monitoring stations and soil depths. The ratio between Fe_{Som} and Al_{Som} and SOC content (mg kg^{-1}) is also reported.

Monitoring Station	Layer (cm)	Fe_{Ox} mg kg^{-1}	Al_{Ox} mg kg^{-1}	Fe_{Som} mg kg^{-1}	Al_{Som} mg kg^{-1}	Fe_{Som}/SOC -	Al_{Som}/SOC -
CE	0-15	1669.2	306.0	561.6	533.0	0.034	0.033
	15-40	1767.1	303.8	562.5	581.2	0.059	0.061
	40-70	1349.4	295.3	695.0	829.9	0.097	0.115
CO	0-15	968.6	276.6	371.7	363.1	0.030	0.029
	15-40	958.8	278.7	410.4	489.9	0.043	0.051
	40-70	358.4	217.7	477.3	631.9	0.076	0.100
VS	0-15	2161.2	235.4	342.3	140.8	0.021	0.009
	15-40	3153.0	354.6	327.7	167.3	0.041	0.021
	40-50	2300.8	296.9	224.1	135.5	0.039	0.023
VN	0-15	2816.3	294.5	375.9	160.1	0.030	0.013
	15-40	2599.4	281.5	287.4	150.3	0.047	0.025
	40-50	2528.4	298.9	148.7	101.5	0.023	0.016

2.4 Discussion

During the 10-months monitoring experiment following herbicide distribution, GLP and AMPA were regularly detected in the topsoil 0-5 cm layer, while they were hardly found in the deeper layers or in pore water samples. However, some rapid transport of GLP to the deepest layers occurred, being firstly detected at 70 cm depth in water samples, e.g. just after 21 days in CE, and 7 days both VS and VN. GLP was first detected more superficially at 10 and 30 cm depth only after 7 (VN) and 30 days (CE). These results have suggested the likely occurrence of some GLP bypass flow in the intermediate layers as also reported by others (Vereecken, 2005; Stone

and Wilson, 2006; Borggaard and Gimsing, 2008), and in turn a limited equilibration between predominantly vertical transport movement – probably only a small fraction of the total pore space was involved – and lateral mixing with surrounding matrix (Jarvis et al., 2016) that reduced filter and buffer functions of soil. This was not the case for CO (**Figure 2.3** and **Table 2.4**), emphasizing that local-specific conditions governing solute movement can occur. It should be noted that the high frequency GLP and AMPA were found in the deepest layer, in both VS and VN, up to water concentrations of 14.1 and 9.4 and μg l^{-1}, respectively. This was likely emphasized by using pan lysimeters that collected the percolation water even from the non-capillary macropores from the overlying layers. Here, GLP could have moved sorbed onto soil particles (Piccolo et al., 1994; De Jonge et al., 2000), enhancing the concentration of the molecule in the suspension. It should be highlighted that the use of suction cups to intercept GLP concentration in pore water does not collect colloid-transported molecules (Lapworth et al., 2005). Furthermore, experimental results about soil moisture in the deeper profiles (**Figure 2.3B**) highlighted differences in water and solute movement dynamics (Jarvis, 2007; Mencaroni et al., 2021) between the sites. Specifically, the soil moisture in CE and CO at 30 and 70 cm depth did not respond to rainfall events earlier than the shallower layer (**Figure 2.3B**). In contrast, this dynamic was observed in VS and VN, which might support the occurrence of solute bypass (Graham and Lin, 2011). Estimates of GLP mobility according to the AF index seem to corroborate the previous results. Despite the AF index suggesting a low risk of groundwater contamination (AF always zero at each station), experimental findings demonstrated that some fast GLP vertical movement occurred. In fact, AF does not include the particular soil structure heterogeneity that might lead to site-specific solute bypass. Moreover, it does not account for single heavy rainfall events, which could have played an effect on moving the herbicide through the soil matrix down to 70 cm depth (Carretta et al., 2021b). Finally, the finding of GLP and AMPA below 30 cm can be due to herbicide interception by the aboveground vegetation, its following translocation into belowground tissues, and its likely release by dead roots below the topsoil (Laitinen et al., 2007).

The monitored experimental sites were characterized by grassland (Valdobbiadene) and grassed vineyard (Conegliano), which could have favored some movement of GLP (Alaoui, 2015) and in turn AMPA due to, e.g., increase in macropores under long-term stabilized soil conditions. About the role of SOC, contrasting results were reported in the literature to increase –or not increase– it (Vereecken, 2005). In our experiment, the SOC content was

mainly split between the topsoil –with SOC values >12.4 g kg^{-1}– and layers below 15 cm values ≤9.6 g kg^{-1}, which reached a minimum of 5.8 g kg^{-1} in the 40-50 cm layer in VS. A significant correlation between Freundlich adsorption coefficient and SOC was not found (**Table 2.8**), although negatively charged organic molecules would suggest the predominance of electrokinetically repulsive forces toward GLP, especially at alkaline soil pH conditions (Borggaard and Gimsing, 2008).

Table 2.8. The Pearson correlation coefficients matrix between sorption coefficients and soil properties in the four monitoring stations (N=13). Different colors indicate a range of p-values.

	Sand	Silt	Clay	SOC	Total N	pH	EC	P Olsen	CEC	Fe_{Ox}	Al_{Ox}	Fe_{Som}	Al_{Som}
Sand	-												
Silt	-0.957	-											
Clay	-0.631	0.380	-										
SOC	-0.243	0.489	-0.535	-									
Total N	-0.367	0.603	-0.445	0.975	-								
pH	0.228	-0.265	-0.017	-0.095	-0.192	-							
EC	-0.656	0.789	-0.018	0.806	0.87	-0.221	-						
P Olsen	0.234	-0.028	-0.674	0.537	0.526	-0.190	0.164	-					
CEC	-0.85	0.916	0.261	0.646	0.734	-0.246	0.925	0.024	-				
Fe_{Ox}	0.624	-0.531	-0.57	-0.041	-0.108	-0.218	-0.374	0.581	-0.478	-			
Al_{Ox}	-0.019	0.030	-0.019	-0.124	-0.083	-0.361	-0.050	0.183	-0.010	0.610	-		
Fe_{Som}	-0.777	0.716	0.563	0.239	0.365	-0.104	0.684	-0.097	0.795	-0.523	-0.053	-	
Al_{Som}	-0.832	0.692	0.805	-0.016	0.104	-0.005	0.507	-0.442	0.687	-0.753	-0.173	0.912	-
$K_{f\text{-}mean}$	-0.876	0.744	0.808	-0.028	0.103	-0.21	0.498	-0.37	0.720	-0.546	0.044	0.894	0.934
p-value ≤	0.001	0.01	0.025	0.05	0.1	0.5	1						

In this context, the significant positive correlations between SOM-chelated Fe and Al and $K_{f\text{-}mean}$ (r = 0.89 and 0.93, respectively, **Table 2.8**) indicated the occurrence of interactions between negatively charged functional groups in SOM and positively charged minerals with high surface area, which likely mitigated unfavorable conditions for adsorption by creating bridges with the GLP phosphonic moiety (Morillo et al., 2000; Fink et al., 2016). Here, the high fraction of SOM-chelated iron and aluminum found in both sites, increased along the soil profile despite the carbon content decreasing, as already observed by Bascomb (1968). The ratio between SOM-chelated metals and SOC (Fe_{Som}/SOC and Al_{Som}/SOC) was also investigated (**Table 2.8**): a high value of this ratio suggests that a large amount of Fe and Al are coupled with the SOM component, and vice versa a low ratio indicates that SOM is associated with a low amount of Fe or Al. The relationship between Fe_{Som}/SOC and Al_{Som}/SOC and $K_{f\text{-}mean}$ is

reported in **Figure 2.6**: as the ratio increases, the sorption capacity is enhanced confirming the effect of cation bridges played by Fe and Al. This was especially observed for Conegliano site, which had greater Fe_{Som}/SOC and Al_{Som}/SOC ratios than Valdobbiadene, and in turn higher $K_{f\text{-}mean}$.

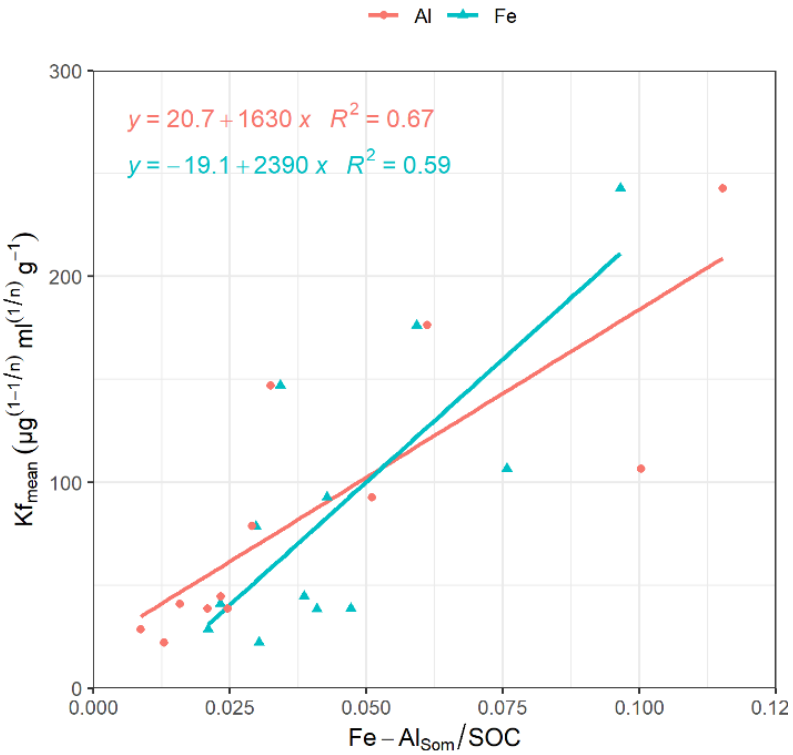

Figure 2.6. Regression lines with coefficient of determination between Al_{Som}/SOC (orange dots) and $K_{f\text{-}mean}$, and between Fe_{Som}/SOC (blue triangles) and $K_{f\text{-}mean}$.

On the other hand, the significant positive correlation of $K_{f\text{-}mean}$ with CEC (r = 0.72), silt and clay (r= 0.74 and 70.81, respectively) and the negative one with sand (r = -0.88) (**Table 2.8**), corroborated the GLP affinity for fine soil particles mainly due to cation bridging (Kah and Brown, 2007). Dollinger et al. (2015) predicted GLP sorption using pedotransfer functions, identifying clay, CEC and SOC as K_f predictors in a multiple regression analysis. By using the same equation, an R^2 = 0.48 (p = 0.01) between experimental and estimated $K_{f\text{-}mean}$ was found (**Table 2.9**). The implementation of multiple regression parameterization accounting for all experimental soil parameters analyzed here revealed that clay and CEC were significant predictors of GLP sorption capacity, similarly to Dollinger et al. (2015). By contrast SOC was not selected, while both amorphous and SOM-chelated metals were significant predictors of $K_{f\text{-}mean}$ leading to an overall R^2 = 0.97 (**Table 2.9**), thus corroborating the major role of

amorphous Fe and Al oxide surfaces (Rampazzo et al., 2013; Maqueda et al., 2017) over SOM-chelated ones.

Table 2.9. Multiple linear regression analysis for estimation of Freundlich sorption coefficient ($K_{f\text{-mean}}$ for experimental and K_f for Dollinger) according to soil parameters and Dollinger et al. (2015). Both unstandardized and standardized (in brackets) regression coefficients ($p < 0.05$) are reported.

		Regression coefficients						
Freundlich coefficient	**Intercept**	**CEC[a]**	**Clay[b]**	**$Fe_{Ox}+Al_{Ox}$[c]**	**$Fe_{Som}+Al_{Som}$[c]**	**SOC[d]**	**R^2**	**p-value**
Experimental	-330.544	6.832 (0.354)	14.602 (0.509)	0.017 (0.218)	0.079 (0.450)	-	0.97	< 0.001
Dollinger et al. (2015)	50.904	9.246	-1.985	-	-	-11.811	0.48	0.001

[a] cmol kg^{-1}; [b] %; [c] mg kg^{-1}; [d] %

The dissipation time (DT_{50}) has been calculated (reported in **Table 2.5**) using Eq. 6 despite the low amount of sampling points in the first 30 days of the experiment. For AMPA, the rate coefficient α was used instead of *k* in Eq. 6. Estimated dissipation of GLP was 28 days in Conegliano and 43 days in Valdobbiadene, highlighting a significant variability between the two experimental sites. In contrast, a low variability within each site can be hypothesized, that is supported by the low variability of both pedogenetic (ARPAV, 2008) and experimental physicochemical analysis of the sites. Anyway, expanding these data to other soils of the Prosecco area with the same pedogenesis must be carefully evaluated, because other factors (e.g. soil management) might strongly affect the dissipation dynamics. In general, DT_{50} - calculated according to first-order kinetic - were slightly longer than that calculated, e.g., in the laboratory in a clay loam agricultural French Cambisol (7 to 26 days) (Mamy et al., 2016), in Argentinian agricultural field trials on silt to loam soils (9 to 38 days) (Bento et al., 2019; Okada et al., 2019), and Danish sandy soils (16.9 days) (Bergström et al., 2011). In Italian agricultural fields, GLP DT_{50} was 9 to 18 days and 99 up to 250 days for AMPA according to different tillage management (Carretta et al., 2021a). To our knowledge, less data are available in the literature about AMPA kinetics, which here averaged 67 days as similarly reported by Bento et al. (2019) (55 to 71 days) and Bergstrom et al. (2011) (35 to 60 days). The GLP dissipation and transformation to AMPA occurred without any lag phase corroborating previous findings (e.g., Nguyen et al., 2018), although the degradation rate could vary widely. From our results, dissipation dynamics of GLP and AMPA in the topsoil under field conditions was the combination of water percolation, runoff and degradation phenomena, while erosion

events were negligible experimental monitoring stations in flat areas being characterized by dense grass cover. Hence, GLP and AMPA dissipation/formation in soil might be predominantly affected by microorganisms degradation (Sprankle et al., 1975) rather than water movement (e.g. enhanced leachability): in this context, greater cumulative rainfall and lower dissipation rate constants were detected in Valdobbiadene than in Conegliano, confirming that heavier rainfall events did not lower the persistence of the molecule in soil by e.g. leaching or run-off. Higher fine particles, CEC, and Fe and Al oxides in soil would suggest greater sorption, an enhanced GLP and AMPA protection against degradation (Bergström, 1990) and in turn higher DT_{50} in Conegliano than Valdobbiadene. In contrast, estimated DT_{50} values were the opposite, suggesting that other factors had likely contributed to GLP and AMPA dissipation, or conservation, in soils. For instance, it is likely that some specific weather conditions contributed to differences between the two experimental sites. After 61 days, both GLP and AMPA concentrations were affected by a sharp reduction, mainly in Valdobbiadene soil and then, at the following sampling date, they increased again (**Figure 2.5**). It is to be noted that a snowfall (~1 cm) in January 2019 and low temperatures (**Table 2.2**) were recorded in the experimental sites, which could have frozen GLP and AMPA in the dead weeds, and then might have been released from the plant material to soil with the gradual increase in temperature (Laitinen et al., 2009).

2.5 Conclusion

The glyphosate application in two soils of the Prosecco DOCG winegrowing area confirmed the general GLP and AMPA low mobility and highlighted the pivotal role of Fe and Al as key factors to mitigate the repulsive forces, especially when complexed with organic molecules. It is therefore suggested to study their content better to predict GLP dynamics. Between experimental sites, Conegliano showed a faster dissipation (about 28 days for GLP, 42 for AMPA) in the 0-5 cm of soil and a higher sorption to soils (depth average $K_{f\text{-}mean}$ = 140.6) than Valdobbiadene (about 43 days for GLP, 92 for AMPA; depth average $K_{f\text{-}mean}$ = 35.6). However, a reduced soil filtering capacity was observed during intense rain events as emphasized by some preferential movements due to likely well-structured soil conditions that could increase groundwater vulnerability to contamination. It follows that, an in-depth water and solute monitoring activity at site-specific level is required after careful definition of homogeneous areas of the Prosecco *terroir*, which goes beyond the estimate of only leachability indexes that do not include the heterogeneity of soil structure and hydraulic properties. This phenomenon might be further exacerbated due to repeated GLP applications in cultivated areas or under particular pedo-climatic conditions that could increase GLP and AMPA dissipation times. Therefore, a sparing use of GLP is suggested, that might be planned after evaluation of most appropriate weather conditions.

References

Ahuja, K., and Raeat, A. (2017). Glyphosate Market Size By Application (Conventional crops, GM crops), Industry Analysis Report, Regional Outlook, Application Potential, Price Trends, Competitive Market Share & Forecast, 2016 – 2024. Selbyville, Delaware, USA.

Alaoui, A. (2015). Modelling susceptibility of grassland soil to macropore flow. *J. Hydrol.* 525, 536–546. doi:10.1016/j.jhydrol.2015.04.016.

Antier, C., Kudsk, P., Reboud, X., Ulber, L., Baret, P. V., and Messéan, A. (2020). Glyphosate use in the European agricultural sector and a framework for its further monitoring. *Sustain.* 12, 1–22. doi:10.3390/su12145682.

ARPAV (2008). Carta dei suoli della Provincia di Treviso 1:50.000. *Agenzia Reg. per la Prev. e Prot. Ambient. del veneto.*, 350.

ARPAV (2019). Carta dei suoli 1:250.000. *Agenzia Reg. per la Prev. e Prot. Ambient. del veneto.*, 156.

ARPAV (2020). Principali variabili meteorologiche (1994-2019). *Agenzia Reg. per la Prev. e Prot. Ambient. del veneto.*

Bascomb, C. L. (1968). Distribution of pyrophosphate-extractable iron and organic carbon in soils of various groups. *J. Soil Sclence*.

Bento, C. P. M., van der Hoeven, S., Yang, X., Riksen, M. M. J. P. M., Mol, H. G. J., Ritsema, C. J., et al. (2019). Dynamics of glyphosate and AMPA in the soil surface layer of glyphosate-resistant crop cultivations in the loess Pampas of Argentina. *Environ. Pollut.* 244, 323–331. doi:10.1016/j.envpol.2018.10.046.

Bento, C. P. M., Yang, X., Gort, G., Xue, S., van Dam, R., Zomer, P., et al. (2016). Persistence of glyphosate and aminomethylphosphonic acid in loess soil under different combinations of temperature, soil moisture and light/darkness. *Sci. Total Environ.* 572, 301–311. doi:10.1016/j.scitotenv.2016.07.215.

Bergström, L. (1990). Use of lysimeters to estimate leaching of pesticides in agricultural soils. *Environ. Pollut.* 67, 325–347. doi:10.1016/0269-7491(90)90070-S.

Bergström, L., Börjesson, E., and Stenström, J. (2011). Laboratory and Lysimeter Studies of Glyphosate and Aminomethylphosphonic Acid in a Sand and a Clay Soil. *J. Environ. Qual.* 40, 98. doi:10.2134/jeq2010.0179.

Bittelli, M., Andrenelli, M. C., Simonetti, G., Pellegrini, S., Artioli, G., Piccoli, I., et al. (2019). Shall we abandon sedimentation methods for particle size analysis in soils? *Soil Tillage Res.* 185, 36–46. doi:10.1016/J.STILL.2018.08.018.

Blake, R., and Pallett, K. (2018). The environmental fate and ecotoxicity of glyphosate. *Outlooks Pest Manag.* 29, 266–269. doi:10.1564/v29_dec_08.

Borggaard, O. K., and Gimsing, A. L. (2008). Fate of glyphosate in soil and the possibility of leaching to ground and surface waters : a review. *Pest Manag. Sci.* 456, 441–456. doi:10.1002/ps.

Carles, L., Gardon, H., Joseph, L., Sanchís, J., Farré, M., and Artigas, J. (2019). Meta-analysis of glyphosate contamination in surface waters and dissipation by biofilms. *Environ. Int.* 124, 284–293. doi:10.1016/j.envint.2018.12.064.

Carretta, L., Cardinali, A., Marotta, E., Zanin, G., and Masin, R. (2019). A new rapid procedure for simultaneous determination of glyphosate and AMPA in water at sub µg/L level. *J. Chromatogr. A* 1600, 65–72. doi:10.1016/j.chroma.2019.04.047.

Carretta, L., Cardinali, A., Onofri, A., Masin, R., and Zanin, G. (2021a). Dynamics of Glyphosate and Aminomethylphosphonic Acid in Soil Under Conventional and Conservation Tillage. *Int. J. Environ. Res.* doi:10.1007/s41742-021-00369-3.

Carretta, L., Masin, R., and Zanin, G. (2021b). Review of studies analysing glyphosate and aminomethylphosphonic acid (AMPA) occurrence in groundwater. *Environ. Rev.*, 1–22. doi:https://doi.org/10.1139/er-2020-0106.

Consorzio di Tutela DOCG Conegliano Valdobbiadene (2019). Protocollo Viticolo del Conegliano Valdobbiadene Prosecco DOCG. Available at: http://repositorio.unan.edu.ni/2986/1/5624.pdf.

Dal Ferro, N., Piccoli, I., Berti, A., Polese, R., and Morari, F. (2020). Organic carbon storage potential in deep agricultural soil layers: Evidence from long-term experiments in northeast Italy. *Agric. Ecosyst. Environ.* 300, 106967. doi:10.1016/j.agee.2020.106967.

De Jonge, H., De Jonge, L. W., and Jacobsen, O. H. (2000). [14C]glyphosate transport in undisturbed topsoil columns. *Pest Manag. Sci.* 56, 909–915. doi:10.1002/1526-4998(200010)56:10<909::AID-PS227>3.0.CO;2-5.

De Jonge, H., De Jonge, L. W., Jacobsen, O. H., Yamaguchi, T., and Moldrup, P. (2001). Glyphosate sorption in soils of different pH and phosphorus content. *Soil Sci.* 166, 230–238. doi:10.1097/00010694-200104000-00002.

de Paz, J. M., and Rubio, J. L. (2006). Application of a GIS-AF/RF model to assess the risk of herbicide leaching in a citrus-growing area of the Valencia Community, Spain. *Sci. Total Environ.* 371, 44–54. doi:10.1016/j.scitotenv.2006.07.018.

De Polo, A., Rossi, S., Bulfoni, I., Bardin, A., Gentili, D., and Cinquetti, S. (2019). From the traces in the wells of the urban aqueduct network to the subsequent prohibition of the use of glyphosate: the case of an area of high-intensity wine production in the province of Treviso, Veneto. *Ig. e sanità pubblica* 75, 451–460.

Dollinger, J., Dagès, C., and Voltz, M. (2015). Glyphosate sorption to soils and sediments predicted by pedotransfer functions. *Environ. Chem. Lett.* 13, 293–307. doi:10.1007/s10311-015-0515-5.

EFSA (2015). Conclusion on the peer review of the pesticide risk assessment of the active substance glyphosate. *EFSA J.* 13. doi:10.2903/j.efsa.2015.4302.

EFSA (2017). Peer review of the pesticide risk assessment of the potential endocrine disrupting properties of glyphosate. *EFSA J.* 15. doi:10.2903/j.efsa.2017.4979.

Fink, J. R., Inda, A. V., Tiecher, T., and Barrón, V. (2016). Iron oxides and organic matter on soil phosphorus availability. *Cienc. e Agrotecnologia* 40, 369–379. doi:10.1590/1413-70542016404023016.

Gairhe, B., Liu, W., Batuman, O., Dittmar, P., Kadyampakeni, D., and Kanissery, R. (2021). Environmental Fate and Behavior of the Herbicide Glyphosate in Sandy Soils of Florida Under Citrus Production. *Front. Environ. Chem.* 2, 1–9. doi:10.3389/fenvc.2021.737391.

Graham, C. B., and Lin, H. S. (2011). Controls and Frequency of Preferential Flow Occurrence: A 175-Event Analysis. *Vadose Zo. J.* 10, 816–831. doi:10.2136/vzj2010.0119.

Grossman, B. R., and Reinsch, T. G. (2002). 2.1 Bulk Density and Linear Extensibility. In: Dane, J.H., Topp, C.G. (Eds.). *Methods Soil Anal. Part 4 Phys. Methods. Soil Sci. Soc. Am.* i, 201–228.

Ibrahim, H. M., and Ali, A. T. M. (2020). Assessment of the environmental risk of pesticides leaching at the watershed scale under arid climatic conditions and low recharge rates. *Water* 12. doi:10.3390/w12020418.

Jarvis, N. J. (2007). A review of non-equilibrium water flow and solute transport in soil macropores: Principles, controlling factors and consequences for water quality. *Eur. J. Soil Sci.* 58, 523–546. doi:10.1111/j.1365-2389.2007.00915.x.

Jarvis, N., Koestel, J., and Larsbo, M. (2016). Understanding Preferential Flow in the Vadose Zone: Recent Advances and Future Prospects. *Vadose Zo. J.* 15, 0. doi:10.2136/vzj2016.09.0075.

Kah, M., and Brown, C. D. (2007). Prediction of the adsorption of lonizable pesticides in soils. *J. Agric. Food Chem.* 55, 2312–2322. doi:10.1021/jf063048q.

Kjær, J., Olsen, P., Ullum, M., and Grant, R. (2003). Vadose Zone Processes and Chemical Transport Leaching of Glyphosate and Amino-Methylphosphonic Acid from Danish Agricultural Field Sites. *J. Environ. Qual.*, 608–620.

Kodešová, R., Kočárek, M., Kodeš, V., Drábek, O., Kozák, J., and Hejtmánková, K. (2011). Pesticide adsorption in relation to soil properties and soil type distribution in regional scale. *J. Hazard. Mater.* 186, 540–550. doi:10.1016/j.jhazmat.2010.11.040.

Laitinen, P., Rämö, S., Nikunen, U., Jauhiainen, L., Siimes, K., and Turtola, E. (2009). Glyphosate and phosphorus leaching and residues in boreal sandy soil. *Plant Soil* 323, 267–283. doi:10.1007/s11104-009-9935-y.

Laitinen, P., Rämö, S., and Siimes, K. (2007). Glyphosate translocation from plants to soil - Does this constitute a significant proportion of residues in soil? *Plant Soil* 300, 51–60. doi:10.1007/s11104-007-9387-1.

Laitinen, P., Siimes, K., Eronen, L., Rämö, S., Welling, L., Oinonen, S., et al. (2006). Fate of the herbicides glyphosate,glufosinate-ammonium, phenmedipham,ethofumesate and metamitron in twoFinnish arable soils. *Pest Manag. Sci.* 62, 473–491. doi:10.1002/ps.1186.

Lapworth, D., Gooddy, D., Harrison, I., Kim, A., and Vane, C. (2005). Colloidal phase transport of pesticides: A review with special reference to major UK aquifers. *Br. Geol. Surv. Intern. Rep.*, 31pp. Available at: http://nora.nerc.ac.uk/4490/.

Lewis, K., and Tzilivakis, J. (2017). Development of a data set of pesticide dissipation rates in/on various plant matrices for the pesticide properties database (PPDB). *Data* 2. doi:10.3390/data2030028.

Mamy, L., Barriuso, E., and Gabrielle, B. (2016). Glyphosate fate in soils when arriving in plant residues. *Chemosphere* 154, 425–433. doi:10.1016/j.chemosphere.2016.03.104.

Maqueda, C., Undabeytia, T., Villaverde, J., and Morillo, E. (2017). Behaviour of glyphosate in a reservoir and the surrounding agricultural soils. *Sci. Total Environ.* 593–594, 787–795. doi:10.1016/j.scitotenv.2017.03.202.

McKeague, J., Brydon, J., and Miles, N. (1971). Differentiation of Forms of Extractable Iron and Aluminum in Soils. *Soil Sci. Soc. Am. Proc.* 35, 33–38.

Mencaroni, M., Dal Ferro, N., Redcliffe, D., and Morari, F. (2021). Preferential solute transport under variably saturated conditions in a silty loam soil: is the shallow water table a driving factor? *J. Hydrol.* 602.

Morillo, E., Undabeytia, T., and Maqueda, C. (1997). Adsorption of glyphosate on the clay mineral montmorillonite: Effect of Cu(II) in solution and adsorbed on the mineral. *Environ. Sci. Technol.* 31, 3588–3592. doi:10.1021/es970341l.

Morillo, E., Undabeytia, T., Maqueda, C., and Ramos, A. (2000). Glyphosate adsorption on soils of different characteristics. Influence of copper addition. *Chemosphere* 40, 103–107. doi:10.1016/S0045-6535(99)00255-6.

Neumann, G., Kohls, S., Landsberg, E., Stock-Oliveira Souza, K., Yamada, T., and Römheld, V. (2006). Relevance of glyphosate transfer to non-target plants via the rhizosphere. *J. Plant Dis. Proctectio, Suppl.* 969, 963–969. doi:http://dx.doi.org/10.1016/j.psychres.2016.04.036.

Nguyen, N. K., Dörfler, U., Welzl, G., Munch, J. C., Schroll, R., and Suhadolc, M. (2018). Large variation in glyphosate mineralization in 21 different agricultural soils explained by soil properties. *Sci. Total Environ.* 627, 544–552. doi:10.1016/j.scitotenv.2018.01.204.

Noori, J. S., Dimaki, M., Mortensen, J., and Svendsen, W. E. (2018). Detection of glyphosate in drinking water: A fast and direct detection method without sample pretreatment. *Sensors (Switzerland)* 18. doi:10.3390/s18092961.

Nowack, B., and Stone, A. T. (2006). Competitive adsorption of phosphate and phosphonates onto goethite. *Water Res.* 40, 2201–2209. doi:10.1016/j.watres.2006.03.018.

OECD (2000). OECD 106 Adsorption - Desorption Using a Batch Equilibrium Method. *OECD Guidel. Test. Chem.*, 1–44. doi:10.1787/9789264069602-en.

Okada, E., Costa, J. L., and Bedmar, F. (2016). Adsorption and mobility of glyphosate in different soils under no-till and conventional tillage. *Geoderma* 263, 78–85.

doi:10.1016/j.geoderma.2015.09.009.

Okada, E., Costa, J. L., and Bedmar, F. (2019). Glyphosate Dissipation in Different Soils Under No-Till and Conventional Tillage. *Pedosphere* 29, 773–783. doi:10.1016/S1002-0160(17)60430-2.

Ololade, I. A., Oladoja, N. A., Oloye, F. F., Alomaja, F., Akerele, D. D., Iwaye, J., et al. (2014). Sorption of Glyphosate on Soil Components: The Roles of Metal Oxides and Organic Materials. *Soil Sediment Contam.* 23, 571–585. doi:10.1080/15320383.2014.846900.

Otto, S., Riello, L., Düring, R. A., Hummel, H. E., and Zanin, G. (1997). Herbicide dissipation and dynamics modelling in three different tillage systems. *Chemosphere* 34, 163–178. doi:10.1016/S0045-6535(96)00356-6.

Perri, M. T., Cassiani, G., Gervasio, I., Deiana, R., and Binley, A. (2012). A saline tracer test monitored via both surface and cross-borehole electrical resistivity tomography: Comparison of time-lapse results. *J. Appl. Geophys.* 79, 6–16. doi:10.1016/j.jappgeo.2011.12.011.

Piccolo, A., Celano, G., Arienzo, M., and Mirabella, A. (1994). Adsorption and desorption of glyphosate in some european soils. *J. Environ. Sci. Heal.*

R Core Team (2020). R: A language and environment for statistical computing. *R Found. Stat. Comput. Vienna, Austria.* Available at: https://www.rstudio.com/wp-content/uploads/2015/03/ggplot2-cheatsheet.pdf%5Cnhttps://www.rstudio.com/wp-content/uploads/2015/06/ggplot2-french.pdf.

Rampazzo, N., Todorovic, G. R., Mentler, A., and Blum, W. E. H. (2013). Adsorption of glyphosate and aminomethylphosphonic acid in soils. *Int. Agrophysics* 27, 203–209. doi:10.2478/v10247-012-0086-7.

Sidoli, P., Baran, N., and Angulo-Jaramillo, R. (2016). Glyphosate and AMPA adsorption in soils: laboratory experiments and pedotransfer rules. *Environ. Sci. Pollut. Res.* 23, 5733–5742. doi:10.1007/s11356-015-5796-5.

Sprankle, P., Meggitt, W. F., and Penner, D. (1975). Adsorption, mobility and microbial degradation of glyphosate in the soil. *Weed Sci.* 23, 229–234. doi:10.1080/03601230802062000.

Stone, W. W., and Wilson, J. T. (2006). Preferential Flow Estimates to an Agricultural Tile Drain with Implications for Glyphosate Transport. *J. Environ. Qual.* 35, 1825–1835. doi:10.2134/jeq2006.0068.

Vereecken, H. (2005). Mobility and leaching of glyphosate: A review. *Pest Manag. Sci.* 61, 1139–1151. doi:10.1002/ps.1122.

Viti, M. L., Alves, P. A. T., Mendes, K. F., Pimpinato, R. F., Guimaraes, A. C. D., and Tornisello, V. L. (2019). Translocation and Root Exudation of Glyphosate by Urochloa brizantha and its Transport on Sugarcane and Citrus Seedlings. *Planta Daninha* 37, 1–8. doi:10.1590/s0100-83582019370100030.

WRB, I. W. G. (2014). World Reference Base for Soil Resources 2014. International Soil Classification System for Naming Soils and Creating Legends for Soil Maps. FAO Rome, Italy.

Zovi, F., Camporese, M., Hendricks Franssen, H. J., Huisman, J. A., and Salandin, P. (2017). Identification of high-permeability subsurface structures with multiple point geostatistics and normal score ensemble Kalman filter. *J. Hydrol.* 548, 208–224. doi:10.1016/j.jhydrol.2017.02.056.

Chapter 3. Glyphosate and AMPA dynamics during the transition towards conservation agriculture: drivers under shallow groundwater conditions*

*Mencaroni M., Longo M., Cardinali A., Lazzaro B., Zanin G., Dal Ferro N., Morari F. Glyphosate and AMPA dynamics during the transition towards conservation agriculture: drivers under shallow groundwater conditions. Soil and Tillage Research (submitted).

Abstract

The environmental fate of glyphosate and its metabolite AMPA were investigated in 8 buried lysimeters in a factorial combination of two cropping systems (conservation and conventional agriculture) and two water table depths (120 and 60 cm). Glyphosate was distributed at a rate of 1.44 kg ha^{-1} a.i., and pore-water was sampled for 48 non-consecutive days along the soil profile (15, 30 and 60 cm) as well as the groundwater. Glyphosate and AMPA concentration in soil was detected to compare the effect of different soil-crop managements on transformation/dissipation dynamics and a full characterization of the soil profile was performed. Freundlich adsorption coefficients were calculated down to 110 cm depth and correlated to laboratory-estimated soil properties. Clay minerals, soil organic carbon, phosphate content, Al and Fe amount were the driving factors influencing most of the glyphosate sorption, regardless of the crop and water management system that did not differentiate between adsorption dynamics. In contrast, conservation practices differently affected glyphosate concentration in the soil profile, although its adoption was limited to two years. Moreover, the occurrence of a shallow water table influenced glyphosate transport in the vadose zone, and its detection in groundwater supported the hypothesis of fast transport of the molecule as mediated by preferential pathways, compromising groundwater quality, especially in agricultural lands. On the contrary, AMPA has never been detected in the groundwater, giving evidence of a diverse adsorption and transport dynamic compared to glyphosate.

3.1 Introduction

The application of glyphosate-based products for weed control is strongly debated due to its extensive use in agricultural lands over several decades. Although concerns have arisen about the risk of soil and water contamination and their impact on human health, analysts have estimated that the glyphosate (GLP) market is likely to increase further, with an expected annual growth rate for herbicide sales of around 6% towards 2024, in Europe and worldwide (Antier et al., 2020). Some authors have highlighted that a possible driver of the growing use in croplands is the expansion of GLP-relying conservation agriculture (CA) practice (Benbrook, 2016), which is often supported through agri-environmental schemes as in the case of Europe. The use of GLP-based products in CA is fundamental to produce a clean seedbed before sowing. However, the investigation of GLP fate under reduced tillage conditions and its comparison with conventional practices is becoming crucial, particularly in European agroecosystems where the use of CA has been traditionally weak among farmers (Basch et al., 2015; Dal Ferro et al., 2020). In this context, still few studies have compared the effect of CA on GLP fate in soil with conventional practices. For example, Prata et al. (2005) observed a faster GLP mineralization in the no-till compared to conventional ones (DT_{50} was 14.5 and 25.8 days, respectively), whereas Carretta et al. (2021a) and Okada et al. (2019) did not find any difference in GLP dissipation time between the two systems. These results highlight that knowledge of the potential influence of CA on GLP dynamics under peculiar soil conditions in different climatic areas is still lacking.

Being a post-emergence herbicide the fraction of GLP not intercepted by weeds may be blocked by crop residues (Khalil et al., 2018), thus impeding subsequent infiltration to soil (Locke et al., 2005). However, the positive impact of these mechanisms on pollution control was recently downplayed by Silburn (2020). The fraction of GLP that reaches the soil surface can be absorbed, degraded by soil biota, or transported through the soil matrix. In soil, GLP is considered immobile or of low mobility (EFSA, 2015) due to its generally high sorption affinity to soil particles. Soil properties mainly affecting sorption are pH, clay minerals, soil organic matter, phosphate content, the occurrence of Al and Fe oxides (Gimsing and Borggaard, 2002; Okada et al., 2016; Ololade et al., 2014), Cu^{2+} (Morillo et al., 2000) or other exchangeable cations (Sprankle et al., 1975).

In soil, besides the adsorption mechanism, GLP is mainly transformed into aminomethylphosphonic acid (AMPA), which has low mobility but high persistence. The dissipation time (DT_{50}) for GLP varies widely from a few days up to 8 months (Bento et al., 2016; Laitinen, 2009), while for AMPA it can be even years (U.S. EPA, 1993), according to different soils and weather conditions. However, both GLP and AMPA are also highly soluble (10.5 and 1466.5 g l^{-1}), highlighting their affinity to the water phase and, in turn, increasing the risk to reach the groundwater.

The presence of GLP and AMPA in groundwater has often been detected in the past years (Carretta et al., 2021b), mainly through macropore-mediated (Kjær et al., 2011) or colloid-facilitated transport (de Jonge et al., 2004) in the soil matrix. Many authors indicated a shallow water table as a critical factor contributing to the risk of pesticide contamination of groundwater resources, especially in agricultural areas (Haarstad and Ludvigsen, 2007; Lutri et al., 2020). Shallow groundwater can enhance preferential flow pathways in the soil matrix by reducing the flow path of the solute and by modifying the flow field, thus compromising the groundwater quality (Mencaroni et al., 2021). This pathway could be emphasized under CA, where undisturbed soil structure is mostly maintained and large biopores (e.g., earthworms and roots) can facilitate the deep transport of contaminants. For this purpose, Okada et al. (2014) suggested that in clayey soils (>35%) under CA practices, the well-preserved soil structure might lead to an increase in the risk of leaching of chemicals. For instance, Cueff et al. (2020) found, through laboratory leaching experiments, that the protective action towards groundwater provided by the high contaminant sorption of CA soils can be offset by a high degree of preferential flow, most likely due to greater continuity of vertically oriented macropores (Wahl et al., 2004). All these phenomena can be particularly relevant in the low-lying Venetian plain of north-eastern Italy, an area where conservation agriculture practices are increasingly used in soils characterized by shallow groundwater conditions (Camarotto et al., 2018). Nevertheless, the only recent conversion to conservation agriculture could slow down the phenomenon, since a transitory phase with slight soil physical changes may occur (Chakraborty et al., 2022; Piccoli et al., 2017). In such peculiar conditions, we hypothesized that the early adoption of CA could favor the mobility of GLP in soil, by offsetting the benefits that conservation practices may provide in relation to increased contaminant adsorption and degradation.

This work aimed to investigate in a set of eight lysimeters, i) the effect of conservation agriculture adoption during the transition period under different shallow water table conditions on GLP and AMPA dynamics and ii) the peculiar interactions of molecules with soil and water, influenced by their dissipation/formation processes, adsorption on soil particles, and transport to groundwater.

3.2 Materials and Methods

3.2.1 Experimental site description

The experimental study was conducted between May and July 2019 at the Experimental Farm "L. Toniolo" of the University of Padova in Legnaro (45°21' N; 11°57' E, 8 m a.s.l.), northeastern Italy. The climate is sub-humid, with a mean annual temperature of 14.3 °C (9.7 and 19.3 °C as yearly min and max) and annual rainfall of about 870 mm, distributed uniformly throughout the year. The experimental site – originally set up in 1984 – consists of twenty drainable lysimeters of 1 m^2 area and 1.5 m depth. The bottom of each lysimeter is funnel-shaped and connected via an underground drain-pipe (1‰ slope) to an external tube equipped with a valve to regulate both the water table level and leaching discharge. Each lysimeter is filled with soil – Fluvi-Calcaric Cambisol (FAO-UNESCO, 2008), silty loam – excavated from the adjacent experimental farm, preserving the original soil horizons. A 20 cm thick of gravel was placed at the bottom of each lysimeter to facilitate water drainage and prevent soil washout. Each lysimeter is equipped with a unique automated monitoring system that serves a dual purpose: i) to monitor the soil water content and matric potential dynamics, with TDR (Time Domain Reflectometry) probes (CS635, Campbell Scientific Inc., Lincoln Nebraska, USA) and electronic tensiometers respectively (T4e, UMS GmbH, Munich, DE), both installed at 15, 30 and 60 cm depths; ii) to collect the pore-water at the same depths with polyethylene/nylon suction cups (SPE20, Meter Group, Munich, DE) with high solute concentration accuracy through automatic regulation of the suction equilibrium with the surrounding soil water tension. This is performed using continuous pore-water sampler vacuum regulation with the surrounding soil water tension, based on matric potential readings (Mencaroni et al., 2021; Morari, 2006). A system composed of a 5-Volt digital-analog conversion module (A04A,

Campbell Scientific Inc., Lincoln Nebraska, USA) connected to an electronic vacuum regulator is employed by incorporating a pressure relief valve (ITV2091, SMC Corporation, Tokyo, J). The imposed negative pressure applied to pore-water samplers was in the range of -2 to -70 kPa. To control water fluxes and preserve the site from destructive weather events, an automated mobile roof was built over the whole area. The site is also equipped with a weather station (Decagon Devices Inc., Pullman, USA).

3.2.2 Lysimeter set-up and herbicide distribution

In the present study, eight out of twenty lysimeters were used to evaluate the soil-water dynamic of GLP and AMPA under a combination of two shallow water table levels at 120 and 60 cm depth (hereafter called WT120 and WT60) and two crop management systems (conservation – CA – vs. conventional – CV – agriculture). The water table level was regulated manually every day (±10 cm from the set reference level) by using a valve at the bottom of each lysimeter or by adding water manually, and a pressure switch was used to measure every 30 min the water level inside each lysimeter. The water table level was kept constant since 2011 (Longo et al., 2021). No-tillage, cover crop cultivation, and crop rotation were the operations applied for conservation agriculture. On the contrary, conventional agriculture consisted of harrowing operations performed at 25 cm depth by manual spading before seeding, incorporation of residues, and bare soil maintenance between growing seasons. The main crops were the same for CA and CV, maize (*Zea mays* L.) in 2018, and grain sorghum (*Sorghum bicolor* (L.) Moench) in 2019. In CA, rye (*Secale cereale* L.) was sown as a cover crop at a seed density of 130 kg ha^{-1} on November 5, 2018 (**Figure 3.1**). The experimental design was a randomized block with two replicates (hereafter referred to as “a” and “b”) for four treatments (CA60, CA120, CV60 and CV120). The commercial herbicide Pantox 360 SUPER™ (Arysta, Barclay chemicals R&D Ltd), containing 360 g l^{-1} of acid glyphosate, was distributed in the eight lysimeters at a constant rate of 1.44 kg ha^{-1} using a manual sprayer at 2.5 bar pressure on May 10, 2019 (**Figure 3.1**). Glyphosate was distributed on rye in CA and on bare soil in CV. Twenty days after the herbicide application, dry rye in CA was cut at the collar, shredded, and left on the soil surface as crop residues, while CV lysimeters were maintained bare during the whole experiment. The water input on each lysimeter was rainfall and

irrigation (194.4 mm in 42 days). To note that GLP has not been used in the experimental plot since 2015.

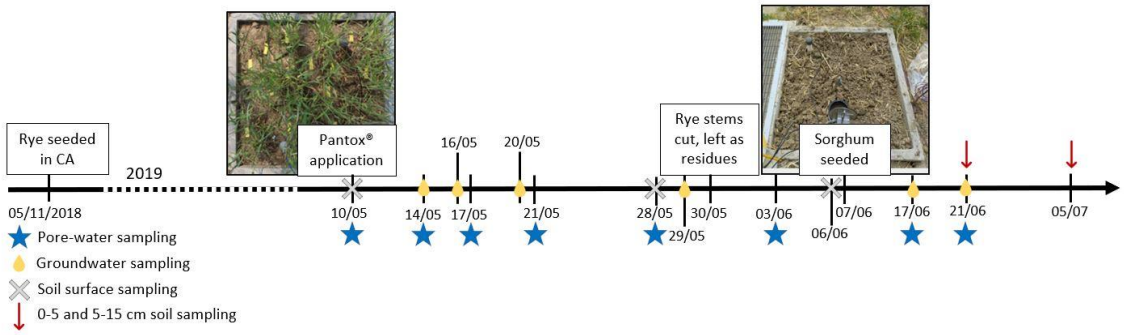

Figure 3.1. Schematic representation of field set-up and water and soil sampling during the time (blue stars, yellow drops, grey crosses and red arrows). Picture of the Pantox application refers to CA treatment (CV were maintained bare).

3.2.3 Characterization of soil profiles

At the end of the experiment, disturbed soil samples were collected with a gouge auger (Ejjkelkamp Soil & Water, Giesbeek, NL) in each lysimeter along the soil profile at the corresponding depth of 0-20, 20-40, 55-70, and 95-110 cm, and later analyzed for chemical and physical properties. The auger had a 5 cm diameter to minimize soil disturbance. Samples were placed in plastic bags and later air-dried, homogenized, crushed with a mortar, and sieved at 2 mm. After sieving, samples were stored at room temperature in the dark until analysis. Soil texture was determined by using a particle size analyzer (Mastersizer 2000, Malvern Panalytical Ltd, Spectris Company, UK) according to the methodology described in Bittelli et al. (2019); soil organic carbon (SOC) and total nitrogen (total N) content were determined by flash combustion with a CNS-analyzer (vario MACRO cube, Elementar Analysensysteme GmbH, Langenselbold, D); pH and electrical conductivity (EC) were measured by an electrode in soil suspensions with soil to water ratio of 1:2.5 (w/v) and the cation exchange capacity (CEC) was determined using the $BaCl_2$-triethanolamine method (**Table 3.1**).

Table 3.1. Average soil chemical and physical properties ± standard errors for CA and CV lysimeters. SOC is the soil organic carbon content (%), N is the total nitrogen (%), EC is the soil electrical conductivity (µS cm^{-1}), CEC is the cation exchange capacity (meq $100g^{-1}$), and Olsen P is the available phosphorous determined through the Olsen method (mg kg^{-1}).

Treatment	Depth	Particle size distribution %			pH	EC	SOC	N	Olsen P	CEC
	cm	Sand	Silt	Clay	-	µS cm^{-1}	%	%	mg kg^{-1}	meq $100g^{-1}$
CA	0-20	27.0± 1.3	56.1± 0.5	16.9± 0.9	7.8± 0.0	263.3± 6.6	0.96± 0.05	0.12± 0.01	47.3± 14.2	14.5± 0.5
	20-40	24.4± 2.1	57.2± 1.3	18.5± 0.9	8.2± 0.0	189.5± 6.8	0.69± 0.05	0.09± 0.01	21.8± 5.6	15.1± 0.4
	55-70	21.4± 2.0	58.8± 2.0	20.0± 0.1	8.3± 0.0	190.5± 3.1	0.57± 0.04	0.08± 0.01	11.2± 3.7	17.7± 0.8
	95-110	18.2± 0.6	61.1± 0.5	20.7± 0.2	8.2± 0.0	191.0± 3.1	0.58± 0.02	0.09± 0.01	14.9± 20.0	17.1± 0.3
CV	0-20	26.7± 0.5	56.9± 0.6	16.5± 0.3	7.8± 0.1	270.5± 20.9	0.88± 0.04	0.12± 0.00	41.2± 10.7	13.9± 0.1
	20-40	26.7± 0.5	56.4± 0.1	17.0± 0.5	8.2± 0.1	194.1± 14.4	0.73± 0.02	0.10± 0.00	21.7± 7.1	14.3± 0.0
	55-70	17.9± 2.7	61.2± 2.1	20.9± 0.6	8.3± 0.0	197.5± 9.8	0.60± 0.01	0.09± 0.00	11.9± 3.5	18.2± 0.5
	95-110	18.5± 0.5	58.8± 1.9	20.2± 0.7	8.3± 0.0	188.0± 6.8	0.64± 0.02	0.09± 0.00	20.1± 4.3	17.2± 0.7

Assimilable phosphorous (P Olsen) was also determined using the Olsen method, and iron (Fe) and aluminum (Al) oxides were analyzed in two forms: (i) poorly ordered Fe and Al oxides – hereafter labeled as Fe_{Ox} and Al_{Ox} – with the ammonium oxalate extraction in darkness method as (McKeague et al., 1971); (ii) SOM-chelated Fe and Al (hereafter labeled as Fe_{Som} and Al_{Som}), with the sodium pyrophosphate extraction method (pH = 10) (Bascomb, 1968). The determination of the extracts was performed by ICP-OES and the content was expressed as mg kg^{-1} (**Table 3.2**). The ratio between Al_{Som} and Fe_{Som} and SOM content (referred to as Al_{Som}/SOM and Fe_{Som}/SOM) was calculated by multiplying the SOC content by 1.72 to convert it to SOM. A high ratio means that, at equivalent SOM content, more Al and Fe are bound to SOM. A representative soil sample of WT60 and WT120 treatments was analyzed by X-ray powder diffraction (XRPD) to determine the soil mineral composition as in Piccoli et al. (2016). Analyses focused on the identification of the mineralogical phase in the bulk soil at different depths (**Table 3.3**). X-ray diffraction data were collected using a Panalytical X'Pert PRO MPD diffractometer equipped with a X'Celerator detector, a Co-anode X-ray tube and operating in Bragg-Brentano reflection geometry. Semiquantitative estimates of individual minerals were obtained by full profile analyses of diffraction data applying the Rietveld method as implemented in Topas v4.1 software.

Table 3.2. Al and Fe characterization of soil profiles as averaged between replicates. Fe_{Ox} and Al_{Ox} (mg kg^{-1}) are poorly-ordered oxides, Fe_{Som} and Al_{Som} (mg kg^{-1}) are SOM-chelated Fe and Al, Fe_{Som}/SOM and Al_{Som}/SOM (%) are the ratio with SOM. The significance was tested for depths and treatments: values followed by the same letter are not statistically different at $p > 0.05$.

Treatment	Depth	Fe_{Ox}	Al_{Ox}	Fe_{Som}	Al_{Som}	Fe_{Som}/SOM	Al_{Som}/SOM
	cm	mg kg^{-1}	mg kg^{-1}	mg kg^{-1}	mg kg^{-1}	%	%
CA60	0-20	1525±46	554±25	260±29	173±16	1.6±0.2	1.0±0.1
	20-40	1615±73	583±30	202±37	150±29	1.6±0.2	1.2±0.2
	55-70	1918±4	649±5	205±38	167±29	2.0±0.3	1.6±0.2
	95-110	2177±128	671±16	215±44	179±37	2.1±0.4	1.7±0.3
CA120	0-20	1842±48	591±17	335±21	231±2	2.1±0.4	1.4±0.2
	20-40	2012±154	645±81	347±10	276±10	3.2±0.6	2.5±0.5
	55-70	2224±272	724±84	388±14	328±13	4.3±0.8	3.7±0.7
	95-110	2070±269	692±74	389±2	325±7	4.2±0.3	3.5±0.2
CV60	0-20	1779±94	573±0	283±16	203±15	2.0±0.0	1.4±0.0
	20-40	1912±290	609±55	313±26	237±24	2.5±0.1	1.9±0.1
	55-70	2000±81	672±1	366±30	297±35	3.5±0.2	2.9±0.3
	95-110	2090±137	706±48	374±40	296±48	3.5±0.2	2.7±0.3
CV120	0-20	1738±203	574±52	289±30	208±30	1.8±0.1	1.3±0.1
	20-40	1663±41	583±6	294±43	228±36	2.3±0.2	1.8±0.2
	55-70	1792±391	603±110	344±61	275±58	3.4±0.6	2.7±0.6
	95-110	1814±93	585±52	398±26	289±47	3.6±0.3	2.6±0.4
Depth	0-20	1720±63 *b*	573±12 *b*	291±14	204±11 *b*	1.9±0.1 *b*	1.3±0.1 *b*
	20-40	1800±9 *ab*	605±22 *ab*	289±24	223±20 *ab*	2.4±0.2 *b*	1.9±0.2 *b*
	55-70	1983±109 *ab*	662±31 *a*	326±31	267±27 *a*	3.3±0.4 *a*	2.7±0.3 *a*
	95-110	2037±82 *a*	663±26 *a*	344±31	272±25 *a*	3.3±0.3 *a*	2.7±0.3 *a*
Treatment	CA60	1809±102	614±20	220±17 *b*	167±12 *b*	1.8±0.1 *b*	1.4±0.1 *c*
	CA120	2037±94	663±32	365±10 *a*	290±15 *a*	3.5±0.4 *a*	2.8±0.4 *a*
	CV60	1945±78	640±24	334±18 *a*	259±20 *a*	2.9±0.3 *a*	2.2±0.2 *a*
	CV120	1752±88	586±25	331±23 *a*	250±21 *a*	2.8±0.3 *a*	2.1±0.3 *b*

Table 3.3. Mineralogical composition of soil (weight %) averaged among treatments ± standard errors divided by layers, determined from XRPD.

	0-20 cm	20-40 cm	55-70 cm	95-110 cm
	weight %			
Dolomite	26.0± 0.0	26.5± 0.5	27.0± 0.0	26.0± 0.0
Quartz	24.5± 0.5	26.0± 1.0	23.0± 0.0	24.5± 0.5
Muscovite	21.0± 0.0	19.5± 0.5	20.0± 0.0	20.5± 0.5
Feldspar	15.0± 0.0	13.5± 0.5	14.0± 0.0	12.5± 0.5
Calcite	7.0± 0.0	7.5± 0.5	8.0± 0.0	8.5± 0.5
Chlorite-like	7.0± 0.0	7.5± 0.5	7.0± 0.0	7.5± 0.5

3.2.4 Adsorption isotherms of glyphosate in the commercial product

Glyphosate sorption isotherms were determined by performing the batch adsorption experiment as reported by the OECD Guideline using the Batch Equilibrium Method (OECD, 2000). The commercial product Pantox 360 SUPER™ was used to better represent the herbicide sorption under field conditions. Five different concentrations of GLP in the range of 1-100 μg g^{-1} of dry soil were tested, with three replicates each. Adsorption isotherms were estimated for all lysimeters in different layers (0-20, 20-40, 55-70 and 95-110 cm) to represent the adsorption dynamic along the full soil profile. Uncontaminated soil, obtained from the sampling at the end of the experiment and checked for the lack of GLP and AMPA, was used for the adsorption experiment. Firstly, a solution of 0.01 M $CaCl_2$ was added to 1 g of the 2 mm-sieved and air-dried soil in 50-mL polypropylene tubes with a corresponding ratio of 1:40 and then shaken at 200 rpm for 24 h at 20 °C. Then, the soil slurry was spiked with the corresponding Pantox® solution and shaken for 24 h. The tubes were centrifuged (6000 rpm for 20 min) and an aliquot of the supernatant was filtered using a regenerated cellulose membrane filter (pore size 0.20 μm) and stored in the fridge at +4 °C before UHPLC-MS analysis. Samples were derivatized as reported in (Carretta et al., 2019).

Adsorption data were fitted by nonlinear regression to the Freundlich adsorption isotherm model:

$$C_s = K_f C_w^{(\frac{1}{n})} \quad [1]$$

where C_s (μg g^{-1}) is the adsorbed amount, C_w (μg ml^{-1}) is the concentration in the aqueous phase, K_f [$\mu g^{1-1/n}$ $(ml)^{1/n}$ g^{-1}] is the Freundlich adsorption coefficient and 1/n is a measure of adsorption intensity and nonlinearity. Small 1/n values indicate the saturation of soil at high GLP contents.

3.2.5 Water sample collection and quantification of glyphosate and AMPA

Pore-water samples were collected with suction cups at 15, 30 and 60 cm depth for a total of seven non-consecutive days, starting on May 14 until June 21, depending on rainfall events. Pore-water samples – around 100 ml or less – were collected in 1000 ml high-density polyethylene bottles (Nalgene™, Thermo Scientific, Waltham, Massachusetts, USA),

transported to the laboratory where they were stored in a refrigerator (+4 °C), and then analyzed by UHPLC-MS for GLP and AMPA concentration using the procedure reported by Carretta et al. (2019) (limit of detection – LOD – and limit of quantification – LOQ – were 0.2 and 0.5 μg l^{-1}, respectively for GLP; 0.05 and 0.1 μg l^{-1} respectively for AMPA). Before the herbicide application, pore-water was sampled in all lysimeters at each depth to measure GLP and AMPA background concentration, which resulted < LOQ. Groundwater was collected at the bottom valve of each lysimeter when the water table was 10 cm above the set level, after rainfall or irrigation, and managed in the same way as reported for pore-water.

3.2.6 Soil sample collection and quantification of glyphosate and AMPA

Soil samples were collected starting on the day of the herbicide application and then after 18 and 27 days. Sampling was performed on two randomly selected points within each lysimeter at about 1 cm depth (hereafter referred to as *surface soil*) and then bulked, resulting in 20 g of soil. To note that, for CA, the sample included residues left in the field from the previous crop. Two additional samplings, on June 21 and July 7 (day 42 and 56 after GLP distribution, respectively), were performed at two depths (0-5 and 5-15 cm) at each lysimeter to determine the residual amount of GLP and AMPA. Once collected in plastic bags, soils were transported to the laboratory. Samples were air-dried (20 °C) and sieved at 2 mm before analysis. The extraction procedure to analyze the concentration of GLP and AMPA in soil samples was performed as reported in Mencaroni et al. (2022). Then the samples were analyzed by HPLC-MS. The LOD and LOQ were 15 and 50 μg kg^{-1} for GLP, and 6 and 20 μg kg^{-1} for AMPA. Soil samples before the herbicide application were also collected and analyzed for the background concentration, resulting to be < LOQ.

3.2.7 Data analysis

Adsorption coefficients (K_f and 1/n) were calculated using the Solver tool in Excel MS Office, minimizing the sum of squared error. Pearson correlation coefficients between K_f and soil properties (N=32) were tested at two significance levels (p=0.05 and p=0.01), and a three-way

ANOVA with a Tukey post-hoc test was performed to test significant differences in K_f and soil properties between soil managements (CA and CV), WT level (120 and 60) and soil depths (0-20, 20-40, 55-70 and 95-110 cm). A Kruskal-Wallis non-parametric test was performed to test the significance ($p < 0.05$) between treatments on GLP concentration in groundwater. When GLP concentration was below the LOQ (censored data were >50%), the value was set as one-half the LOQ to estimate the summary statistics, as reported by Gilbert (1988). Statistical analyses were performed using R (R Core Team, 2020).

3.3 Results

3.3.1 Soil properties

Soil properties showed a differentiation among soil layers (**Table 3.1** and **Table 3.2**). Silt was the predominant texture fraction which slightly increased with depth, from 56% in 0-20 cm to about 60% in the deepest layers (> 55cm). A similar trend was observed for clay, which ranged from 17% to 20% with no relevant differences between CA and CV. Profile stratification was also reflected in the chemical properties, showing contrasting values of pH (7.8 vs 8.2), SOC (0.9 vs 0.6%) and P Olsen (> 40 vs 17 mg kg^{-1}) between the top layer and the deepest ones. Some slight increase of SOC content was found in 0-20 cm in CA (0.97±0.05%) than CV (0.88±0.04%). Cation exchange capacity (CEC) increased with depth, reaching a maximum of 18 meq 100 g^{-1} in 55-70 cm, being more affected by clay than SOC content. Fe_{Ox} and Al_{Ox} – as well as Fe_{Som} and Al_{Som} – were also found to increase with depth, from an average of 1721±63 and 573±12 mg kg^{-1} in 0-20 cm to 2038±82 and 663±27 mg kg^{-1} in 95-110 cm respectively (**Table 3.2**). The ratio between Fe and Al with SOM almost doubled with depth due to their opposite trends within the soil profile. The mineralogical composition of the soil was similar among layers (**Table 3.3**), highlighting the predominance of layered silicates (~66%) – of which 42% were aluminosilicates (muscovite and chlorite-like fraction) – in the carbonate phase (dolomite and calcite, 34%).

3.3.2 Glyphosate adsorption isotherms

The Freundlich equation described with good accuracy the soil-water GLP repartition (**Table 3.4**, $R^2 \geq 0.90$) for all depths and in the different management systems (**Figure 3.2**). The 1/n parameter was always < 1, suggesting that non-linear adsorption occurred in all cases. Some 1/n reduction was found at increasing depth of investigation, which revealed the skewness of the curve was enhanced along the soil profile. To note that at 55-70 cm layer, 1/n reached the lowest average value (0.39±0.00), and then increased again (0.60±0.06 at 95-110 cm) regardless the groundwater and cultivation management. On the contrary, K_f has always increased with soil depth, highlighting that GLP-soil particle interaction was enhanced from 0-20 cm (27.5±2.0) to 20-40 cm (46.5±2.1), 55-70 cm (56.0±2.7) and 95-110 cm (74.0±3.7).

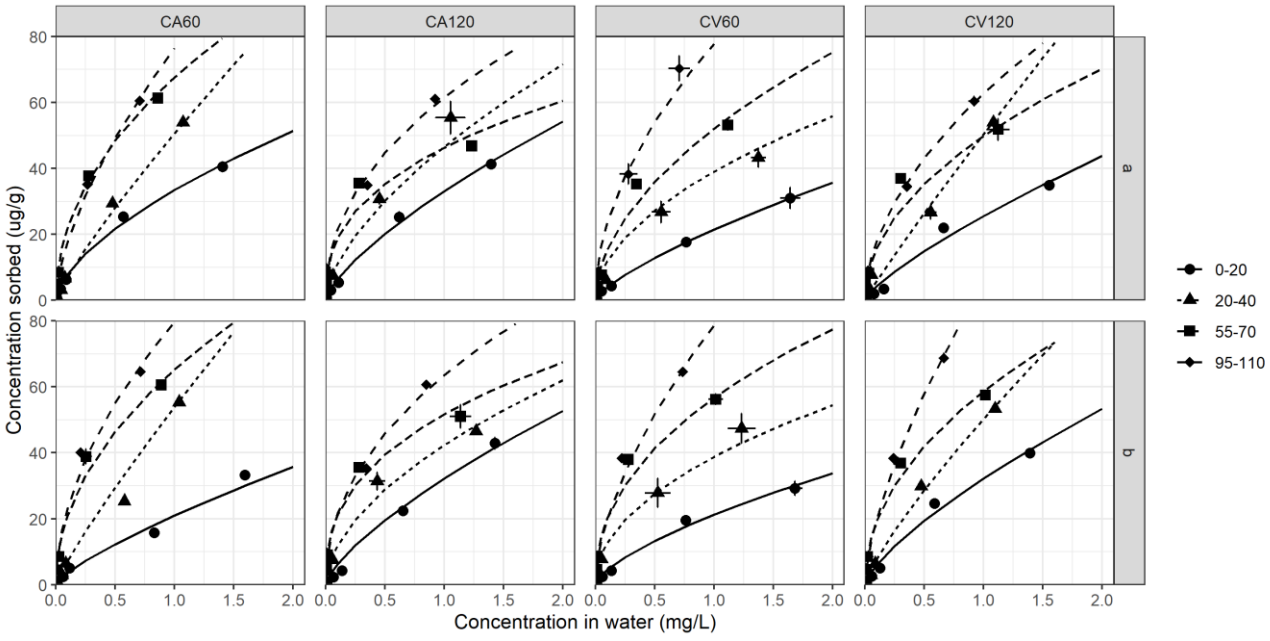

Figure 3.2. Freundlich adsorption isotherms of GLP at different depths in the four treatments and replicates. Symbols are observed values reported as the mean ± standard error and lines represent the fitting curves.

Several soil properties significatively affected GLP adsorption (**Table 3.5**), positively like clay and CEC (r = 0.75 and 0.62), and negatively like Olsen P, SOC content and EC (r =-0.57, -0.69 and -0.67 respectively). Furthermore, SOM-chelated Al and Fe – reported as Al_{Som}/SOM and Fe_{Som}/SOM – slightly influenced GLP adsorption, having r = 0.37 in both ($p < 0.05$).

Table 3.4. Freundlich adsorption coefficients averaged between replicates (K_f and 1/n) for GLP for different treatments and different soil depths ± standard errors. The significance is reported for depths and treatments: values followed by the same letter are not statistically different at $p > 0.05$.

Treatment	Depth	K_f	1/n	R^2
CA60	0-20	27.2± 6.2	0.78± 0.16	0.905
	20-40	52.3± 1.6	0.86± 0.01	0.985
	55-70	66.4± 1.2	0.48± 0.00	0.957
	95-110	78.0± 1.6	0.58± 0.05	0.980
CA120	0-20	32.2± 0.5	0.86± 0.15	0.985
	20-40	44.4± 2.1	0.59± 0.04	0.937
	55-70	49.0± 2.7	0.39± 0.00	0.922
	95-110	62.6± 1.0	0.46± 0.01	0.980
CV60	0-20	21.3± 0.1	0.70± 0.03	0.968
	20-40	38.9± 0.1	0.50± 0.01	0.914
	55-70	54.3± 2.3	0.49± 0.04	0.903
	95-110	78.2± 0.5	0.56± 0.04	0.967
CV120	0-20	28.9± 3.3	0.75± 0.02	0.956
	20-40	50.4± 0.0	0.87± 0.06	0.924
	55-70	54.2± 4.4	0.49± 0.01	0.940
	95-110	77.0± 14.3	0.60± 0.06	0.945

Depth	0-20	27.5±2.0 *c*	0.77±0.05 *a*
	20-40	46.5±2.1 *b*	0.70±0.06 *a*
	55-70	56.0±2.7 *b*	0.46±0.02 *b*
	95-110	74.0±3.7 *a*	0.55±0.03 *b*
Treatment	CA60	56.0±7.3	0.68±0.07
	CA120	47.1±4.1	0.57±0.07
	CV60	48.2±7.9	0.56±0.03
	CV120	52.6±7.1	0.68±0.06

Table 3.5. Pearson's correlation coefficients (r) between estimated Freundlich adsorption coefficients (K_f and 1/n) for GLP and selected soil properties (N=32). Values with ** indicate that the correlation is significant at 0.01 level, and * at 0.05.

	Sand	Silt	Clay	SOC	pH	EC	CEC	Olsen P	Al_{Ox}	Fe_{Ox}	Al_{Som}/SOM	Fe_{Som}/SOM	K_f
Sand	-												
Silt	-0.951**	-											
Clay	-0.892**	0.709**	-										
SOC	0.584**	-0.464**	-0.655**	-									
pH	-0.552**	0.440*	0.618**	-0.853**	-								
EC	0.438*	-0.326	-0.523**	0.720**	-0.897**	-							
CEC	-0.736**	0.603**	0.798**	-0.697**	0.666**	-0.547**	-						
P Olsen	0.607**	-0.486**	-0.677**	0.859**	-0.869**	0.737**	-0.716**	-					
Al_{Ox}	-0.278	0.197	0.346	-0.575**	0.471**	-0.358*	0.422*	-0.540**	-				
Fe_{Ox}	-0.247	0.211	0.255	-0.502**	0.428*	-0.365*	0.335	-0.438*	0.917**	-			
Al_{Som}/SOM	-0.478**	0.434*	0.456**	-0.723**	0.674**	-0.501**	0.641**	-0.642**	0.725**	0.658**	-		
Fe_{Som}/SOM	-0.461**	0.425*	0.432*	-0.695**	0.648**	-0.468**	0.617**	-0.579**	0.670**	0.610**	0.987**	-	
K_f	-0.671**	0.533**	0.753**	-0.690**	0.692**	-0.671**	0.621**	-0.573**	0.311	0.300	0.373*	0.370*	-
1/n	0.578**	-0.512**	-0.571**	0.709**	-0.592**	0.411*	-0.712**	0.729**	-0.482**	-0.516**	-0.671**	-0.646**	-0.408*

3.3.3 Glyphosate and AMPA concentration in soil

At the soil surface (0-1 cm), GLP was found at very high concentrations (**Table 3.6**), ranging from 9174 to 13529 µg kg^{-1} a few hours after the distribution (day 0, hereafter referred to C_0). After 18 days, GLP sharply decreased compared to the initial concentration (from -88.3% to a maximum of -97.2%), ending to an almost complete dissipation on day 27, when GLP was less than 1.5% of C_0.

Table 3.6. GLP and AMPA concentration in the soil surface (0-1 cm layer) at increasing day intervals in the eight lysimeters. Day 0 refers to the day of herbicide distribution (May 10, 2019). The percentage of GLP dissipated and the formation of AMPA (GLP_{Diss} and $AMPA_{Formed}$) are also reported.

		GLP	AMPA	GLP_{Diss}	$AMPA_{Formed}$
Treatment	**Day**	**µg/kg**	**µg/kg**	**%**	**%**
	0	13525.7	1121.8		11.2
CA60 a	18	472.2	579.1	96.5	5.8
	27	112.8	233.6	99.2	2.3
	0	13418.5	1022.1		10.3
CA60 b	18	377.3	536.8	97.2	5.4
	27	70.4	90.6	99.5	0.9
	0	9174.3	656.9		9.8
CA120 a	18	681.4	516.1	92.6	7.7
	27	87.1	179.1	99.1	2.7
	0	10734.7	531.2		7.0
CA120 b	18	810.7	516.7	92.4	6.8
	27	87.1	256.8	99.2	3.4
	0	12034.8	1812.4		18.6
CV60 a	18	779.1	1042	93.5	10.7
	27	153.3	411.8	98.7	4.2
	0	13524.1	1884.9		17.4
CV60 b	18	1586	1447.7	88.3	13.4
	27	254.4	499.3	98.1	4.6
	0	12904	1977.2		18.8
CV120 a	18	782.1	1282.7	93.9	12.2
	27	148.6	490.6	98.8	4.7
	0	13529	2137.3		19.3
CV120 b	18	1102.5	1309.1	91.9	11.8
	27	104.6	258.9	99.2	2.3

Generally, CA showed a lower amount of GLP at day 0 (11713±1064 µg kg^{-1}) than CV (12998±353 µg kg^{-1}), due to the presence of rye which intercepted part of the herbicide spray.

As for the parent molecule, AMPA was already detected few hours after the distribution with a significant difference between treatments, being the average concentration of 833±142 and 1953±70 µg kg^{-1} in CA and CV, respectively. A similar difference was found on day 18 when the average AMPA concentration was 537±15 in CA and 1270±84 µg kg^{-1} in CV. At day 18, the AMPA reduction was 48% in CA60 and 12% in CA120, highlighting different rates of transformation/dissipation according to WT. After 27 days, AMPA in CA was reduced to 190±37 and in CV to 415±56 µg kg^{-1}. A different dynamic between crop managements was found at 0-5 and 5-15 cm depth (**Table 3.7**). Infact, GLP was always < LOQ in CA in both layers, suggesting that a full dissipation already occurred at day 42. In CV, GLP was found in 2 out of 4 times in both sampling days 42 and 56 at 0-5 cm depth, mostly with a shallower water table. Conversely, AMPA was detected in CA in 3 out of 4 samples (42 days, 81.1±5.6 µg kg^{-1}) at 0-5 cm, and down to 15 cm only in one lysimeter at 56 days. In CV, the metabolite was always detected on both layers (157.3±45.3 and 90.5±16.6 µg kg^{-1} at 0-5 and 5-15 cm respectively at 42 days), except for CV120a where AMPA was < LOQ at 0-5 cm on day 56.

Table 3.7. GLP and AMPA concentration in soil at 0-5 and 5-15 cm at 42 and 56 days after application in the eight lysimeters. When the molecule concentration was below the limit of quantification, "<LOQ" is reported in the Table.

Treatment	Day	GLP		AMPA	
		0-5 cm µg/kg	5-15 cm µg/kg	0-5 cm µg/kg	5-15 cm µg/kg
CA60 a	42	< LOQ	< LOQ	72.2	< LOQ
	56	< LOQ	< LOQ	68.0	< LOQ
CA60 b	42	< LOQ	< LOQ	< LOQ	< LOQ
	56	< LOQ	< LOQ	< LOQ	< LOQ
CA120 a	42	< LOQ	< LOQ	91.5	< LOQ
	56	< LOQ	< LOQ	< LOQ	< LOQ
CA120 b	42	< LOQ	< LOQ	79.7	< LOQ
	56	< LOQ	< LOQ	< LOQ	78.7
CV60 a	42	98.3	< LOQ	239.7	140.1
	56	86.3	48.7	214.1	94.8
CV60 b	42	< LOQ	< LOQ	72.2	78.0
	56	52.6	48.7	170.8	101.0
CV120 a	42	69.3	< LOQ	231.6	68.0
	56	< LOQ	< LOQ	< LOQ	137.7
CV120 b	42	< LOQ	< LOQ	85.8	76.0
	56	< LOQ	< LOQ	81.9	90.4

3.3.4 Glyphosate and AMPA dynamic in soil pore-water

A total of 142 pore-water samples were collected and analyzed for GLP and AMPA content. GLP was > LOQ in 53% of CA samples with deep water table level (120 cm), a frequency that increased to 81% in CV60. The maximum peak of GLP was reached after 4 days at 15 cm depth (**Figure 3.3**), with the highest detected in CV120a (131.1 µg l^{-1}) and the lowest in CA60b (42.3 µg l^{-1}). On the same day, GLP was found at 60 cm depth at concentrations ranging from 20.5 to 94.1 µg l^{-1} (in CA60a and CV60b respectively). In some cases, the maximum peak at 30 and 60 cm depth was delayed at day 7 instead of 4. After 7 days, GLP concentration started to decrease mostly at 15 cm and after 11 days, it was sharply reduced to an average value of 4.1±1.9 µg l^{-1}. In intermediate and deepest layers, GPL was only occasionally detected. Some lysimeters showed a delayed increment, like CA60a at 15 cm (day 38, 33.1 µg l^{-1}) and CV60b at 30 cm depth (day 24, 54.2 µg l^{-1}). Moreover, at WT60 and 60 cm sampling depth, GLP reached an average of 6.9±0.2 µg l^{-1} after 20 days, which only slightly changed until the end of the experiment (**Figure 3.3**). In general, CV lysimeters showed higher GLP concentration at 15 cm – 18.9±8.0 and 30.3±13.3 µg l^{-1} for CV60 and CV120 respectively – then decreasing at 30 and 60 cm.

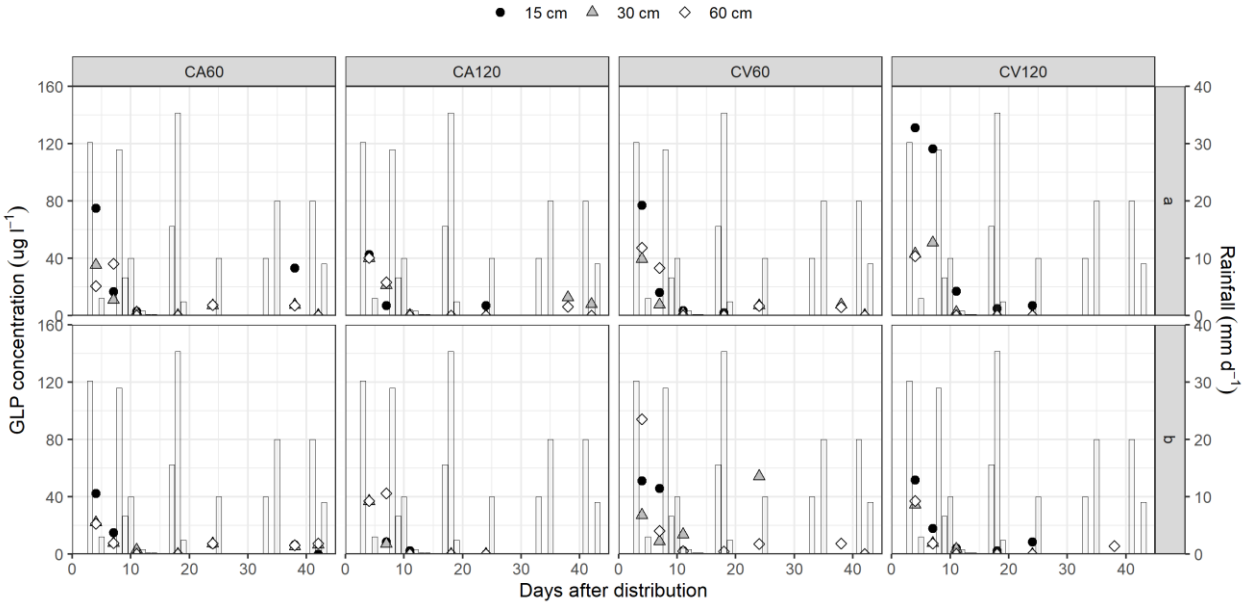

Figure 3.3. GLP concentration in soil pore-water at the three different depths (15 cm - black circle, 30 cm - grey triangle, 60 cm - white rhombus) for the eight studied lysimeters. Bars refer to simulated rainfall amount (mm) during the sampling period.

Contrary to GLP, AMPA was detected only in 5% of CA, regardless the water table level, 14% of samples in CV60 and 32% in CV120. It was only found at 15 cm, starting from day 4 until 24 after the distribution (**Figure 3.4**), while at 60 cm it was only detected in CV120a after 7 days (2.7 µg l^{-1}).

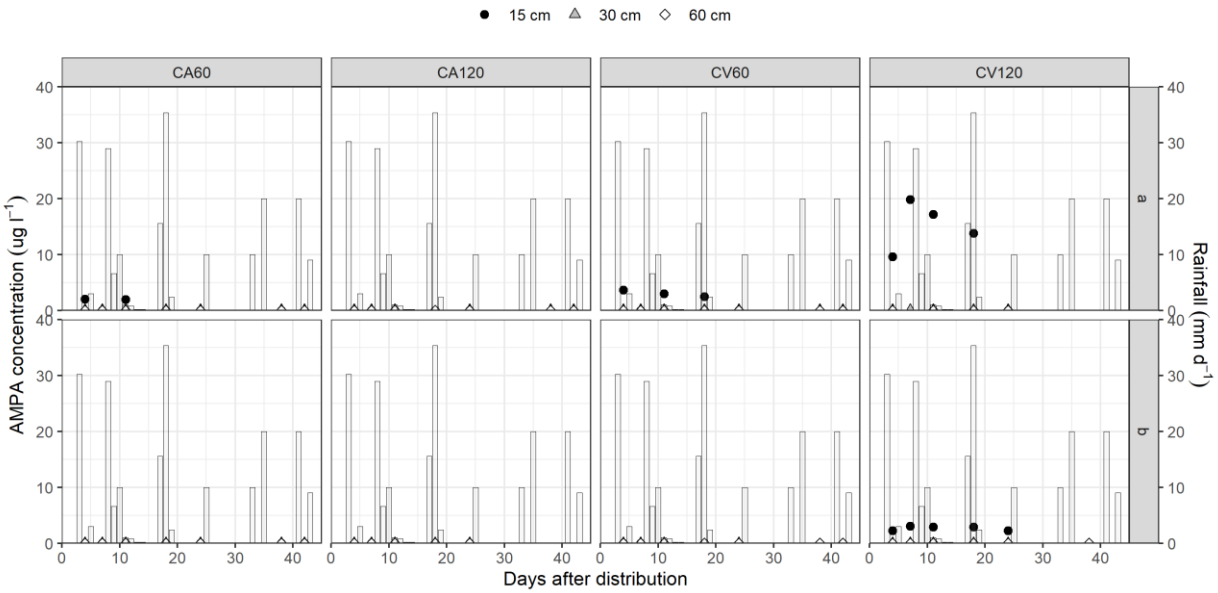

Figure 3.4. AMPA concentration in soil pore-water at the three different depths (15 cm - black circle, 30 cm - grey triangle, 60 cm - white rhombus) for the eight studied lysimeters. Bars refer to simulated rainfall amount (mm) during the sampling period.

3.3.5 Glyphosate and AMPA in the groundwater

During the experiment, groundwater was monitored from May 14 (day 4) to June 27 (day 48) for a total of 44 analyses. The GLP detection frequency was higher in CV than CA (**Figure 3.5**). On day 4, GLP was firstly detected in all lysimeters after 30 mm of rainfall, at an average concentration of 7.2±0.1 µg l^{-1}. On day 6, GLP was found in WT120, ranging from 7.5 to 22.1 µg l^{-1}, while it was < LOQ in WT60 (except for CV60b). After a cumulative rainfall of 51 mm (i.e. 17-18 days from the herbicide distribution), GLP was detected again in all lysimeters at concentrations of 6.9±0.3 µg l^{-1}. The concentration was < LOQ in almost all cases after 38 days, while at day 48 GLP only occurred in CV (2 out of 4 lysimeters). All along the experimentation, GLP median concentrations were lower in CA (WT60 and WT120 were 0.3±1.1 and 3.4±2.4 µg l^{-1}) than CV (WT60 and WT120 were 6.6±1.5 and 7.0±1.5 µg l^{-1}), but the high variability made differences not statistically significant $p<0.05$ (**Figure 3.6**). Contrary to GLP, AMPA was always < LOQ in the groundwater.

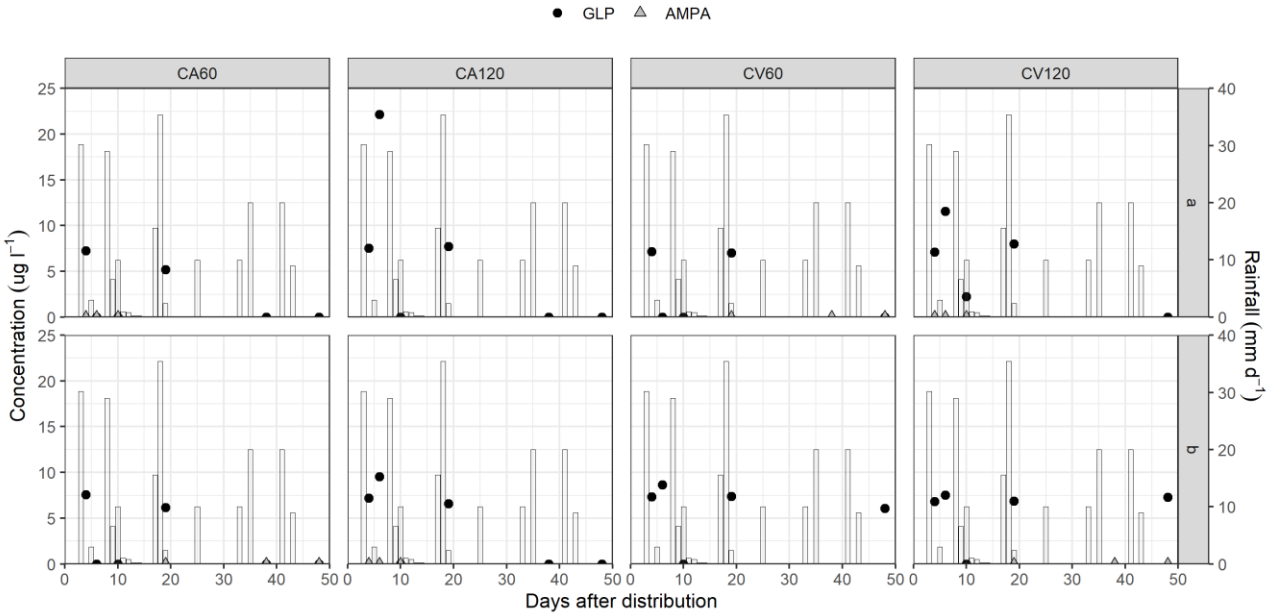

Figure 3.5. GLP (black circles) and AMPA (grey triangles) concentration in groundwater for the eight studied lysimeters. Bars refer to simulated rainfall amount (mm) during the sampling period.

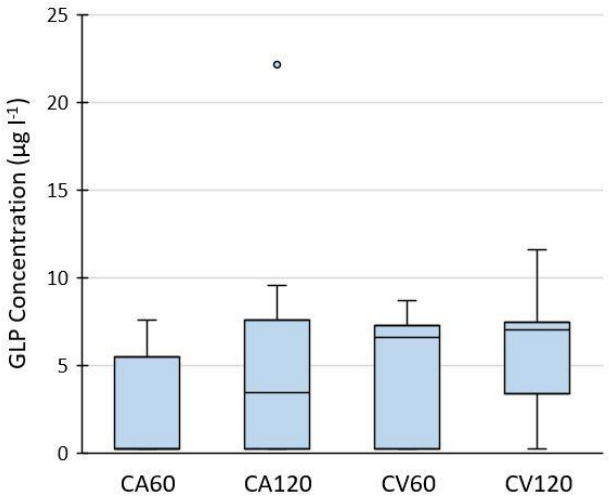

Figure 3.6. Glyphosate concentration in groundwater for the four treatments. Blue rhombuses refer to the median value for each treatment.

3.4 Discussion

3.4.1 Adsorption of glyphosate and AMPA to soil particles

Results about GLP adsorption isotherms indicated that most of the variability was observed with depth, regardless the management practices. The adsorption coefficient (K_f) resulted approximately three times greater in the deepest layer than in the surface layer, and 1/n decreased at increasing depth. Despite such variability, it was generally observed a low affinity for the soil phase of the Cambisol under investigation, with K_f that never exceeded 80, which is a relatively low coefficient compared to other studies (Candela et al., 2007; Piccolo et al., 1994; Okada et al., 2016). This might be explained by the alkaline reaction of the soil under investigation, which has maximized the negative electrical charges of GLP at high pH, thus limiting its adsorption to soil particles due to its polyprotic nature (De Gerónimo and Aparicio, 2021; Borggaard and Gimsing, 2008). Similar values were found by Accinelli et al. (2005), which performed an adsorption study on a surface soil layer (0-20 cm) having pH = 8.1 and clay content similar to ours (14%), resulting in a K_f of 43. Conversely, other authors reported higher adsorption than ours (K_f = 166) at lower pH (6.1) and similar clay content (17%) (Autio et al., 2004). Noteworthy is also the work of Carretta et al. (2021a), which analyzed GLP adsorption in the same soil as in the present study, but only in the surface layer. The authors compared the effect of conventional and no-tillage practices on GLP adsorption, highlighting a K_f that was statistically lower in the first than in the second treatment (around 28 and 51, respectively) in the 0-20 cm profile. In our study, the surface layer K_f was on average 27.5±2 and did not statistically differ between treatments (**Table 3.6**). The missing difference between agricultural management can be due to the recent conversion of the soil to CA practices (about 2 years) which might have masked the potential effect of CA on the adsorption dynamic of GLP, e.g., due to an increase in SOC (Page et al., 2020; Patle et al., 2013) which might favor the formation of poorly-order Fe and Al oxides (Borggaard and Gimsing, 2008). In the present work, the slight difference in soil properties between CA and CV, did not affect differently K_f between managements. Similarly, the WT management did not affect significantly the GLP adsorption, suggesting that a prolonged change in soil moisture condition was not a driver able to modify the physicochemical soil properties that could affect it.

Multiple soil properties contributed to the adsorption dynamic of GLP in the studied soil (**Table 3.5**), as emphasized by the positive correlation of K_f with both clay and CEC, and the negative one with phosphorus (Olsen P) that emphasized the strong competition for the same sorption sites (De Jonge et al., 2001; Gimsing and Borggaard, 2002; Munira et al., 2016). This phenomenon is particularly relevant in intensive agricultural systems such as those of the low-lying Venetian plain, where progressive saturation of soil sorption capacities can occur due to continuous application of P-rich mineral and organic fertilizers (Pizzeghello et al., 2011), enhancing the risk of GLP mobility to groundwater. This was also corroborated by the positive correlation that was found between 1/n and Olsen P (**Table 3.7**), which suggests a low rate of GLP sorption (1/n closer to 1) onto soil particles as the competition with P increased. The SOC content, like EC, seemed to have a negative influence on K_f: In this case, the effect of repulsive negative charges of SOM might have blocked available sorption sites for GLP, reducing its adsorption (Borggaard and Gimsing, 2008). Despite GLP is in general highly adsorbed onto variable-charged surfaces, like Al and Fe oxides, no significant correlations were found between K_f and Al_{Ox} or Fe_{Ox}. On the contrary, SOM-chelated Al and Fe, which are metals complexed with humic substances, have likely acted as metal bridges (Gerke, 2010), influencing GLP sorption in a limited way, due to the increasing Al and Fe amount at equal SOM along with the soil profile (**Table 3.2**), as also found in other northern soils of the Veneto region (Mencaroni et al., 2022). A strong correlation was found between 1/n and Al and Fe bound to SOM, as with poorly-ordered Al and Fe oxides, suggesting that at high Al and Fe content the non-linearity of the curve increased, thus reflecting a tendency to decrease the sorption at increasing GLP concentrations in solution. Worth of note was also the slight change in the soil mineralogy found at different soil depths (**Table 3.3**), such as the calcite that was found to increase along the soil profile. Some authors reported that anionic pesticides are slightly adsorbed by calcite (Clausen et al., 2001), indicating that this fraction cannot play a major role in pesticides adsorption as compared with clay and oxide minerals (e.g. gibbsite or ferrihydrite), but may emphasize it. In addition, the mineralogical composition of the soil was characterized by the predominance of silicate minerals. Although layered silicates have only few permanent and negatively charged adsorption sites (OH groups) in the octahedral layer (Borggaard and Gimsing, 2008) and are a limited source of exchangeable cations in soils due to the low CEC (Kumari and Mohan, 2021), it can be hypothesized a complexation of GLP by

cations released from clay silicates via a cation-exchange reaction with solution protons, as reported by Glass (1987).

3.4.2 Mobility and occurrence of glyphosate and AMPA along the soil profile

Glyphosate in water was detected soon after its application at all depths and in groundwater, regardless of agricultural and WT management, emphasizing the likely occurrence of bypass flow and reduced GLP adsorption when rainfall time was close to its distribution (Jarvis, 2007), enhancing the leaching potential of the molecule to the groundwater (Székács et al., 2015; Pazikowska-Sapota et al., 2020). Despite the Cambisol under investigation being poorly structured, previous research that combined modeling and X-ray µCT analysis demonstrated that shallow water table conditions can enhance solute movement through non-equilibrium preferential pathways (Mencaroni et al., 2021) due to a pronounced macropore structure, emphasizing the risk of groundwater contamination. When more time passed since the GLP application, further detection of GLP in soil and water showed different mobility according to the agricultural system and WT management. Particularly, after 24 days GLP was detected at 30 and 60 cm depth only in WT60 (18.8±11.8 and 7.1±0.1 µg l^{-1} respectively), and once again on day 38 at concentrations of 6.7± 0.7 and 6.5± 0.4 µg l^{-1} at the same depths. In contrast, GLP concentration was < LOQ in WT120 at both depths on day 24, and only sporadically found on days 38 and 42. Mencaroni et al. (2021) found that under close-to-saturation conditions only the non-capillary macropores were empty, as in the surface layer of WT60. In such conditions, additional water input would converge part of water and solutes stored in the soil matrix into preferential pathway (Radolinski et al., 2022) by making the macropores more active (Krzeminska et al., 2014).

Consequently, the risk of fast movement and contamination may occur even in case of leaching events far from spraying distribution (Milan et al., 2022), especially when shallow water table conditions occur. When detected in the groundwater, GLP was found in WT60 up to 48 days after the distribution only in CV lysimeters (**Figure 3.5**), and generally at concentrations much higher than the European drinking water limit (0.1 µg l^{-1}). Glyphosate was mostly found in concomitance of a high water input (≥ 30 mm), which has increased the leaching transport of the molecule. However, it must be noted that such intense rainfall events

are not as common as usually monitored in the study area (Dal Ferro et al., 2017), emphasizing that GLP fast movement and findings in the groundwater might be partially overestimated.
On the other hand, AMPA was seldom detected in the pore-water at 15 cm depth (**Figure 3.4**), mostly in CV lysimeters, emphasizing a diverse occurrence between agricultural systems. Furthermore, AMPA had never reached the groundwater in all treatments, suggesting different adsorption and transport dynamics in soil compared to the parent molecule. This was likely due to the higher adsorption potential of AMPA than GLP towards soil (Sidoli et al., 2016) which might have reduced the mobility and in turn its transport through the soil matrix. Regarding the dynamic in soil, in this study, dissipation rates were not estimated but concentrations of the herbicide found at the surface layer supported the hypothesis of a slightly faster dissipation of GLP under CA compared to CV management. A minor amount of GLP reached the soil surface in the case of CA (-10%), due to the presence of rye which partially intercepted the spray. Besides the effect of crop interception, it is important to highlight that on day 18 in CA, on average, only 5±1% of the initial amount of GLP was still detected in the surface layer, compared to the 8±1% left in CV. To note that GLP was < LOQ down to 15 cm after 42 days in CA (**Table 3.5**), but AMPA only occasionally. On the contrary, GLP and AMPA were still found in CV, suggesting faster mobility under conventional than conservation management. Furthermore, a faster AMPA formation was found at day 0 in CV compared to CA, likely due to the higher amount of GLP that reached the ground in bare soil and to a likely diverse contribution of the microbial degradation according to soil management (Habig and Swanepoel, 2015).

3.5 Conclusion

Our findings did not fully support the hypothesis that conservation practices during the transition period affected GLP dynamics in soil and water under shallow groundwater conditions. Indeed, GLP adsorption did not discriminate between different shallow water tables and agricultural systems, rather was the soil layering that modified GLP adsorption properties resulting to be mostly affected by clay fraction, SOC content, P Olsen and the presence of Al and Fe bonded to SOM. Neither two-year agricultural management nor long-term shallow water table conditions were effective drivers that did not modify the main physicochemical properties that affect adsorption. In contrast, the tested treatments affected dissipation and movement dynamics of both GLP and AMPA. Glyphosate transport through the soil profile was fast, with the likely formation of non-equilibrium preferential pathways that allowed GLP to bypass the soil matrix and directly reach the groundwater soon after its application. In particular, the shallower water table (WT60) increased the solute mobility down to the deepest layer. AMPA never reached the groundwater, being detected only at 15 cm depth. Despite differentiation between agricultural systems were still transitory and did not change the main soil properties, a higher dissipation of GLP and AMPA was found when conservation agriculture was adopted. It follows that the peculiar management conditions of CA, such as the occurrence of surface residues and a faster degradation in soil, might have mitigated the risk of groundwater contamination.

References

Accinelli, C., Koskinen, W.C., Seebinger, J.D., Vicari, A., Sadowsky, M.J., 2005. Effects of incorporated corn residues on glyphosate mineralization and sorption in soil. J. Agric. Food Chem. 53, 4110–4117. https://doi.org/10.1021/jf050186r

Antier, C., Kudsk, P., Reboud, X., Ulber, L., Baret, P. V., Messéan, A., 2020. Glyphosate use in the European agricultural sector and a framework for its further monitoring. Sustain. 12, 1–22. https://doi.org/10.3390/su12145682

Autio, S., Siimes, K., Laitinen, P., Rämö, S., Oinonen, S., Eronen, L., 2004. Adsorption of sugar beet herbicides to Finnish soils. Chemosphere 55, 215–226. https://doi.org/10.1016/j.chemosphere.2003.10.015

Basch, G., Friedrich, T., Kassam, A., Gonzalez-Sanchez, E., 2015. Conservation Agriculture in Europe, in: Farooq, M., Siddique, K. (Eds.), Conservation Agriculture. Springer, Cham, pp. 357–389.

Bascomb, C.L., 1968. Distribution of pyrophosphate-extractable iron and organic carbon in soils of various groups. J. Soil Sclence.

Benbrook, C.M., 2016. Trends in glyphosate herbicide use in the United States and globally. Environ. Sci. Eur. 28, 1–15. https://doi.org/10.1186/s12302-016-0070-0

Bento, C.P.M., Yang, X., Gort, G., Xue, S., van Dam, R., Zomer, P., Mol, H.G.J., Ritsema, C.J., Geissen, V., 2016. Persistence of glyphosate and aminomethylphosphonic acid in loess soil under different combinations of temperature, soil moisture and light/darkness. Sci. Total Environ. 572, 301–311. https://doi.org/10.1016/j.scitotenv.2016.07.215

Bittelli, M., Andrenelli, M.C., Simonetti, G., Pellegrini, S., Artioli, G., Piccoli, I., Morari, F., 2019. Shall we abandon sedimentation methods for particle size analysis in soils? Soil Tillage Res. 185, 36–46. https://doi.org/10.1016/j.still.2018.08.018

Borggaard, O.K., Gimsing, A.L., 2008. Fate of glyphosate in soil and the possibility of leaching to ground and surface waters : a review 456, 441–456. https://doi.org/10.1002/ps

Camarotto, C., Dal Ferro, N., Piccoli, I., Polese, R., Furlan, L., Chiarini, F., Morari, F., 2018. Conservation agriculture and cover crop practices to regulate water, carbon and nitrogen cycles in the low-lying Venetian plain. Catena 167, 236–249. https://doi.org/10.1016/j.catena.2018.05.006

Candela, L., Álvarez-Benedí, J., Condesso de Melo, M.T., Rao, P.S.C., 2007. Laboratory studies on glyphosate transport in soils of the Maresme area near Barcelona, Spain: Transport model parameter estimation. Geoderma 140, 8–16. https://doi.org/10.1016/j.geoderma.2007.02.013

Carretta, L., Cardinali, A., Marotta, E., Zanin, G., Masin, R., 2019. A new rapid procedure for simultaneous determination of glyphosate and AMPA in water at sub μg/L level. J. Chromatogr. A 1600, 65–72. https://doi.org/10.1016/j.chroma.2019.04.047

Carretta, L., Cardinali, A., Onofri, A., Masin, R., Zanin, G., 2021a. Dynamics of Glyphosate and Aminomethylphosphonic Acid in Soil Under Conventional and Conservation Tillage. Int. J. Environ. Res. https://doi.org/10.1007/s41742-021-00369-3

Carretta, L., Masin, R., Zanin, G., 2021b. Review of studies analysing glyphosate and aminomethylphosphonic acid (AMPA) occurrence in groundwater. Environ. Rev. 1–22. https://doi.org/https://doi.org/10.1139/er-2020-0106

Chakraborty, P., Singh, N., Bansal, S., Sekaran, U., Sexton, P., Bly, A., Anderson, S.H., Kumar, S., 2022. Soil & Tillage Research Does the duration of no-till implementation influence depth distribution of soil organic carbon , hydro-physical properties , and computed tomography-derived macropore characteristics ? Soil Tillage Res. 222, 105426. https://doi.org/10.1016/j.still.2022.105426

Clausen, L., Fabricius, I., Madsen, L., 2001. Adsorption of Pesticides onto Quartz, Calcite, Kaolinite, and α-Alumina. J. Environ. Qual. 30, 846–857. https://doi.org/10.2134/jeq2001.303846x

Cueff, S., Alletto, L., Bourdat-Deschamps, M., Benoit, P., Pot, V., 2020. Water and pesticide transfers in undisturbed soil columns sampled from a Stagnic Luvisol and a Vermic Umbrisol both cultivated under conventional and conservation agriculture. Geoderma 377, 114590. https://doi.org/10.1016/J.GEODERMA.2020.114590

Dal Ferro, N., Camarotto, C., Piccoli, I., Berti, A., Mills, J., Morari, F., 2020. Stakeholder Perspectives to Prevent Soil Organic Matter Decline in Northeastern Italy. Sustainability 12, 378. https://doi.org/10.3390/su12010378

Dal Ferro, N., Zanin, G., Borin, M., 2017. Crop yield and energy use in organic and conventional farming: A case study in north-east Italy. Eur. J. Agron. 86, 37–47. https://doi.org/10.1016/j.eja.2017.03.002

De Gerónimo, E., Aparicio, V.C., 2021. Changes in soil pH and addition of inorganic phosphate affect glyphosate adsorption in agricultural soil. Eur. J. Soil Sci. 1–16. https://doi.org/10.1111/ejss.13188

De Jonge, H., De Jonge, L.W., Jacobsen, O.H., Yamaguchi, T., Moldrup, P., 2001. Glyphosate sorption in soils of different pH and phosphorus content. Soil Sci. 166, 230–238. https://doi.org/10.1097/00010694-200104000-00002

de Jonge, L.W., Kjaergaard, C., Moldrup, P., 2004. Colloids and colloid-facilitated transport of contaminants in soils: An introduction. Vadose Zo. J. 3, 321–325. https://doi.org/10.2113/3.2.321

EFSA, 2015. Conclusion on the peer review of the pesticide risk assessment of the active substance glyphosate. EFSA J. 13. https://doi.org/10.2903/j.efsa.2015.4302

FAO-UNESCO, 2008. Soil map of the world. Revised Legend, FAO, Rome.

Gerke, J., 2010. Humic (organic matter)-Al(Fe)-phosphate complexes: An underestimated

phosphate form in soils and source of plant-available phosphate. Soil Sci. 175, 417–425. https://doi.org/10.1097/SS.0b013e3181f1b4dd

Gilbert, R.O., 1988. Statistical Methods for Environmental Pollution Monitoring, Technometrics. https://doi.org/10.2307/1270090

Gimsing, A.L., Borggaard, O.K., 2002. Effect of phosphate on the adsorption of glyphosate on soils, clay minerals and oxides. Int. J. Environ. Anal. Chem. 82, 545–552. https://doi.org/10.1080/0306731021000062964

Glass, R.L., 1987. Adsorption of glyphosate by soils. J. Agric. Food Chem. 35, 497–500. https://doi.org/10.1002/ps.2780070407

Haarstad, K., Ludvigsen, G.H., 2007. Ten years of pesticide monitoring in norwegian ground water. Gr. Water Monit. Remediat. 27, 75–89. https://doi.org/10.1111/j.1745-6592.2007.00153.x

Habig, J., Swanepoel, C., 2015. Effects of conservation agriculture and fertilization on soil microbial diversity and activity. Environ. - MDPI 2, 358–384. https://doi.org/10.3390/environments2030358

Jarvis, N.J., 2007. A review of non-equilibrium water flow and solute transport in soil macropores: principles, controlling factors and consequences for water quality. Eur. J. Soil Sci. 71, 279–302. https://doi.org/10.1111/ejss.12973

Khalil, Y., Flower, K., Siddique, K.H.M., Ward, P., 2018. Effect of crop residues on interception and activity of prosulfocarb, pyroxasulfone, and trifluralin. PLoS One 13, e0208274. https://doi.org/10.1371/JOURNAL.PONE.0208274

Kjær, J., Ernsten, V., Jacobsen, O.H., Hansen, N., de Jonge, L.W., Olsen, P., 2011. Transport modes and pathways of the strongly sorbing pesticides glyphosate and pendimethalin through structured drained soils. Chemosphere 84, 471–479. https://doi.org/10.1016/j.chemosphere.2011.03.029

Krzeminska, D.M., Bogaard, T.A., Debieche, T.H., Cervi, F., Marc, V., Malet, J.P., 2014. Field investigation of preferential fissure flow paths with hydrochemical analysis of small-scale sprinkling experiments. Earth Surf. Dyn. 2, 181–195. https://doi.org/10.5194/esurf-2-181-2014

Kumari, N., Mohan, C., 2021. Basics of Clay Minerals and Their Characteristic Properties. IntechOpen Clay and C. https://doi.org/10.5772/intechopen.97672

Laitinen, P., 2009. Fate of the organophosphate herbicide glyphosate in arable soils and its relationship to soil phosphorus status.

Locke, M.A., Zablotowicz, R.M., Bauer, P.J., Steinriede, R.W., Gaston, L.A., 2005. Conservation cotton production in the southern United States: herbicide dissipation in soil and cover crops. Weed Sci. 53, 717–727. https://doi.org/10.1614/ws-04-174r1.1

Longo, M., Jones, C.D., Izaurralde, R.C., Cabrera, M.L., Dal Ferro, N., Morari, F., 2021. Testing

the EPIC Richards submodel for simulating soil water dynamics under different bottom boundary conditions. Vadose Zo. J. 1–18. https://doi.org/10.1002/vzj2.20142

Lutri, V.F., Matteoda, E., Blarasin, M., Aparicio, V., Giacobone, D., Maldonado, L., Becher Quinodoz, F., Cabrera, A., Giuliano Albo, J., 2020. Hydrogeological features affecting spatial distribution of glyphosate and AMPA in groundwater and surface water in an agroecosystem. Córdoba, Argentina. Sci. Total Environ. 711, 134557. https://doi.org/10.1016/j.scitotenv.2019.134557

McKeague JA, Brydon JE, Miles NM, 1971. Differentiation of Forms of Extractable Iron and Aluminum in Soils 35, 33–38.

Mencaroni, M., Dal Ferro, N., Redcliffe, D., Morari, F., 2021. Preferential solute transport under variably saturated conditions in a silty loam soil: is the shallow water table a driving factor? J. Hydrol. 602.

Mencaroni M., Cardinali A., Costa L., Morari F., Salandin P., Zanin G. and Dal Ferro N. (2022), Glyphosate and AMPA have low mobility through different soil profiles of the prosecco wine production area: A monitoring study in north-eastern Italy. Front. Environ. Sci. 10:971931. doi: 10.3389/fenvs.2022.97193

Milan, M., Vidotto, F., Fogliatto, S., 2022. Leaching of Glyphosate and AMPA from Field Lysimeters. Agronomy 12. https://doi.org/10.3390/agronomy12020328

Morari, F., 2006. Drainage Flux Measurement and Errors Associated with Automatic Tension-controlled Suction Plates. Soil Sci. Soc. Am. J. 70, 1860. https://doi.org/10.2136/sssaj2006.0009

Morillo, E., Undabeytia, T., Maqueda, C., Ramos, A., 2000. Glyphosate adsorption on soils of different characteristics. Influence of copper addition. Chemosphere 40, 103–107. https://doi.org/10.1016/S0045-6535(99)00255-6

Munira, S., Farenhorst, A., Flaten, D., Grant, C., 2016. Phosphate fertilizer impacts on glyphosate sorption by soil. Chemosphere 153, 471–477. https://doi.org/10.1016/j.chemosphere.2016.03.028

OECD, 2000. OECD 106 Adsorption - Desorption Using a Batch Equilibrium Method. OECD Guidel. Test. Chem. 1–44. https://doi.org/10.1787/9789264069602-en

Okada, E., Costa, J.L., Bedmar, F., 2019. Glyphosate Dissipation in Different Soils Under No-Till and Conventional Tillage. Pedosphere 29, 773–783. https://doi.org/10.1016/S1002-0160(17)60430-2

Okada, E., Costa, J.L., Bedmar, F., 2016. Adsorption and mobility of glyphosate in different soils under no-till and conventional tillage. Geoderma 263, 78–85. https://doi.org/10.1016/j.geoderma.2015.09.009

Okada, E., Costa, J.L., Bedmar, F., Barbagelata, P., Irizar, A., Rampoldi, E.A., 2014. Effect of conventional and no-till practices on solute transport in long term field trials. Soil Tillage

Res. 142, 8–14. https://doi.org/10.1016/j.still.2014.04.002

Ololade, I.A., Oladoja, N.A., Oloye, F.F., Alomaja, F., Akerele, D.D., Iwaye, J., Aikpokpodion, P., 2014. Sorption of Glyphosate on Soil Components: The Roles of Metal Oxides and Organic Materials. Soil Sediment Contam. An Int. J. 23, 571–585. https://doi.org/10.1080/15320383.2014.846900

Page, K.L., Dang, Y.P., Dalal, R.C., 2020. The Ability of Conservation Agriculture to Conserve Soil Organic Carbon and the Subsequent Impact on Soil Physical, Chemical, and Biological Properties and Yield. Front. Sustain. Food Syst. 4, 1–17. https://doi.org/10.3389/fsufs.2020.00031

Patle, G.T., Bandyopadhyay, K.K., Singh, D.K., 2013. Impact of conservation agriculture and resource conservation technologies on carbon sequestration - A review. Indian J. Agric. Sci. 83, 3–13.

Pazikowska-Sapota, G., Galer-Tatarowicz, K., Dembska, G., Wojtkiewicz, M., Duljas, E., Pietrzak, S., Dzierzbicka-Glowacka, L.A., 2020. The impact of pesticides used at the agricultural land of the Puck commune on the environment of the Puck Bay. PeerJ 2020, 1–21. https://doi.org/10.7717/peerj.8789

Piccoli, I., Camarotto, C., Lazzaro, B., Furlan, L., Morari, F., 2017. Conservation Agriculture Had a Poor Impact on the Soil Porosity of Veneto Low-lying Plain Silty Soils after a 5-year Transition Period. L. Degrad. Dev. 28, 2039–2050. https://doi.org/10.1002/ldr.2726

Piccoli, I., Chiarini, F., Carletti, P., Furlan, L., Lazzaro, B., Nardi, S., Berti, A., Sartori, L., Dalconi, M.C., Morari, F., 2016. Disentangling the effects of conservation agriculture practices on the vertical distribution of soil organic carbon . Evidence of poor carbon sequestration in North- Eastern Italy. "Agriculture, Ecosyst. Environ. 230, 68–78. https://doi.org/10.1016/j.agee.2016.05.035

Piccolo, A., Celano, G., Arienzo, M., Mirabella, A., 1994. Adsorption and desorption of glyphosate in some eropean soils.

Pizzeghello, D., Berti, A., Nardi, S., Morari, F., 2011. Phosphorus forms and P-sorption properties in three alkaline soils after long-term mineral and manure applications in north-eastern Italy. Agric. Ecosyst. Environ. 141, 58–66. https://doi.org/10.1016/j.agee.2011.02.011

Prata, F., Lavorenti, A., Regitano, J.B., 2005. Seção Ii - Química E Mineralogia Do Solo Glyphosate Behavior in a Rhodic Oxisol Under No-Till and Conventional 61–69.

R Core Team, 2020. R: A language and environment for statistical computing. R Found. Stat. Comput. Vienna, Austria.

Radolinski, J., Le, H., Hilaire, S.S., Xia, K., Scott, D., Stewart, R.D., 2022. A spectrum of preferential flow alters solute mobility in soils. Sci. Rep. 12, 1–11. https://doi.org/10.1038/s41598-022-08241-w

Sidoli, P., Baran, N., Angulo-Jaramillo, R., 2016. Glyphosate and AMPA adsorption in soils: laboratory experiments and pedotransfer rules. Environ. Sci. Pollut. Res. 23, 5733–5742. https://doi.org/10.1007/s11356-015-5796-5

Silburn, D.M., 2020. Pesticide Retention, Degradation, and Transport Off-Farm. No-till Farming Syst. Sustain. Agric. 281–297. https://doi.org/10.1007/978-3-030-46409-7_17

Sprankle, P., Meggitt, W.F., Penner, D., 1975. Adsorption, mobility and microbial degradation of glyphosate in the soil. Weed Sci. 23, 229–234. https://doi.org/10.1080/03601230802062000

Székács, A., Mörtl, M., Darvas, B., 2015. Monitoring Pesticide Residues in Surface and Ground Water in Hungary: Surveys in 1990–2015. J. Chem. 2015. https://doi.org/http://dx.doi.org/10.1155/2015/717948 Research

U.S. EPA, 1993. Reregistration Eligibility Decision (RED) Glyphosate.

Wahl, N.A., Bens, O., Buczko, U., Hangen, E., Hüttl, R.F., 2004. Effects of conventional and conservation tillage on soil hydraulic properties of a silty-loamy soil. Phys. Chem. Earth, Parts A/B/C 29, 821–829. https://doi.org/10.1016/J.PCE.2004.05.009

Chapter 4. Preferential solute transport under variably saturated conditions in a silty loam soil: is the shallow water table a driving factor?*

*Mencaroni M., Dal Ferro N., Radcliffe D. E., Morari F. (2021). Preferential solute transport under variably saturated conditions in a silty loam soil: Is the shallow water table a driving factor? J. Hydrol. X. 602, 126733. doi: 10.1016/j.jhydrol.2021.126733

Abstract

A shallow water table might enhance preferential solute movement by modifying both the water flow and solute dynamics. In this study, we estimated soil hydraulic and solute transport parameters through a tracer experiment in lysimeters comparing different water table levels. In a set-up of 12 lysimeters, the bottom boundary condition was set as a water table depth of 120 cm, or 60, or as free drainage. A tracer solution of bromide (250 mg l^{-1}, 40 mm) was added to each lysimeter, and soil water was sampled with suction cups at different depths for the following 174 days. Soil water content and matric potential were monitored using TDR probes and electronic tensiometers at the same depths. Soil hydraulic and solute transport parameters in different soil layers were estimated by inverse modeling using HYDRUS 1D. Soil hydraulic parameters were estimated from the Mualem-van Genuchten equations, while both the advection-dispersion (ADE) and physical non-equilibrium mobile-immobile water (MIM) models were used to describe the solute transport. Moreover, the soil pore network was analyzed by means of 3D X-ray microtomography. Results showed different solute dynamics between contrasting water table managements. With free drainage, solute in the immobile domain was negligible, and its transport was fully associated with the mobile water flow. In contrast, a shallow water table affected the tracer transport, by modifying a) the soil pore network, with an increase of the macropores and a reduction of the pore connectivity; b) the flow field, with an increase of immobile water and a reduction of α_{MIM}, indicating slow exchange between mobile and immobile regions, in turn promoting preferential pathways. Hence, groundwater pollution might be worsened by preferential solute transport of agrochemicals occurring with shallow water table conditions.

4.1 Introduction

Nonpoint-source pollution of groundwater caused by fertilizers and agrochemicals is a major issue worldwide (Chae et al., 2004; Wu and Sun, 2016). Although the genesis of diffuse agriculture pollution has been investigated for decades, understanding solute dynamics in the vadose zone is still challenging. Soil hydraulic properties show a nonlinear behavior under variably saturated conditions that can vary greatly, due to spatial and temporal heterogeneity of the soil pore system (Kabat et al., 1997; Vogel et al., 2000), and a favorite soil air displacement by water in the laboratory than field conditions (Basile et al., 2003). Soil structure can be affected by shrinkage or swelling processes due to drying and wetting cycles, or tillage operations, that might increase the formation of macropores (Herbrich and Gerke, 2017; Jirků et al., 2013), and in turn enhance the occurrence of preferential flow pathways (Jarvis et al., 2016; Kumahor et al., 2015).

Further uncertainty in understanding pollutant transport is related to the groundwater table condition. Some studies emphasized that evapotranspiration and upward fluxes increased at shallower water table conditions, thus minimizing drainage and the risk of groundwater pollution (Groh et al., 2016). In contrast, other authors reported that a shorter residence time can be observed in the unsaturated zone when the distance between soil surface and groundwater was reduced by particular meteorological and lower boundary conditions (Haria et al., 2003; Sprenger et al., 2016; Wossenyeleh et al., 2020), besides the type of land use. This condition would lead to a higher probability of the contaminant reaching the groundwater (Rahman, 2008) and a lower degree of pollutant-soil matrix reaction (Maher, 2010).

The water table depth might affect the magnitude of solute movement by changing the water content inside the soil system, likely leading to preferential solute pathways. For instance, Guo and Lin (2018) and Haria et al. (2003) found that preferential solute movement occurred under shallow water table conditions, increasing the risk of solute bypass (Hendrickx and Flury, 2001; Beven and Germann, 1982). It was hypothesized that above the capillary fringe, the water stored in the soil matrix could be moved to preferential flow pathways when a low amount of rainfall is added to the system (Krzeminska et al., 2014). Vegetation could play an additional effect, which in presence of a shallow water table might grow roots until the water pool, leading to the formation of new root channels that enhance macropore flow (Mitchell et al., 1995). Furthermore, preferential flows naturally occur in presence of drying cracks, fissures

and biopores (e.g., caused by earthworms) (Gerke, 2006), when dry soil conditions can favor hydrophobicity (Deurer and Bachmann, 2007), or in soils affected by swelling and shrinking processes depending on soil water content changes (Beven and Germann, 1982). The geometry and connectivity of water flow might change in porous media, where the spatial arrangement between void and solid phases depends on drying-wetting cycles (Sayem and Kong, 2016; Vervoort et al., 1999). This can be originated by shallow water table fluctuations that can affect both soil hydraulic and physical properties, especially within weakly structured soils (Pagliai et al., 1989) or loamy soils with a high organic matter content (Gérard et al., 2004).

Modeling methodologies to predict diffuse nutrient and agrochemical pollution are fundamental to identify management zones (e.g. Nitrate Vulnerable Zones) and assess alternatives of agroecosystem management. Solute movement in both saturated and unsaturated porous media is usually simulated with the advection-dispersion equation (ADE). Application of the ADE under equilibrium conditions requires knowledge of dispersive transport parameters, such as the dispersivity, that are cumbersome to measure directly. They can be estimated by inverse modeling fitting ADE to field transport data (Jury and Roth, 1990). However, difficulties in establishing geochemical conditions (Goldberg and Kabengi, 2010), and incorrect assumptions about water and solute dynamics and boundary conditions (Durner et al., 2007), can lead to unrealistic estimation of transport parameters, such as in the case of non-equilibrium flow. Moreover, inverse modelling can be affected by different optimization strategies that, e.g., consider simultaneously or sequentially different type of observation data (matric potential, solute concentration, etc.) in the objective function (Groh et al., 2018).

Observations conducted at the lysimeter scale can help to assess the solute behavior when they are combined with numerical simulations (Klier et al., 2008; Thuyet et al., 2010). In some circumstances, lysimeters could lead to a bias due to field boundaries that are difficult to reproduce, e.g., providing a lower boundary exposure to atmospheric pressure (Flury et al., 1999; Isch et al., 2019) or the disruption of water flow and the hydraulic gradient due to the bottom of the lysimeter itself. Recently, new technologies have been developed to overcome bottom boundary related problem: Pütz et al. (2016) in a high-precision lysimeter-network adjusted the matric potential at the bottom of the soil profile to the potential measured from the surrounding soil, enabling the upward or downward water flux across the bottom of the lysimeter. A similar process is described in Von Unold and Fank (2008). However, even in their

traditional set-up, they are still key tools to represent real-world conditions in a controlled manner better than laboratory columns.

Here, an experiment was set-up on twelve lysimeters under two different water table depth conditions and free drainage. Lysimeters were equipped with probes for continuous monitoring of soil water content and matric potential at different depths, and with automated suction cups for soil-water sampling. We estimated soil hydraulic and solute transport parameters through a bromide tracer experiment and inverse modeling applying both the ADE and mobile-immobile (MIM) models in a multi-layer soil profile. Our hypothesis was that a shallow water table could affect the solute movement by modifying soil properties and generating preferential solute pathways.

4.2 Materials and Methods

4.2.1 Description of the experimental site

This study was conducted at the Experimental Farm "L. Toniolo" of the University of Padova in Legnaro (45°21′ N; 11°57′ E, 8 m a.s.l.), northeastern Italy. The study site was originally set up in 1984, consisting of twenty 1 m × 1 m × 1.5 m (length × width × depth) drainable lysimeters. The bottom of each lysimeter is funnel-shaped and connected via an underground drain-pipe (1‰ slope) to an external tube equipped with a valve that regulates both the water table level and leaching discharge (**Figure 4.1A**). Each lysimeter was filled in 1984 with soil excavated from the adjacent experimental farm, in a way that preserved the original soil horizons. To facilitate water drainage and prevent soil washout, a 15 cm-thick layer of gravel (30–50 mm diameter) covers the bottom of each lysimeter. The soil is Fluvi-Calcaric Cambisol (FAO-UNESCO, 2008) (**Table 4.1**), which represents about 50% of the low-lying Venetian plain.

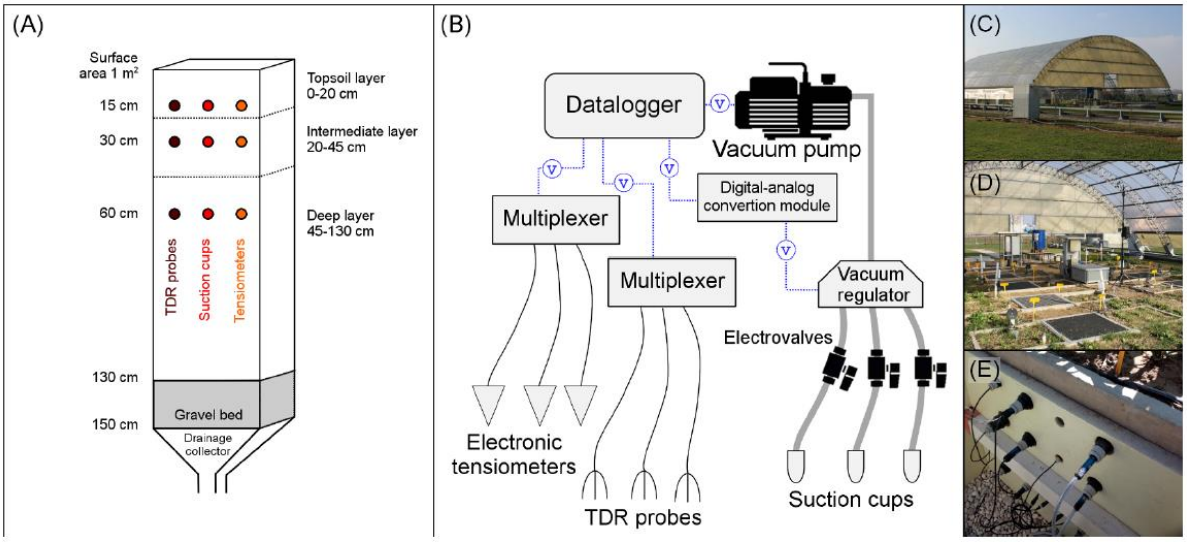

Figure 4.1. Schematic lysimeter and probes design (A), and scheme of the automated monitoring and pore-water sampling (B). Pictures about the experimental site report details about the mobile roof (C), the lysimeter system (D) and the soil probes (E).

Table 4.1. Average soil properties of tested lysimeters.

Soil Properties	**Soil depth**	
	0-60 cm	**60-130 cm**
Sand (%)	36	33
Silt (%)	49	47
Clay (%)	15	20
pH	8.2	8.1
Total Nitrogen (‰)	0.9	1.1
Organic Matter (g $100g^{-1}$)	1.1	1.3
Total Carbonates (%)	33	19
Active Carbonates (%)	4.1	3.2
EC (mS cm^{-1})*	0.28	0.35
Available P (mg kg^{-1})**	16	50
Exchangeable K (mg kg^{-1})**	49	132

*Electrical conductivity
**Available phosphorus
***Exchangeable potassium

Soil particle size distribution (sand, silt and clay content) was determined by using a particle size analyzer (Mastersizer 2000, Malvern Panalytical Ltd, Spectris Company); pH and EC were measured by an electrode in soil suspensions with a soil to water ratio of 1:2.5 and 1:2 (w/v)

respectively: total nitrogen was analyzed with the Kjeldahl method; soil organic carbon content was determined with a CNS-analyzer (vario MACRO cube, Elementar Analysensysteme GmbH); total and active carbonates with the Dietrich-Fruehling calcimeter and ammonium oxalate titration method respectively; available phosphorus with the Olsen method and exchangeable potassium by the extraction with ammonium acetate. An automated mobile roof was built over the whole area, allowing control of rain events and water fluxes on lysimeters and preserving the site from destructive weather events. A weather station (Decagon Devices Inc., Pullman, WA) consisting of an anemometer, wind direction, temperature/relative humidity probe, pyranometer and pluviometer, was installed near the experimental site to monitor site-specific conditions. Data were collected using a datalogger (Em50 Data Collection System, Decagon Devices Inc., Pullman, WA).

4.2.2 Automated monitoring and pore-water sampling systems

An automated monitoring system was installed in 2011 in twelve out of twenty lysimeters with sensors at depths of 15, 30 and 60 cm. The system consisted of CS635 TDR (Time Domain Reflectrometry) probes (Campbell Scientific Inc., Lincoln Nebraska – USA) to estimate the volumetric water content, T4e electronic tensiometers (UMS GmbH, Munich - DE) to measure the soil matric potential, and SPE20 polyethylene/nylon suction cups (Meter Group, Munich - DE) to collect the mobile water. The TDR, calibrated in the laboratory, had an accuracy of ±1.5%. To ensure continuity between soils and probes, tensiometers and suction cups were installed in horizontal cavities forcing the excess soil slurry, previously used to fill the cavities, to discharge. TDR and tensiometer probes were connected to a CR-10X datalogger (Campbell Scientific Inc., Lincoln Nebraska – USA) through a series of multiplexers. The automatized system continuously kept suction equilibrium with the surrounding soil water tension (Morari, 2006) by integrating soil matric potential measurements, acquired by the electronic tensiometers, with pore water samplers (**Figure 4.1B**). Since vacuum applied to the sampling media was constantly regulated during the sampling period, the sample solute concentration was more accurate compared with other soil water samplers (Farsad et al., 2012). To regulate continuously the vacuum in pore water samplers based on matric potential, a system composed of a 5-Volt digital-analog conversion module (A04A, Campbell Scientific Inc., Lincoln

Nebraska – USA) connected to an electronic vacuum regulator incorporating a pressure relief valve (ITV2091, SMC Corporation, Tokyo, Japan) was employed. In this way, only the solutes that were involved in the mobile flow were sampled by the pore water samplers. The imposed negative pressure applied to soil-water samplers was in the range of -2 to -70 kPa and was maintained close to the soil water tension readings. To overcome pore water sampler resistance and the force with which water was held by soil, the imposed negative pressure was set at -2 kPa less than the soil water matric potential readings in the surrounding soil (Masarik et al., 2004). The system overcame frequent vacuum fluctuations of traditional systems that control the suction application duration, or are subjected to vacuum pressure leakage in vacuum tanks (Farsad et al., 2012). In drier soil conditions, the automated suction control system was not activated, because of the extremely low soil hydraulic conductivity making water sampling inoperative.

4.2.3 Experimental Design and Tracer Test

Twelve lysimeters were used in this experiment to evaluate the effect of groundwater management on solute movement. The bottom boundary condition was set with a water table level at 120 cm (WT120), 60 cm (WT60), and as free drainage (FD). Four replicates (hereafter labeled a, b, c, d) were used to better govern the soil variability and evaluate differences between treatments. The valve at the bottom of each lysimeter was used to regulate manually every day the water table level to the expected values (120 cm or 60 cm). Despite that, groundwater level fluctuations could occur within a maximum of ±10 cm. In order to investigate solute transport, a saline tracer solution of KBr containing a Br^- concentration of 250 mg l^{-1} was added to every lysimeter on bare soil at the beginning of the soil-water monitoring, on November 5th 2013 (10 g of Br^- in total) with a simulated rain event of 40 mm. Prior to the tracer test, background Br^- concentration of the soil solution was assessed at different depths and in the leaching water. Concentrations were below the detection limits (0.05 mg l^{-1}). The water sampling, started on November 6th 2013, was carried out on a daily time scale in the first week, and subsequently at increasing intervals until the end of the experiment (April 27th 2014), when the pore water was lastly sampled to evaluate any residual Br^- concentration. Once collected, the water samples were stored at -20 °C and then analyzed with Ion Chromatography (Dionex ICS-900, provided with a conductivity detector - Model DS

5 - and a column Ion Pac CS12A, Thermo Scientific) to measure bromide concentration. During the experiment the soil was maintained bare, such that total atmospheric water loss was due to evaporation. The water input was due only to irrigation, referred as simulated rainfall events (**Figure 4.2**).

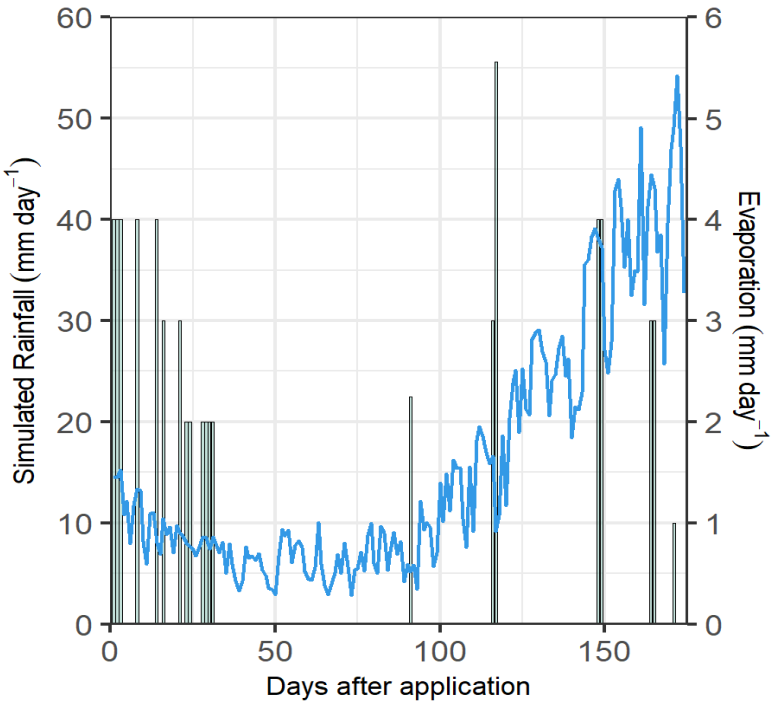

Figure 4.2. Rainfall events (grey bars) and potential evaporation from bare soil (blue line) during the experiment.

4.2.4 Advection-dispersion and mobile-immobile water solute transport equations in soil

The Advection-Dispersion Equation (ADE) is widely used to describe solute transport for Fickian flow when all the water molecules are taking part in the flow. The ADE for transient flow in soil is presented in Equation [1] when no adsorption occurs:

$$\frac{\partial(\theta C)}{\partial t} = \frac{\partial}{\partial z} \cdot \left(\theta D \frac{\partial C}{\partial z}\right) - \frac{\partial (J_w C)}{\partial z} \qquad [1]$$

where C is the solute concentration (mg cm^{-3}), ϑ is the soil water content (cm^3 cm^{-3}), D is the dispersion coefficient (cm^2 d^{-1}) that takes into account both hydrodynamic dispersion and molecular diffusion (Šimůnek and van Genuchten, 2008), J_w is the flux term for water (cm d^{-}

[1]), t is time (d) and z is the space coordinate (cm). The dispersion coefficient (D), accounting for both molecular diffusion and hydrodynamic dispersion, is equal to:

$$D = \xi(\Theta) \cdot D_l^w + v\lambda \quad [2]$$

where $\xi(\Theta)$ is the dimensionless tortuosity factor, D_l^w is the molecular diffusion coefficient in free water (cm^2 d^{-1}), v is the averaged pore water velocity (cm d^{-1}) and λ is the longitudinal dispersivity (cm), a parameter that expresses the mixing length of the solute in the soil. The ADE equation is widely used to simulate solute transport, but it cannot sufficiently describe transport in heterogeneous and unsaturated porous media (Gao et al., 2010). When physical non-equilibrium occurs, the mobile-immobile (MIM) equation (van Genuchten and Wierenga, 1976) is applied as a modified version of the ADE, assuming that the water inside micropores (mainly intraggregate pores) is stagnant, and the solute can be trapped in it. Hence, the water flow, and so the solute movement, is restricted only to the macropores (mainly interaggregate pores and fractures) (Šimůnek and van Genuchten, 2008). In the MIM model the water content ϑ is divided into two fractions: the mobile phase (ϑ_{mo}), which plays a key role in solute leaching, and the immobile phase (ϑ_{im}):

$$\theta = \theta_{mo} + \theta_{im} \quad [3]$$

The MIM model uses two equations, one for the mobile domain (Eq. 4) and the other for the immobile domain (Eq. 5), without the sorption terms, as reported by Šimůnek and van Genuchten (2008):

$$\frac{\partial \theta_{\mathrm{mo}} c_{\mathrm{mo}}}{\partial t} = \frac{\partial}{\partial z}\left(\theta_{\mathrm{mo}} D_{\mathrm{mo}} \frac{\partial c_{\mathrm{mo}}}{\partial z}\right) - \frac{\partial q_{\mathrm{mo}} c_{\mathrm{mo}}}{\partial z} - \phi_{\mathrm{mo}} - \Gamma_s \quad [4]$$

$$\frac{\partial \theta_{\mathrm{im}} c_{\mathrm{im}}}{\partial t} = \Gamma_s - \phi_{\mathrm{im}} \quad [5]$$

where c_{mo} and c_{im} are concentrations in the mobile and immobile region (mg cm^{-3}) respectively, D_{mo} is the dispersion coefficient in the mobile region (cm^2 d^{-1}), q_{mo} is the fluid flux density in the mobile region (cm d^{-1}), ϕ_{mo} and ϕ_{im} are sink-source terms (mg cm^{-3} d^{-1}), Γ_{s} is the rate of mass transfer between the two domains (mg cm^{-3} d^{-1}) that includes the first-order mass transfer coefficient α_{MIM} (d^{-1}) and is equal to:

$$\Gamma_{\mathrm{s}} = \alpha_{\mathrm{MIM}}(c_{\mathrm{mo}} - c_{\mathrm{im}}) \quad [6]$$

The dispersion coefficient D_e for the MIM model is described as the following Eq. 7 reported from Radcliffe and Šimůnek (2010):

$$D_e = \frac{D_{mo}\theta_{mo}}{\theta} \quad [7]$$

where the term on the right side of the equation represents the contribution of dispersion (D_{mo}) in the mobile phase.

4.2.5 Estimation of soil hydraulic and solute transport properties using HYDRUS 1D

HYDRUS 1D (Šimůnek et al., 2009) was used to numerically solve the Richards equation for variably saturated water flow under equilibrium flow conditions. Solute transport under equilibrium and physical non-equilibrium state was simulated with ADE and MIM equations, respectively.

First, the water flow was modeled applying the inverse solution approach. The difference between observed and simulated volumetric soil water content and matric potential at depths of 15, 30 and 60 cm, was minimized in the objective function which was defined as (Eq. 8):

$$\varphi(b, y) = \sum_{j=i}^{m} v_j \sum_{i=1}^{n_j} w_{i,j} \left[y_j^*(z, t_i) - y_j(z, t_i, b)\right]^2 \quad [8]$$

where φ is the target function, m is the number of variables measured, n_j is the numbered measurements for the variable j, v and w are weighting factors for individual measurements associated with the variable j and with each individual value i of j, y_j^* is the variable observed at time t and space z, y_j is the corresponding model predicted value at the same t and z, while b is the vector of parameters to be optimized (soil hydraulic –ϑ_s, α_{VG}, n, K_s– and solute transport parameters –λ_{ADE}, λ_{MIM}, α_{MIM} and ϑ_{Im}). For the soil hydraulic parameters estimation, the maximum number of iterations was set at 100 with a number of observed soil water contents and matric potentials at daily time scale that ranged between 880 and 1005 in total. Matric potential data that were out of range and outliers were not used for the inverse modelling. Soil hydraulic parameters of the Mualem-van Genuchten function (ϑ_s, α_{VG}, n and K_s) were estimated for the 0-20, 20-45 and 45-130 cm layers for the 174 days of the trial (November 4th 2013 to April 27th 2014). The residual soil water content (ϑ_r) was set 0.01 cm^3

cm^{-3} according to previous analysis on the same soil (Morari, 2006), and the conductivity tortuosity (*l*) was 0.5 (Mualem, 1976). Fixed values were used: a) to reduce the number of unknowns parameters; b) because preliminary analysis including ϑ_r and *l* as variables did not improve the accuracy of the results; c) due to their low sensitivity due to specific soil experimental conditions (e.g., mostly in the wet range) (Wösten and van Genuchten, 1988). Potential evapotranspiration rates and rainfall events were set as upper boundary conditions, while a seepage face in free drainage (FD) and variable pressure heads, describing daily fluctuations of water table levels in WT60 and WT120, were set as bottom boundary conditions. Potential evapotranspiration (ET_0) was calculated using the Hargreaves equation multiplied by the crop coefficient for bare soil (K_c = 1.15) (Allen et al., 2005), hereafter referred as potential evaporation as reported in Figure 2. Initial conditions were set in soil water content by using soil moisture data recorded by TDRs at the beginning of the experiment.

After soil hydraulic properties, solute transport parameters at different depths were estimated. The objective function was defined in terms of bromide concentration flux data, weighted by the standard deviation. For this purpose, two different equations were used: a) the ADE, to estimate dispersivity (λ_{ADE}); b) the MIM physical non-equilibrium model, to estimate dispersivity (λ_{MIM}), mass-transfer coefficient (α_{MIM}) and immobile soil water content (ϑ_{Im}). Boundary conditions for solute transport were set as concentration flux of the infiltrating water (250 mg l^{-1} of bromide), and lower zero concentration gradient at the outflow. Bromide water diffusion was set at 1.6 cm^2 d^{-1} (Leistra and Boesten, 2010; Lide, 2003) and the soil-water adsorption coefficient (K_d) was set as zero due to the conservative behavior of bromide and its negligible sorption (Celestino Ladu and Zhang, 2011). The maximum number of iterations was set at 10 with a number of observed bromide flux concentrations in the objective function that ranged between 25 and 100. Previously estimated soil hydraulic parameters were used as soil information for the solute transport simulations.

To test the goodness of fit between observed and predicted values, three statistical approaches were used: the coefficient of determination (R^2), the Nash-Sutcliffe Efficiency coefficient (NSE) and the Root Mean Square Error (RMSE). These statistical parameters were chosen for their ability to compare comprehensively the goodness of fit of simulation models (Power, 1993; Zeng et al., 2014). In general, the best fit was represented by RMSE close to 0 and NSE and R^2 close to 1.

Afterward, the fraction of mobile water (β) was calculated as the ratio between the mobile ($\vartheta_{mo} = \vartheta - \vartheta_{lm}$, see Eq. [3]) and the total soil water content (ϑ), when no adsorption occurs (Van Genuchten and Wierenga, 1976). Since β is dependent on ϑ, the average ϑ during the experimental trial was calculated and used.

4.2.6 Procedure of inverse modeling for parameter optimization

The procedure of inverse modelling in a multi-layer soil profile can be applied using a simultaneous (Groh et al., 2018) or a sequential (Šimůnek et al., 2001) approach for the estimation of soil hydraulic and solute parameters. In our case, the sequential approach was necessary to minimize problems of non-uniqueness due to the high number of parameters to be optimized (Hopmans et al., 2002; Jacques et al., 2002). A stepwise layer-by-layer procedure starting from the top, applied to each lysimeter, was performed. First, the soil profile was assumed homogeneous and hydraulic parameters were optimized against daily soil water contents (measured by TDRs) and matric potentials (measured by tensiometers) at the corresponding depth. The initial values of hydraulic parameters were estimated based on the pedotransfer functions already implemented in HYDRUS 1D, using particle size distribution and bulk density data. After the first run, the obtained hydraulic parameters were fixed in the first layer (0-20 cm), and a two-layer soil profile (0-20, 20-130 cm) was defined to optimize the parameters in the second one. The procedure was performed until parameters in all three layers were optimized. When all the hydraulic parameters were estimated, some further tuning was done by re-estimating the same parameters of different layers until no further improvement was achieved. After that, solute transport parameters were optimized, starting from initial values of 5 cm, 0.1 $cm^3\ cm^{-3}$ and 0.5 d^{-1} for λ, θ_{im}, and α_{MIM}, respectively. Parameter optimization for both hydraulic and solute transport modeling was based on the Levenberg-Marquardt method to minimize the target function (Marquardt, 1963). The weights associated with the observed data were manually set as 1 since data were automatically weighted by standard deviation by HYDRUS 1D (Isch et al., 2019).

4. 2.7 X-ray computed microtomography

To identify additional pore structure properties, one undisturbed soil core (7 cm diameter × 5 cm height) was collected after the tracer test in each tested lysimeter (totally 12), using as hand auger (Eijkelkamp, The Netherlands), at a depth of 25-to-30 cm, and analyzed by means of X-ray microtomography (µCT). Before analysis, soil cores were equilibrated at –60 cm matric potential with a sandbox apparatus to ensure uniform conditions, after that they were gently removed from stainless steel cylinders and reduced in size to allow higher greyscale contrast of acquired projections between soil porosity and matrix. Undisturbed samples (*ca*. 2 cm diameter × 4 cm height) were obtained from the center of the cores using a knife and then wrapped in parafilm. Scanning was done using a Skyscan 1172 µCT (Bruker microCT, Belgium) at 88 kV and 112 µA, and projections were acquired during a 180° sample rotation at 0.27° angular incremental steps. Beam hardening artefacts were minimized during data acquisition with a 0.5 mm Al filter. Projections were reconstructed using NRecon software version 1.6.9.4 (Bruker microCT, Belgium) to obtain a stack of at least 1500 2D images in 8-bit depth. The final voxel resolution was 27.25 µm in all three directions. After reducing noise with a 3×3×3 median filter, the reconstructed greyscale volumes were segmented into binary images (i.e., soil pores and matrix) using a clustering-based threshold method (Otsu, 1979). Total porosity was calculated by dividing the number of pore voxels by the total number of voxels of the analyzed volume. The 3D mean pore diameter and pore size classes were estimated by using a sphere-fitting method (at intervals of two voxels) that determines the local thickness of every medial axis pore voxel (Remy and Thiel, 2002). Pore classes were divided into micropores (27.25-327.00 µm) and macropores (> 327.00 µm) to emphasize the contribution of the large pores to possible non-equilibrium flow (Jarvis, 2007). The Euler number –by calculating the number of redundant connections between pores per unit volume (mm^{-3})– was used as an estimate of local pore connectivity, that becomes increasing by negative with increasing connectivity and increasing by positive with decreasing connectivity (Vogel et al., 2010). Digital image processing and analysis was done using CTAn software version 1.17.7.2 (Bruker microCT, Belgium).

4.3 Results

4.3.1 Experimental soil water content, pressure heads and meteorological data

Total water input as simulated rainfall during the experimental period was 638.1 mm (**Figure 4.2**), starting November 5th with 40 mm. The highest input was observed on March 1st, when 55.6 mm of simulated rain fell on the lysimeters in one day. From the beginning until February 16th, the potential evaporation from bare soil was always lower than 1.6 mm d^{-1}, and after it increased to a maximum value of 5.4 mm d^{-1} on April 25th. Soil water content dynamics observed during the experimental trial (November 5th 2013 – April 27th 2014) showed that free drainage (FD) lysimeters were always drier than WT120 and WT60 (**Figure 4.3**). At the beginning of the experiment, before any simulated rainfall event, the soil water content was mainly affected by the water table management condition. In fact, the free drainage lysimeters showed soil water content of about 0.129±0.024 cm^3 cm^{-3} at 15 cm and increased up to 0.193±0.006 cm^3 cm^{-3} and 0.222±0.001 cm^3 cm^{-3}, respectively at 30 cm and 60 cm depth. Higher initial soil water content within the soil profile was observed in WT120 (0.257±0.006, 0.332±0.023, 0.412±0.002 cm^3 cm^{-3}) and WT60 with maximum values in WT60 (0.334±0.02, 0.370±0.011 and 0.414±0.004 cm^3 cm^{-3}). After subsequent simulated rainfall events that amounted to 120 mm (November 5th - 7th 2013), soil water content in FD rapidly increased, reaching 0.280±0.018, 0.363±0.006 and 0.370±0.012 cm^3 cm^{-3} at 15, 30 and 60 cm, respectively. In particular, stronger fluctuations were observed at 15 cm that were smoothed and slightly delayed in deeper layers. During the experimental trial, FD had on average 0.266±0.017 cm^3 cm^{-3}, 0.357±0.006 cm^3 cm^{-3} and 0.390±0.002 cm^3 cm^{-3} at 15, 30 and 60 cm respectively, while the maximum and minimum values were 0.349 and 0.141, 0.403 and 0.183, 0.441 and 0.220 cm^3 cm^{-3}, at the same depth.

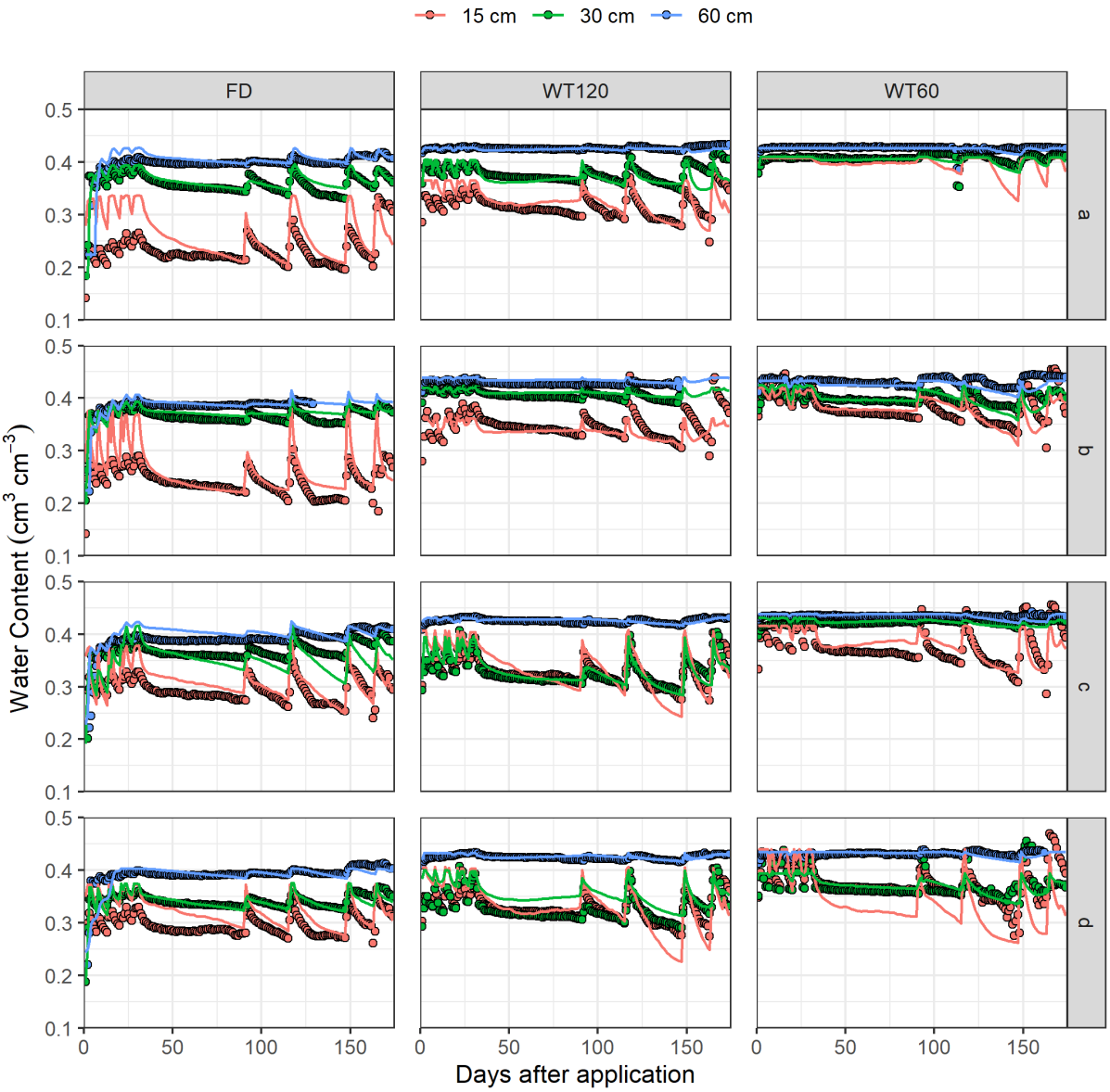

Figure 4.3. Observed (dots) and simulated (lines) water content (cm^3 cm^{-3}) in lysimeters with different water table managements (FD, left; WT120, centre; WT60, right) and replicates (a, b, c, d) during the experiment. Colors indicate different monitoring depths: 15 cm (red), 30 cm (green) and 60 cm (blue). Where dots are missing, no data were available.

In general, during the experiment, soil water content in the surface layer was always lower than at 30 cm and 60 cm. Similar soil water content dynamics were observed in WT120 and WT60 at 15 cm and 30 cm, showing a peak after each rainfall event. In contrast, at 60 cm the soil water content was slightly affected by additional water input due to higher initial soil water content conditions. The soil water content gradient was reduced in WT120 and WT60 compared to FD mainly at 15 cm. This was particularly noticeable in WT60 when the topsoil

water content reached similar values –or even higher– than those in the subsoil, at 30 and 60 cm due to simulated rainfall events. Notably, similar soil water contents close to saturation (about 0.43 cm^3 cm^{-3}) were found at 60 cm in both WT120 and WT60, despite being managed according to different water table levels. Furthermore, in WT lysimeters maximum and minimum values were higher with respect to the free drainage condition, showing similar maximum water contents reached along the depths. Minimum values recorded were lower mostly in WT60 (0.160, 0.336 and 0.386 cm^3 cm^{-3} at 15, 30 and 60 cm), than WT120 (0.248, 0.291 and 0.409 cm^3 cm^{-3} at 15, 30 and 60 cm), except for the intermediate depth, suggesting wider fluctuations in WT60 lysimeters.

Similar observations were reported by measured pressure head dynamics (**Figure 4.4**), with wider fluctuations that were found in FD lysimeters compared to smoother dynamics as observed in WT120 and especially WT60. After each simulated rainfall event, the matric potential increased sharply until values always > -50 cm in all lysimeters, regardless the water table management. Notably, the effect of a shallow water table was recorded by the tensiometers, with values above 0 cm especially when the water table was set at 60 cm. In some cases, this was also observed in WT120, when simulated rainfalls of at least 40 mm occurred with high frequency.

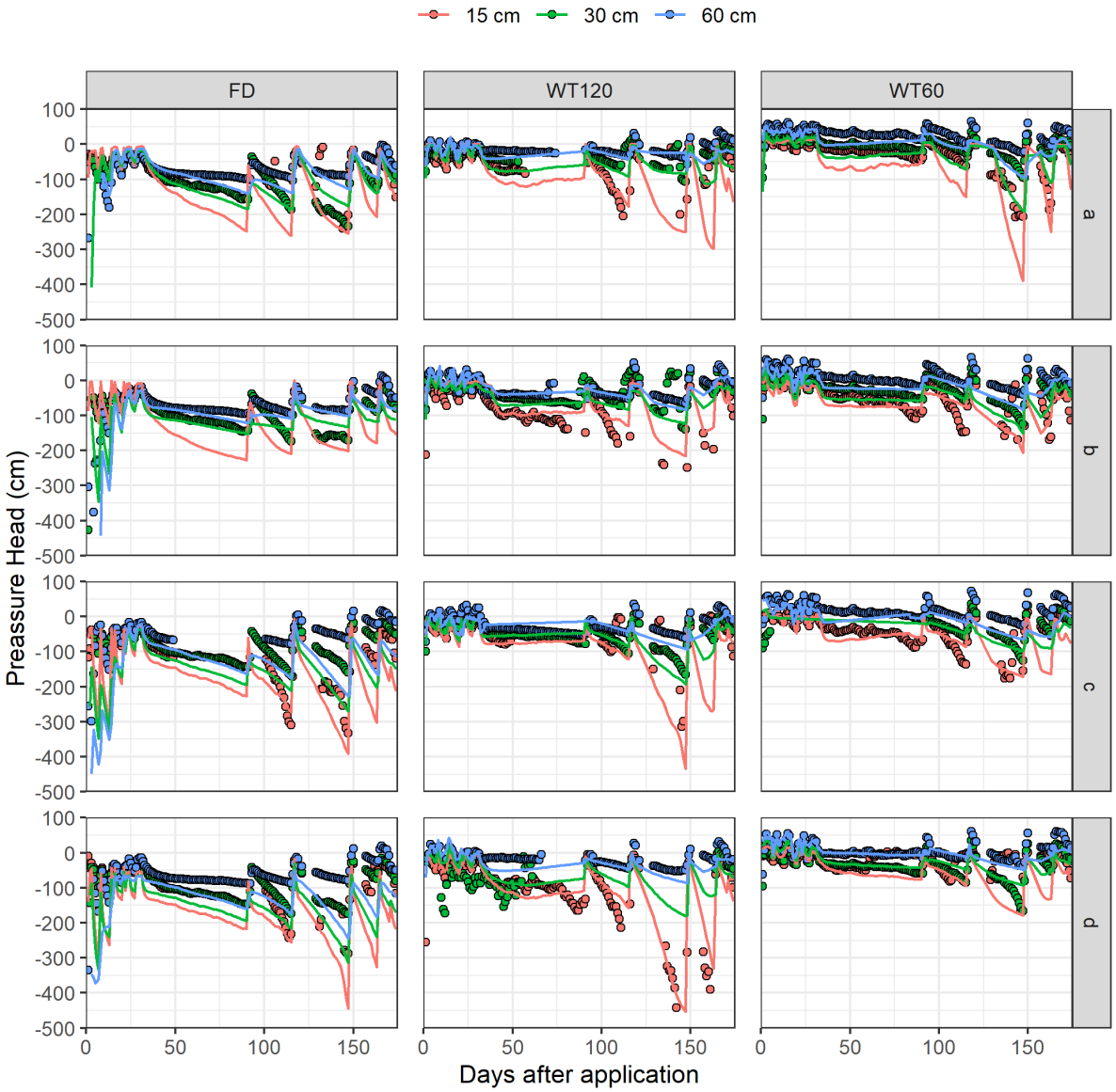

Figure 4.4. Observed (dots) and simulated (lines) pressure heads (cm) in lysimeters with different water table managements (FD, left; WT120, centre; WT60, right) and replicates (a, b, c, d) during the experiment. Colors indicate different monitoring depths: 15 cm (red), 30 cm (green) and 60 cm (blue). Where dots are missing, no data were available or out of range.

4.3.2 Soil Water Dynamics and Hydraulic Parameters Estimation with HYDRUS 1D

Soil water contents were well simulated by HYDRUS 1D (**Figure 4.3**), but in some cases (mostly at -15 cm), the model showed an excessive sensitivity to predict wide and frequent soil water content fluctuations, particularly in FD lysimeters. In contrast, the sharp increase of volumetric water content after rainfall events at 30 and 60 cm depth, and the following slower drying dynamics were well described. In case of pressure heads simulation (**Figure 4.4**) the model showed higher fluctuations at 15 cm, as reported for water contents, but good predictions at the deeper depths. Indeed, the close fitting between measured and modeled water contents indicated the goodness of inverse operations (**Table 4.2**) for all the treatments: generally, the best fit was found in WT120, while the lowest was in WT60d (R^2=0.619, RMSE=0.030, NSE=0.198). In general, water contents in FD lysimeters were well estimated, according to high R^2 and NSE, and low RMSE. Furthermore, inverted parameters well described the soil water dynamics of all lysimeters at the three soil layers (**Figure 4.3**). The goodness of fit of simulated vs. observed matric heads was generally lower than water contents (**Table 4.2**). The best fit was found for WT lysimeters (R^2 ranging from 0.284 to 0.786), except for WT60a which showed a negative NSE (-0.124).

Table 4.2. Statistical analysis for water content and matric potential estimation with HYDRUS 1D. Coefficient of Determination (R^2), Root Mean Square Error (RMSE) and Nash-Sutcliffe Efficiency (NSE) coefficients are reported for each lysimeter.

	Water Content (cm^3 cm^{-3})			**Matric Head (cm)**		
	R^2	**RMSE**	**NSE**	**R^2**	**RMSE**	**NSE**
FDa	0.866	0.025	0.830	0.573	22.142	0.339
FDb	0.888	0.021	0.861	0.475	15.952	0.301
FDc	0.724	0.024	0.700	0.430	25.267	-1.222
FDd	0.777	0.017	0.739	0.377	16.973	-2.416
WT120a	0.892	0.014	0.891	0.284	23.588	0.417
WT120b	0.853	0.016	0.811	0.470	26.934	0.395
WT120c	0.875	0.019	0.854	0.322	21.248	0.212
WT120d	0.821	0.021	0.784	0.557	26.890	0.602
WT60a	0.731	0.006	0.684	0.786	24.126	-0.124
WT60b	0.651	0.015	0.627	0.581	20.853	0.475
WT60c	0.770	0.013	0.762	0.516	23.286	0.456
WT60d	0.619	0.030	0.198	0.414	24.569	0.259

Similar results were reported for FDc and FDd (R^2 = 0.430 and 0.377; NSE = -1.222 and -2.416, respectively), mostly due to a general underestimation of the matric potential by the model. Estimated saturated soil water content (**Table 4.3**) increased by depth, from 0.397 cm^3 cm^{-3} at the topsoil layer to 0.406 cm^3 cm^{-3} and 0.429 cm^3 cm^{-3} at the intermediate (20-45 cm) and deep (45-130 cm) layers, with slight variability between treatments. Most of the variability was found among soil layers. The saturated water content was generally lower in the topsoil layer (0.392±0.015 cm^3 cm^{-3}) and increased with the soil depth (0.429±0.004 cm^3 cm^{-3} at 45-130 cm). At the topsoil, the air entry potential (α_{VG}) was 0.013±0.003 cm^{-1}, similar to the intermediate one (0.010±0.001 cm^{-1}), while the deep layers showed halved α_{VG} (0.006±0.002 cm^{-1}). A tendency to lower *n* values was observed in the 45-130 cm layer (1.17±0.02) compared to 0-20 (1.34±0.00) and 20-45 cm (1.20±0.01), which indicated a flatter pore size distribution at the greatest depth (**Table 4.3**). Saturated hydraulic conductivity varied between treatments, in general showing higher values in FD (45.70±28.76 cm d^{-1} on average), while in WT120 and WT60 values were 14.21±6.20 cm d^{-1} and 19.26±3.38 cm d^{-1}. Greatest K_s values were found in the deepest layer of FD (101.11±25.62 cm d^{-1}), showing a most pronounced increase with depth than WT lysimeters.

Table 4.3. Soil hydraulic parameters estimated by HYDRUS 1D at different layer depths and according to different water table management: ϑ_s, saturated water content; α_{VG}, air entry suction; n, slope of the water retention curve; K_s, saturated hydraulic conductivity (first line). Standard errors are reported in the second line of each treatment.

	0-20 cm				20-45 cm				45-130 cm			
	θ_s	α_{VG}	n	K_s	θ_s	α_{VG}	n	K_s	θ_s	α_{VG}	n	K_s
	($cm^3\ cm^{-3}$)	(cm^{-1})	(-)	($cm\ d^{-1}$)	($cm^3\ cm^{-3}$)	(cm^{-1})	(-)	($cm\ d^{-1}$)	($cm^3\ cm^{-3}$)	(cm^{-1})	(-)	($cm\ d^{-1}$)
FDa	0.338	0.009	1.50	5.29	0.400	0.008	1.17	26.20	0.432	0.018	1.07	108.12
	0.008	0.000	0.03	0.32	0.002	0.000	0.00	1.61	0.002	0.001	0.00	10.46
FDb	0.380	0.027	1.30	7.37	0.402	0.006	1.18	34.93	0.417	0.012	1.10	140.49
	0.010	0.002	0.08	2.34	0.007	0.001	0.03	14.70	0.006	0.001	0.02	12.35
FDc	0.390	0.008	1.36	3.59	0.433	0.007	1.41	39.16	0.427	0.004	1.19	15.27
	0.005	0.000	0.01	0.47	0.012	0.001	0.00	7.77	0.002	0.000	0.01	2.37
FDd	0.373	0.005	1.21	2.06	0.383	0.011	1.23	25.42	0.410	0.006	1.21	140.49
	0.002	0.000	0.01	0.59	0.002	0.000	0.00	1.34	0.001	0.000	0.01	0.14
WT120a	0.365	0.007	1.32	1.48	0.406	0.015	1.18	8.34	0.428	0.003	1.20	12.09
	0.001	0.000	0.01	0.05	0.001	0.000	0.00	0.22	0.001	0.000	0.06	1.30
WT120b	0.364	0.005	1.38	0.58	0.420	0.003	1.21	16.03	0.439	0.003	1.15	8.83
	0.002	0.000	0.03	0.02	0.001	0.000	0.02	4.29	0.002	0.000	0.02	0.97
WT120c	0.405	0.009	1.35	6.52	0.401	0.015	1.20	16.57	0.431	0.004	1.14	69.87
	0.009	0.004	0.01	1.31	0.001	0.001	0.00	0.26	0.009	0.000	0.02	9.71
WT120d	0.406	0.011	1.36	7.71	0.402	0.017	1.19	11.5	0.433	0.005	1.13	11.01
	0.003	0.001	0.03	1.02	0.002	0.002	0.02	0.91	0.001	0.001	0.01	2.34
WT60a	0.408	0.003	1.40	0.23	0.410	0.004	1.16	1.67	0.427	0.003	1.17	1.51
	0.001	0.000	0.03	0.05	0.001	0.001	0.02	0.55	0.001	0.000	0.06	0.41
WT60b	0.421	0.007	1.42	50.3	0.425	0.010	1.22	15.9	0.433	0.009	1.16	26.25
	0.005	0.002	0.03	0.02	0.001	0.000	0.03	0.25	0.002	0.001	0.02	0.45
WT60c	0.416	0.010	1.32	2.36	0.431	0.006	1.12	59.70	0.439	0.004	1.33	15.78
	0.003	0.000	0.03	0.12	0.002	0.000	0.02	12.19	0.002	0.000	0.05	0.97
WT60d	0.440	0.049	1.21	45.57	0.394	0.013	1.25	3.31	0.435	0.008	1.20	8.53
	0.004	0.004	0.01	4.57	0.005	0.010	0.02	6.54	0.002	0.002	0.05	2.58

4.3.3 Experimental bromide movement in lysimeters

Experimental bromide concentration dynamics at different depths (mg l^{-1}) are shown in **Figure 4.5** (dots), describing the 174-day monitoring from November 5th 2013 until April 27th 2014. In FD, the first water sampling was delayed until November 13th because of the very dry conditions at the beginning of the experiment (**Figure 4.3** and **Figure 4.4**), almost two weeks after application of Br^- and 160 mm of simulated rainfall. The highest concentrations were detected at 15 cm, reaching 75 mg l^{-1} in lysimeters FDb and FDc. Concentrations sharply decreased to values <5 mg l^{-1} one month after application. At increasing depths, concentration peaks were shifted a few days later (1 to 8). Bromide concentrations were never higher than 40 mg l^{-1} at 30 cm depth, and even lower at 60 cm. Thirty days after the Br^- application and 360 mm of water input, bromide concentrations were almost steady at values close to 1 mg l^{-1} or below.

WT treatments exhibited earlier initial arrival of Br^- than FD. Bromide was first detected the day after application (6th of November) at concentrations up to 90 mg l^{-1}. The fast Br^- movement was emphasized in WT120, when it showed a peak at 30 cm on November 8th (48.4 mg l^{-1}, on average), followed by a peak at 60 cm starting November 12th (especially in lysimeter WT120a, reaching a maximum concentration of 35 mg l^{-1}). WT60 showed a similar trend compared to WT120 at the surface and intermediate sampling points. In all WT60 lysimeters, the Br^- had a peak above 80 mg l^{-1}, detected at 15 cm, that gradually dropped to about 5 mg l^{-1} after one month. At 30 cm the peak was reached on November 12th (detected also at 15 cm due to a 40 mm irrigation) and then decreased to approximately 10 mg l^{-1} at the end of the experiment. At 60 cm, Br^- was detected immediately after the 15 and 30 cm sampling, but a peak of concentration was never found. These dynamics highlighted the fluctuating effect of the shallow water table, which likely enhanced Br^- dilution as well hindered its complete leaching.

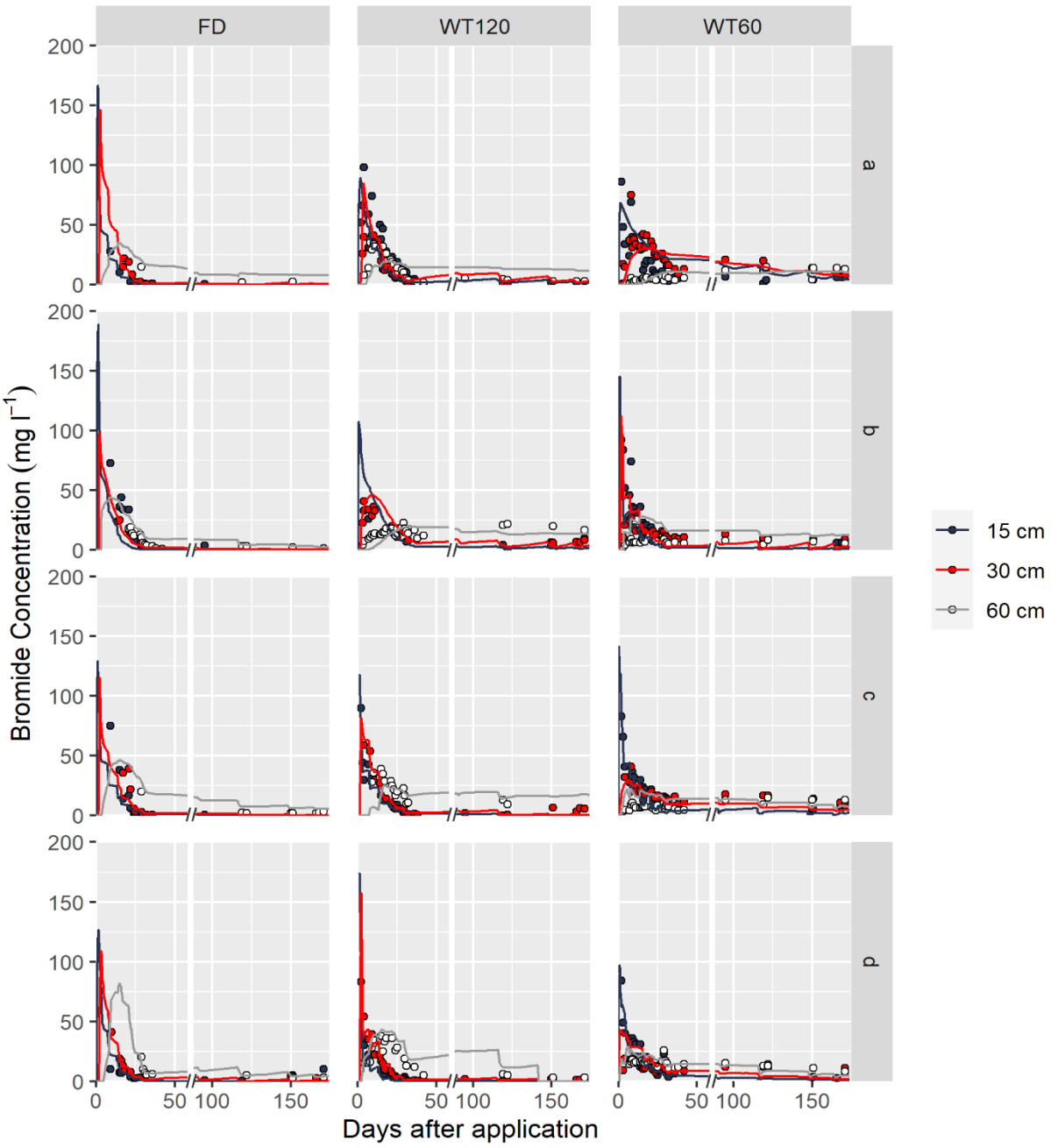

Figure 4.5. Experimental Br^- concentration (dots) and simulated (line) dynamics obtained by solute modeling applying MIM in differerent treatments: FD (left), WT120 (centre) and WT60 (right), each on the four lysimeters (a, b, c, d). Different colors indicate different depths of soil-water sampling: 15 cm (black), 30 cm (red) and 60 cm (grey).

4.3.4 Modeled Solute Transport Dynamics and Parameterization with HYDRUS 1D

Model performance metrics of bromide dynamic using ADE and MIM are reported in **Table 4.4**. The fitting showed better values with MIM than ADE in all the treatments. In general, R^2 and NSE were higher and RMSE lower using MIM, confirming a better model efficiency. The model performance with MIM also changed between lysimeters, indicating that in a few cases unsatisfactory predictions occurred (e.g., WT60b in which NSE was negative).

Table 4.4. Statistical analysis for bromide concentration with HYDRUS 1D using ADE and MIM. Coefficient of Determination (R^2), Root Mean Square Error (RMSE) and Nash-Sutcliffe Efficiency (NSE) coefficients are reported for each lysimeter.

	ADE			MIM		
	R^2	RMSE	NSE	R^2	RMSE	NSE
FDa	0.602	2.475	0.447	0.917	1.365	0.695
FDb	0.504	6.160	0.484	0.417	5.47	0.072
FDc	0.328	6.040	0.239	0.693	3.844	0.400
FDd	0.816	3.821	0.783	0.830	3.203	0.807
WT120a	0.423	12.931	0.359	0.443	13.499	0.357
WT120b	0.387	16.489	-3.272	0.783	7.149	0.037
WT120c	0.621	9.110	0.620	0.696	8.338	0.694
WT120d	0.745	7.993	0.719	0.773	8.555	0.724
WT60a	0.630	14.885	0.038	0.591	19.707	0.594
WT60b	0.067	25.726	-0.763	0.038	19.191	-0.889
WT60c	0.111	19.752	-13.340	0.527	9.607	0.406
WT60d	0.224	10.226	-0.110	0.410	12.832	0.324

Modeled dynamics with MIM are shown in **Figure 4.5**. HYDRUS 1D simulated initially high peaks of bromide mostly in the FD treatment (max 170 mg l^{-1}) at 15 and 30 cm depths, followed by a fast decrease (black and red lines) that reached concentrations close to 0 mg l^{-1} after 35-40 days. In FD, Br- at 60 cm depth (grey line) showed delayed and lower peaks (< 40 mg l^{-1}) compared to -15 and -30 cm, with final estimated concentrations close to 5 mg l^{-1}. In contrast, WT lysimeters mostly showed lower initial peaks of bromide than FD lysimeters that flattened after 20 days to concentrations close to 0 mg l^{-1} at 15 and 30 cm, except for WT60a. At 60 cm, HYDRUS 1D was not always able to predict Br^- concentration dynamics as observed in the upper layers (**Figure 4.5**, e.g. WT120c).

Solute transport parameters from inverse modeling are shown in **Table 4.5** for the ADE and **Table 4.6** for the MIM model. Very high dispersivity (λ_{ADE}) was found at the surface layer of both WT120 (211.5±38.5 cm) and WT60 (152.3±45.7 cm) lysimeters. In FD λ_{ADE} was much lower, generally decreasing with depth as WT lysimeters. Large values of λ and the poor fit (**Table 4.4**) using ADE indicated likely non-equilibrium conditions (Radcliffe and Šimůnek, 2010).

Table 4.5. Dispersivity (λ_{ADE}) values estimated using ADE at different layer depths and according to different water table management (first line). Standard errors are reported in the second line of each WT treatment.

	λ_{ADE} (cm)		
	0-20 cm	**20-45 cm**	**45-130 cm**
FDa	16.5	0.07	10.92
	8.21	0.02	4.46
FDb	243.58	15.37	90.36
	70.21	9.92	38.16
FDc	39.29	8.8	10.42
	7.70	0.77	2.27
FDd	9.42	3.52	0.24
	4.74	2.82	0.01
WT120a	250.00	2.69	72.85
	515.34	1.59	7.11
WT120b	250.00	4.10	17.52
	150.52	1.61	4.36
WT120c	96.11	6.42	0.55
	47.58	2.04	0.01
WT120d	250.00	1.66	5.71
	92.15	0.75	4.43
WT60a	87.97	10.71	1.27
	46.75	1.87	1.94
WT60b	197.62	40.87	73.55
	381.51	5.44	17.59
WT60c	250.00	20.01	28.57
	81.04	4.26	17.92
WT60d	73.77	122.54	11.01
	6.28	32.01	6.71

Table 4.6. Dispersivity (λ_{MIM}), immobile water content (ϑ_{Im}) and mass exchange coefficient (α_{MIM}) estimated using MIM divided for WT management and layer depth (first line). Standard errors are reported in the second line of each WT treatment.

	0-20 cm			20-45 cm			45-130 cm		
	λ_{MIM} (cm)	ϑ_{Im} ($cm^3\ cm^{-3}$)	α_{MIM} (d^{-1})	λ_{MIM} (cm)	ϑ_{Im} ($cm^3\ cm^{-3}$)	α_{MIM} (d^{-1})	λ_{MIM} (cm)	ϑ_{Im} ($cm^3\ cm^{-3}$)	α_{MIM} (d^{-1})
FDa	14.63	0.004	108.56	0.10	0.007	22.57	84.80	0.052	1.75
	2.97	0.067	75.11	0.08	0.046	12.21	12.57	0.150	7.15
FDb	15.02	0.000	343.52	19.70	0.014	10.8	20.12	0.000	0.13
	0.01	0.000	2.87	0.19	0.000	0.79	0.13	0.000	0.00
FDc	76.6	0.000	20.91	0.13	0.075	12.92	15.77	0.009	0.05
	17.1	0.002	4.28	0.01	0.002	1.51	3.59	0.032	0.14
FDd	12.49	0.065	340.49	0.54	0.072	0.00	0.27	0.019	0.01
	5.86	0.027	99.77	2.14	0.027	0.00	0.00	0.040	0.37
WT120a	49.11	0.079	0.14	0.17	0.352	0.01	44.06	0.147	61.04
	0.96	0.016	0.02	0.00	0.005	0.01	22.94	0.082	30.78
WT120b	35.02	0.199	0.10	1.96	0.278	0.12	5.18	0.256	30.82
	5.18	0.283	0.11	0.30	0.016	0.03	0.95	0.021	6.62
WT120c	46.66	0.088	0.06	0.17	0.112	1.34	15.10	0.136	64.00
	2.77	0.011	0.00	0.00	0.019	0.11	1.45	0.005	5.44
WT120d	0.06	0.146	0.06	0.08	0.235	0.10	1.75	0.298	13.29
	0.00	0.003	0.01	0.04	0.007	0.02	0.47	0.120	6.43
WT60a	46.07	0.184	0.02	6.23	0.128	0.04	15.01	0.201	0.08
	10.99	0.117	0.01	1.87	0.012	0.07	4.47	0.002	0.24
WT60b	23.72	0.251	0.12	0.09	0.120	0.08	20.54	0.139	0.05
	12.03	0.003	0.11	0.00	0.049	0.84	4.18	0.025	0.51
WT60c	2.53	0.340	0.10	54.11	0.344	0.05	15.85	0.357	0.07
	0.02	0.004	0.02	2.22	0.003	0.02	1.40	0.002	0.01
WT60d	14.57	0.340	0.47	31.87	0.224	0.09	7.31	0.349	0.09
	3.71	0.045	0.06	5.67	0.072	0.02	1.35	0.003	0.07

By applying the physical non-equilibrium model, the MIM dispersivity (λ_{MIM}) was reduced compared to the ADE in WT treatments. Mobile-immobile dispersivity at the surface layer (0-20 cm) of WT60 was 21.7±9.2 cm on average, whereas higher values were found in WT120 (32.7±11.3 cm). In contrast, WT120 showed larger λ_{MIM} than WT60 at the deepest soil layer, with an average value of 16.5±9.6cm and 14.7±2.7 cm respectively. In some cases, λ_{MIM} in FD showed values similar to results reported using ADE – FDa and FDd mostly. Results from inverse modeling showed that the degree of solute exchange between the immobile and mobile region, α_{MIM} (d^{-1}), changed among treatments. This suggested a diverse contribution of immobile water to solute transport, either slow –as described by small α_{MIM} values (mostly

in WT treatments)– or fast –as described by large α_{MIM} values (mostly in the topsoil layer in FD and deepest layer in WT120). Free drainage was strongly differentiated from WT even in terms of mobile water fraction, in that β estimates for free drainage were generally close to 1 (ϑ_{Im} very low) whereas for WT treatments they were much lower (revealed by higher ϑ_{Im}).

4.3.5 Pore network characterization by means of X-ray computed microtomography

Total porosity in the range 27.25-2834.00 µm, decreased from 0.15±0.01 cm^3 cm^{-3} in FD, to 0.11±0.03 cm^3 cm^{-3} in WT120, and 0.08 cm^3 cm^{-3} in WT60 (**Table 4.7**).

Table 4.7. Soil porosity and structure parameters calculated with X-ray microtomography analysis on undisturbed soil samples collected in 25-32 cm soil layers. The threshold identifying macropores that can generate preferential flow was set at 327 µm according to Jarvis (2007).

	Total porosity (cm^3 cm^{-3})	Micropore* Frequency (%)	Macropore** Frequency (%)	Mean pore diameter (µm)	Euler number (mm^{-3})	Degree of anisotropy
Fda	0.13	63.20	36.76	300.6	-4.92E-03	0.11
FDc	0.13	85.40	14.56	238.1	-1.68E-02	0.13
FDd	0.18	71.60	28.44	267.8	-1.25E-02	0.09
FDb	0.16	38.50	61.49	636.8	-2.59E-03	0.19
WT120c	0.08	55.70	44.30	510.4	-1.46E-03	0.12
WT120d	0.14	67.30	32.71	306.1	-5.21E-03	0.07
WT120a	0.16	73.40	26.63	251.3	-9.65E-03	0.14
WT120b	0.05	51.60	48.38	516.2	-1.64E-03	0.10
WT60a	0.10	69.20	30.78	326.4	-1.83E-03	0.10
WT60b	0.08	45.10	54.87	485.3	-1.53E-03	0.05
WT60c	0.08	38.20	61.80	560.3	-9.64E-04	0.08
WT60d	0.06	44.60	55.41	543.1	-5.22E-04	0.08

*54-327 µm

**327-2800 µm

The macroporosity (>327.00 µm) was 35.3±9.9% of the total porosity in FD, while increased up to 40.4±3.6% in WT120 and 50.7±6.8% in WT60. To note the high pore size class variability of FD, that was due to a single macropore observed in just one soil core (i.e., FDb). The Euler number was always negative, suggesting that pores with multiple connections dominated over single isolated pores. Lower Euler number values were found in FD (-0.92±0.33 10^{-2} mm^{-3}), compared to WT120 (-0.45±0.19 10^{-2} mm^{-3}) and WT60 (0.12±0.03 10^{-2} mm^{-3}). A visual

inspection of the pore structure in some example images (**Figure 4.6**) highlighted the different network organization between treatments, with an increasing number of large macropores where the water table occurred.

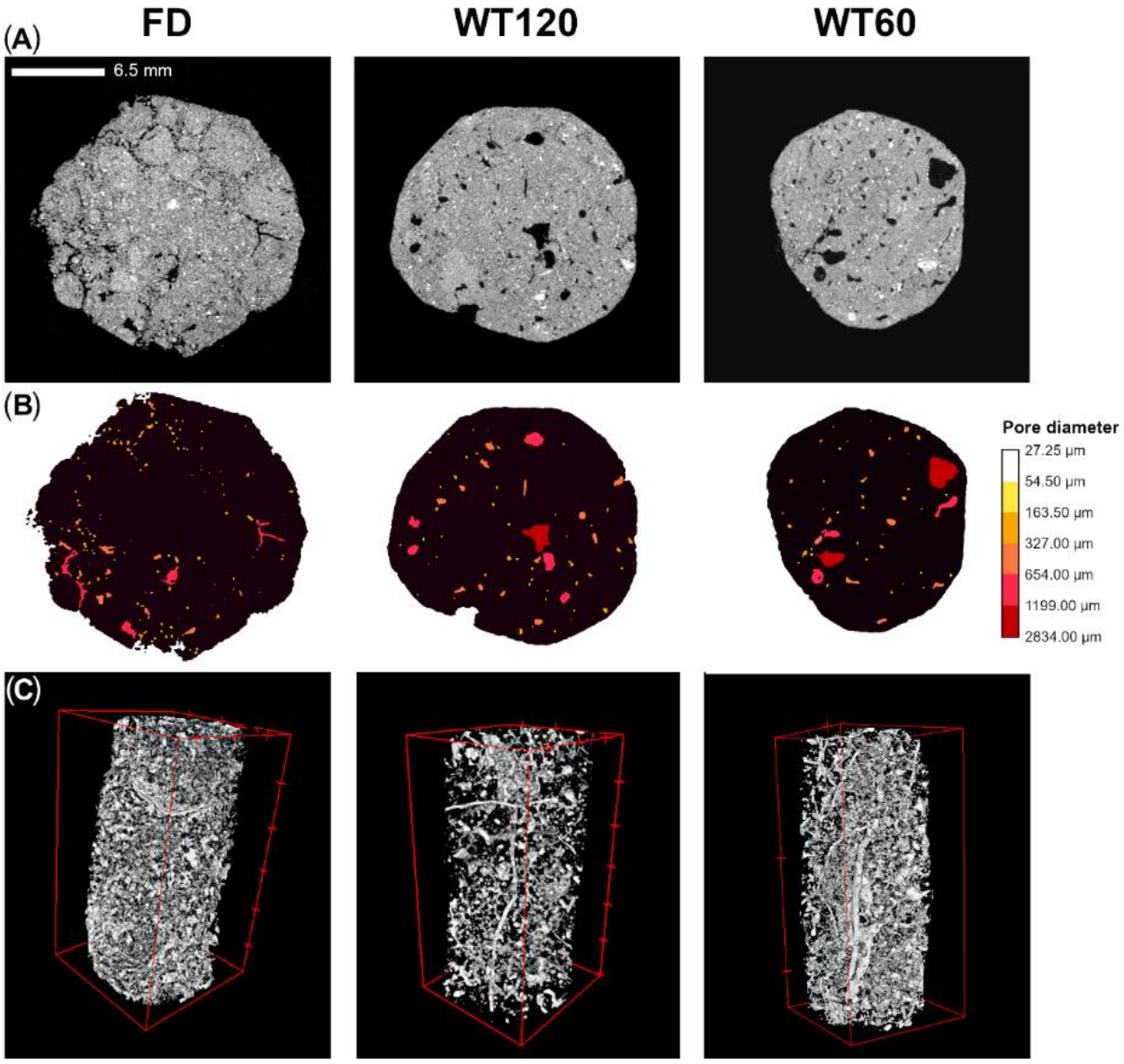

Figure 4.6. 2D sections (A, B) and 3D porosity (C) of selected soil cores collected at 25-30 cm depth under different water table (WT60, WT120) and free drainage (FD) treatments. Pore size diameter in soil sections (b) are classified according to different colors, while the soil matrix is colored in black.

4.4 Discussion

Modeling of soil hydraulic parameters with HYDRUS 1D highlighted only slight differences of soil water retention parameters between groundwater management systems. Similar water retention and saturated conductivity data were already reported in previous studies using the same Cambisol (Dal Ferro et al., 2015; Morari, 2006), emphasizing the accuracy of the inverse modeling as well as the ability of the water flow equilibrium model to describe soil water content dynamics. Nevertheless, some uncertainty in hydraulic parameter estimation was observed, especially in soil layers with permanent high soil water content (Isch et al., 2019). A detailed investigation of the pore network, provided by µCT analysis, revealed some subtle structure changes between treatments (**Figure 4.6**), with an increase in the macropore structure > 327 µm when the water table was set at 120 and 60 cm (**Table 4.5**). Consequently, we cannot exclude that a fraction of water was moved by preferential flow, especially at the beginning of the experiment when dry soil conditions occurred. However from our experimental results –the deeper layers did not respond to rainfall events earlier than the shallower (Graham and Lin, 2011) – and from simulations, its magnitude was not relevant to justify the use of water flow non-equilibrium models. This contrasts with results on solute transport, where the physical MIM non-equilibrium model seemed the most suitable to describe Br^- movement (**Table 4.3**), especially under WT treatments. According to our results, previous studies adopted similar estimation process of soil hydraulic properties –the use of single porosity models in variably saturated porous media– and solute transport parameters with both ADE and MIM (Isch et al., 2019; Abbasi et al., 2004; Jacques et al., 2002), highlighting that physical non-equilibrium processes can take place when the soil profile is non-uniform and the structure heterogeneity can create differences either in water pressure, or solute concentrations, or both (Jarvis, 2007).

Modeling of Br^- movement with the ADE showed limitations in describing the solute movement in the WT treatment soils because dispersivity (λ_{ADE}), especially in the unsaturated layers, was often much higher than the transport distance (with high standard errors) (**Table 4.3** and **Table 4.4**), suggesting preferential solute movement (Vervoort et al., 1999). The ADE assumes a high degree of mixing among flow paths that is unlikely to occur when macropores extend a column length, as suggested by contrasting results between FD and WT treatments. The only exception was the saturated layer in the WT treatments (45-130 cm), where λ_{ADE}

never exceeded the transport distance. This is in accordance with some authors which indicated that the ADE is suitable to describe solute movement under saturated conditions (Padilla et al., 1999). In contrast, the MIM model was able to describe the solute exchange between mobile and immobile regions of the soil pores (Maraqa et al., 1997; Zeng et al., 2014) above the shallow water table. The modelling results were supported by experimental µCT analyses on the pore structure. Despite being conducted on small cores and at a single depth, the higher frequency of macropores under WT conditions, compared to FD, was associated with rapid non-equilibrium flow (Jarvis, 2007). The only exception was FDb, whose macropores represented > 60% of total investigated porosity (range 27.25-2834.00 µm). It follows that some effect of shallow water table fluctuations in modifying the soil-pore arrangement cannot be completely excluded (Guo and Lin, 2018), despite the soil under investigation was a silt loam with low organic matter content, thus swelling or shrinkage processes would be limited. These findings were further supported by the positive relationship that was observed between the macropore class and the weighted dispersivity (λ_{ADE}) value that was calculated for each lysimeter (**Figure 4.7A**). It is worth of note the high representativeness of macropores in FDb –an outlier with respect to the other FD– that was associated with very high modelled dispersivity. In addition, macropores frequency weas negatively correlated with the Euler number (**Figure 4.7B**)–the lower the value, the higher the degree of pore connectivity– supporting the conceptual model described by Jarvis et al. (2012) and also validated by Larsbo et al. (2014), according to which the strongest preferential transport would occur in soils that contain macropores that lack well-connected networks with smaller pores.

Dispersivity was different in the WT120 and WT60 treatments using the MIM model, especially in the topsoil layer: here, higher λ_{MIM} in the WT120 treatment than the WT60 treatment might be associated with unsaturated conditions that likely increased the tortuous path of mechanical dispersion, sometimes exceeding the transport distance (λ_{MIM} > 20 cm). The behavior of β and α_{MIM} parameters indirectly supports the hypothesis of preferential solute movement under WT treatment conditions.

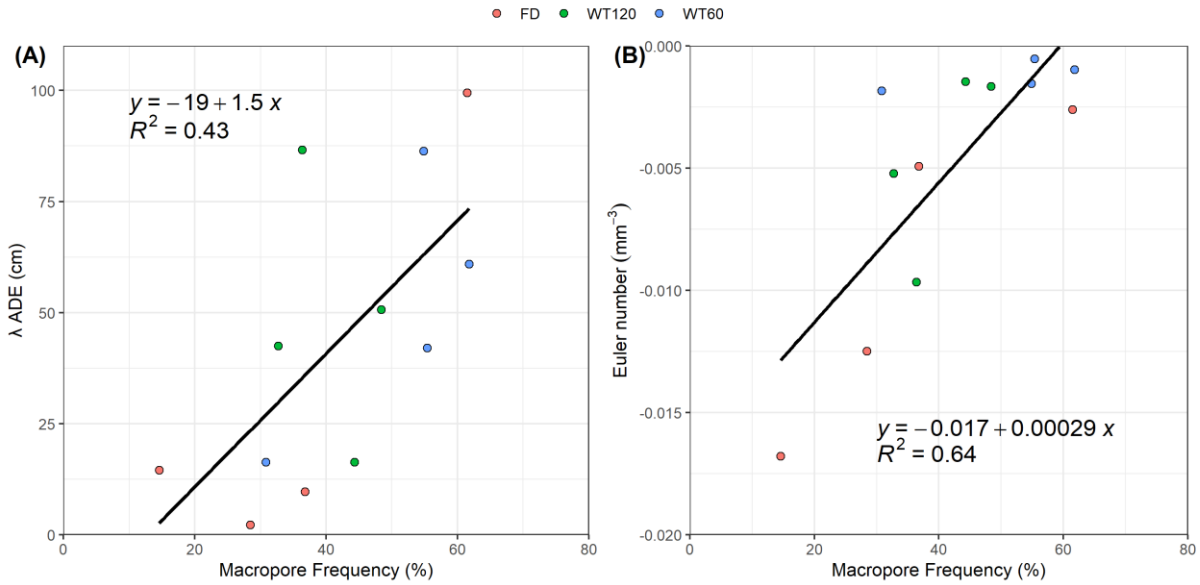

Figure 4.7. Regression lines with coefficient of determination between (A) macropore (>327 µm) frequency (%) and mean λ_{ADE} and (B) macropore (>327 µm) frequency (%) and Euler number. Different colors indicate different treatments: FD in red, WT120 in green and WT60 in blue.

Theoretically, when β equals 1 and α_{MIM} is high, the MIM results align with ADE results, downplaying the role of preferential solute movement as observed in FD lysimeters. Therefore, in the FD treatment, solute in the immobile domain was negligible, in turn, making the transfer coefficient, α_{MIM}, no longer relevant (Comegna et al., 2001). Instead, in the WT treatment, the β parameter changed with depth due to water table fluctuations, which created intermittent saturated-unsaturated conditions (**Figure 4.3** and **Figure 4.4**). Especially under intermediate soil water contents (about 0.30-0.40 cm^3 cm^{-3}), the fraction of mobile water was broadly variable, decreasing from 0.65±0.08 when the soil water content was relatively low (< 0.35 cm^3 cm^{-3} in WT120 topsoil layer), to 0.30±0.06 when the soil water content increased to values > 0.35 cm^3 cm^{-3} (in WT120, 20-130 cm layer; WT60, topsoil layer). On the contrary, it was found that β slightly increased when close-to-saturation conditions were found, i.e. below the 20 cm layer under WT60 (0.55±0.12 and 0.37±0.14 at the intermediate and deep layer respectively) and at the deepest layer of WT120 (0.54±0.09). This might suggest that different solute dynamics occurred with varying groundwater management and soil water contents. This was confirmed also by α_{MIM} estimation: in the deepest layer (close-to-saturation conditions) of the WT120 treatment, the average value was 42.29±12.23 d^{-1}, while under the WT60 treatment it was widely lower (0.07±0.01 d^{-1}),

highlighting a diverse contribution of the immobile water domain on solute dynamic according to WT management. According to Comegna et al. (2001), low values of β and α_{MIM} are indication of preferential solute transport. To note that even FDb, despite being characterized by a soil structure similar to WT, followed the same solute transport dynamics as per the other free drainage lysimeters, in turn corroborating that solute mixing and flow was due to the combined effect of structure properties (Jarvis et al., 2012) and soil water content conditions (Kumahor et al., 2015) affecting the connectivity of the water phase.

The relationship between soil water content and β, reported in **Figure 4.8**, corroborated our previous findings. Notably, β decreased as the soil water content increased until close-to-saturation conditions, due to the shallow water table. A similar dynamic was previously observed by Toride and Inoue (2003) in a column experiment using dune sand in unsaturated conditions. Vervoort et al. (1999) observed a different mobile water dynamics according to different saturation levels: in fact, for frequently and intermittent saturated horizons (i.e. deep and intermediate layers of WT), they found that β had low to moderate values, while for unsaturated horizons (e.g. FD and topsoil layer in WT120) β resulted in higher values.

In accordance with that, we observed that preferential solute transport increased under shallow water table conditions until non-capillary macropores were empty. In such conditions, a significant capillary fringe can take place, and additional water input would converge part of water and solutes stored in the soil matrix into preferential pathways, thus making macropores more active (Krzeminska et al., 2014). It follows that a likely hydraulic instability between the water-filled network of smaller pores and the macropores occurred leading to large variation of local transport velocities (Beven and Germann, 1982; Larsbo et al., 2014). In contrast, free drainage conditions did not follow the same dynamic, revealing that water was mainly mobile. This behavior led to inaccurate predictions of solute movement with the ADE under shallow groundwater conditions, raising the need to apply a model that accounts for a dual-porosity soil-medium (MIM) that can better describe the solute transport under unsaturated conditions.

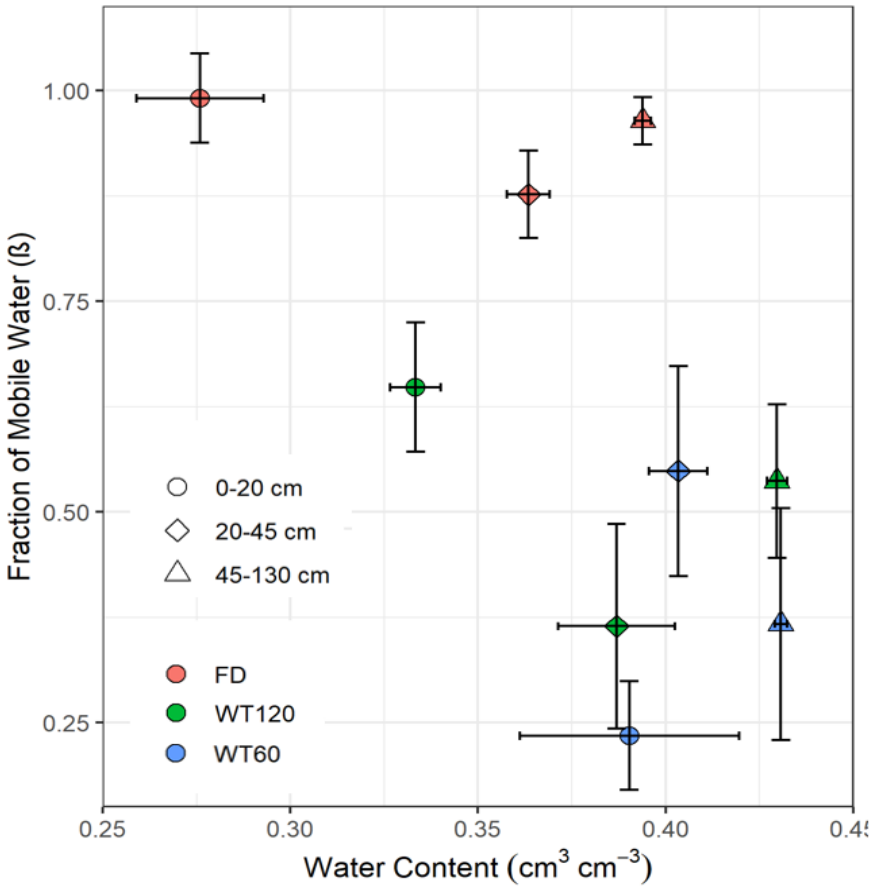

Figure 4.8. Mean mobile water fraction (*β*) as a function of the mean soil volumetric water content (cm^3 cm^{-3}) divided for treatment (FD, red; WT120, green; WT60, blue). Different simbols indicate different soil layers. Error bars refer to standard deviation of the mean water content and *β*.

4.5 Conclusion

Coupling tracer experiment and inverse modeling with HYDRUS 1D revealed that solute transport was likely affected by the water table depth, which modified the flow field in a silty loam soil. Solute transport under free drainage conditions was better predicted with the ADE equation since the mobile-immobile equation indicated the predominance of the mobile phase and high exchange between dead-end pores and transfer pores. In contrast, tracer movement was better described with the MIM model under shallow water table conditions (WT lysimeters), highlighting that the solute was mostly distributed between the two domains with a low mobile-immobile interaction. Therefore, wetter conditions in the WT treatments induced a strong reduction in λ_{MIM} and β compared to the FD treatment. Moreover, with shallow water table conditions that strongly modified the soil water content, some soil structure changes occurred at the microscale, such that solute transport properties were modified. We conclude that groundwater pollution might be worsened by the preferential movement of agrochemicals occurring with shallow water table conditions.

Appendix

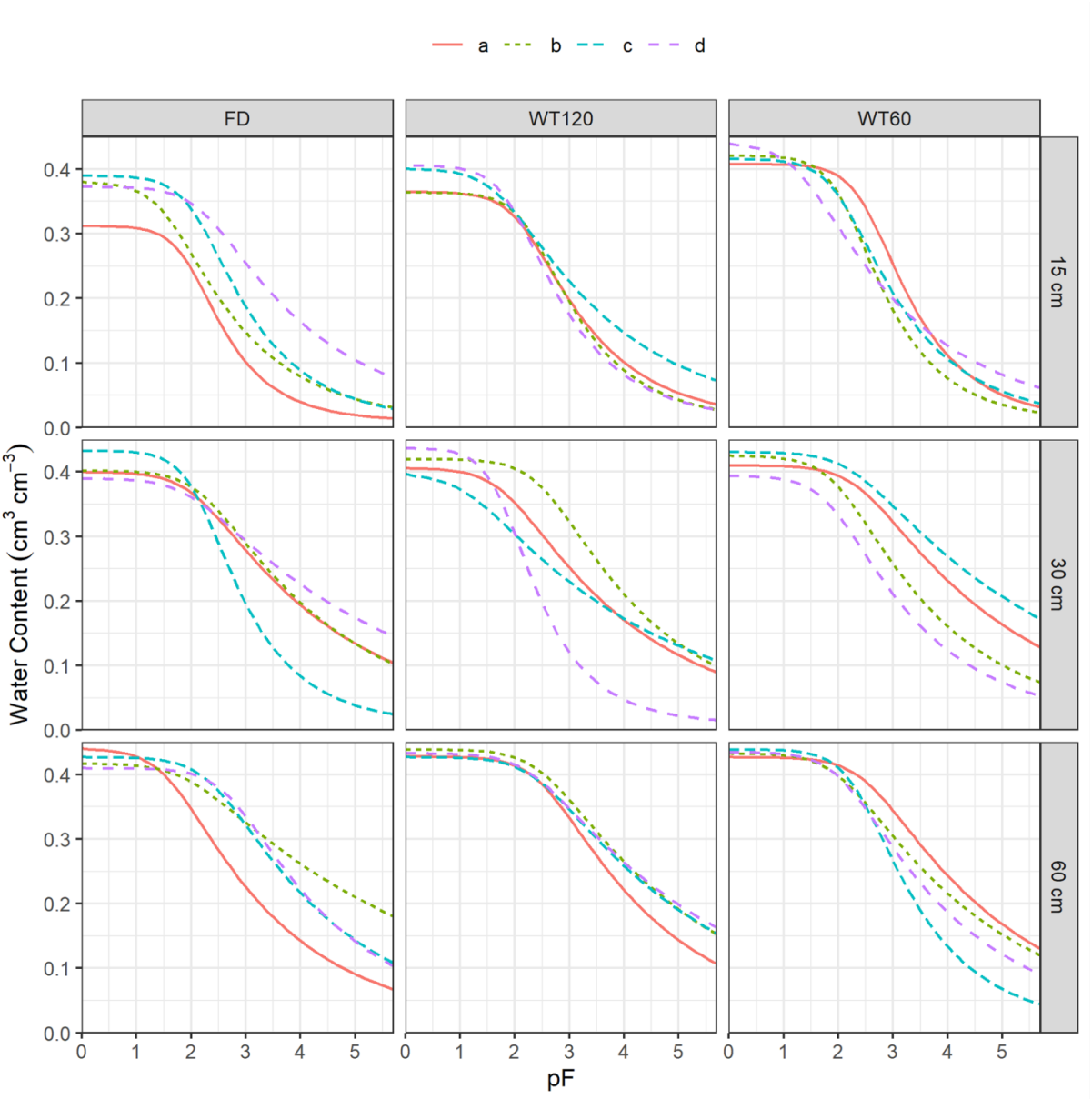

Figure S1. Water retention curves estimated with HYDRUS 1D divided for treatments and depths. Different colors indicate replicates.

References

Abbasi, F., Feyen, J., Van Genuchten, M.T., 2004. Two-dimensional simulation of water flow and solute transport below furrows: Model calibration and validation. J. Hydrol. 290, 63–79. https://doi.org/10.1016/j.jhydrol.2003.11.028

Allen, R.G., Pruitt, W.O., Raes, D., Smith, M., Pereira, L.S., 2005. Estimating Evaporation from Bare Soil and the Crop Coefficient for the Initial Period Using Common Soils Information. J. Irrig. Drain. Eng. 131, 14–23. https://doi.org/10.1061/(asce)0733-9437(2005)131:1(14)

Basile, A., Ciollaro, G., Coppola, A., 2003. Hysteresis in soil water characteristics as a key to interpreting comparisons of laboratory and field measured hydraulic properties. Water Resour. Res. 39, 1–12. https://doi.org/10.1029/2003WR002432

Beven, K., Germann, P., 1982. Macropores and water flow in soils. Water Resour. Res. 18, 1311–1325. https://doi.org/10.1029/WR018i005p01311

Celestino Ladu, J.L., Zhang, D.R., 2011. Modeling atrazine transport in soil columns with HYDRUS-1D. Water Sci. Eng. 4, 258–269. https://doi.org/10.3882/j.issn.1674-2370.2011.03.003

Chae, G.T., Kim, K., Yun, S.T., Kim, K.H., Kim, S.O., Choi, B.Y., Kim, H.S., Rhee, C.W., 2004. Hydrogeochemistry of alluvial groundwaters in an agricultural area: An implication for groundwater contamination susceptibility. Chemosphere 55, 369–378. https://doi.org/10.1016/j.chemosphere.2003.11.001

Comegna, V., Coppola, A., Sommella, A., 2001. Effectiveness of equilibrium and physical non-equilibrium approaches for interpreting solute transport through undisturbed soil columns. J. Contam. Hydrol. 50, 121–138. https://doi.org/10.1016/S0169-7722(01)00100-0

Dal Ferro, N., Strozzi, A.G., Duwig, C., Delmas, P., Charrier, P., Morari, F., 2015. Application of smoothed particle hydrodynamics (SPH) and pore morphologic model to predict saturated water conductivity from X-ray CT imaging in a silty loam Cambisol. Geoderma 255–256, 27–34. https://doi.org/10.1016/j.geoderma.2015.04.019

Deurer, M., Bachmann, J., 2007. Modeling Water Movement in Heterogeneous Water-Repellent Soil: 2. A Conceptual Numerical Simulation. Vadose Zo. J. 6, 446–457. https://doi.org/10.2136/vzj2006.0061

Donald W . Marquardt, 1963. An Algorithm for Least-Squares Estimation of Nonlinear Parameters. Soc. Ind. Appl. Math. 11, 431–441.

Durner, W., Jansen, U., Iden, S.C., 2007. Effective hydraulic properties of layered soils at the lysimeter scale determined by inverse modelling. Eur. J. Soil Sci. 0, 071026202618002-??? https://doi.org/10.1111/j.1365-2389.2007.00972.x

FAO-UNESCO, 2008. Soil map of the world. Revised Legend, FAO, Rome.

Farsad, A., Herbert, S.J., Hashemi, M., Sadeghpour, A., 2012. An Automated Suction Lysimeter for Improved Soil Water Sampling. Vadose Zo. J. 11, 0. https://doi.org/10.2136/vzj2012.0003

Flury, M., Yates, M. V., Jury, W.A., 1999. Numerical Analysis of the Effect of the Lower Boundary Condition on Solute Transport in Lysimeters. Soil Sci. Soc. Am. J. 63, 1493–1499. https://doi.org/10.2136/sssaj1999.6361493x

Gao, G., Zhan, H., Feng, S., Fu, B., Ma, Y., Huang, G., 2010. A new mobile-immobile model for reactive solute transport with scale-dependent dispersion. Water Resour. Res. 46, 1–16. https://doi.org/10.1029/2009WR008707

Gérard, F., Tinsley, M., Mayer, K.U., 2004. Preferential Flow Revealed by Hydrologic Modeling Based on Predicted Hydraulic Properties. Soil Sci. Soc. Am. J. 68, 1526. https://doi.org/10.2136/sssaj2004.1526

Gerke, H.H., 2006. Preferential flow descriptions for structured soils. J. Plant Nutr. Soil Sci. 169, 382–400. https://doi.org/10.1002/jpln.200521955

Goldberg, S., J. Kabengi, N., 2010. Bromide Adsorption by Reference Minerals and Soils. Vadose Zo. J. 9, 780–786. https://doi.org/10.2136/vzj2010.0028

Graham, C.B., Lin, H.S., 2011. Controls and Frequency of Preferential Flow Occurrence: A 175-Event Analysis. Vadose Zo. J. 10, 816–831. https://doi.org/10.2136/vzj2010.0119

Groh, J., Stumpp, C., Lücke, A., Pütz, T., Vanderborght, J., Vereecken, H., 2018. Inverse Estimation of Soil Hydraulic and Transport Parameters of Layered Soils from Water Stable Isotope and Lysimeter Data. Vadose Zo. J. 17, 0. https://doi.org/10.2136/vzj2017.09.0168

Groh, J., Vanderborght, J., Pütz, T., Vereecken, H., 2016. How to Control the Lysimeter Bottom Boundary to Investigate the Effect of Climate Change on Soil Processes? Vadose Zo. J. 15, vzj2015.08.0113. https://doi.org/10.2136/vzj2015.08.0113

Guo, L., Lin, H., 2018. Addressing Two Bottlenecks to Advance the Understanding of Preferential Flow in Soils. Adv. Agron. 147. https://doi.org/https://doi.org/10.1016/bs.agron.2017.10.002 #

Haria, A.H., Hodnett, M.G., Johnson, A.C., 2003. Mechanisms of groundwater recharge and pesticide penetration to a chalk aquifer in southern England. J. Hydrol. 275, 122–137. https://doi.org/10.1016/S0022-1694(03)00017-9

Hendrickx, J.M.H., Flury, M., 2001. Uniform and preferential flow, mechanisms in the vadose zone. Conceptual Models of Flow and Transport in the Fractured Vadose Zone. Natl. Acad. Sci.

Herbrich, M., Gerke, H.H., 2017. Scales of Water Retention Dynamics Observed in Eroded Luvisols from an Arable Postglacial Soil Landscape. Vadose Zo. J. 16, vzj2017.01.0003. https://doi.org/10.2136/vzj2017.01.0003

Hopmans, J.W., Šimůnek, J., Romano, N., Durner, W., 2002. 3.6.2. Inverse modeling of transient water flow. Methods Soil Anal. Part 1, Phys. Methods 963–1008.

Isch, A., Montenach, D., Hammel, F., Ackerer, P., Coquet, Y., 2019. A comparative study ofwater and bromide transport in a bare loam soil using lysimeters and field plots. Water (Switzerland) 11, 1–25. https://doi.org/10.3390/w11061199

J. Šimůnek, M. Šejna, H. Saito, M. Sakai, and M.T. van G., 2009. The HYDRUS-1D Software Package for Simulating the One-Dimensional Movement of Water, Heat, and Multiple Solutes in Variably-Saturated Media.

Jacques, D., Šimůnek, J., Timmerman, A., Feyen, J., 2002. Calibration of Richards' and convection-dispersion equations to field-scale water flow and solute transport under rainfall conditions. J. Hydrol. 259, 15–31. https://doi.org/10.1016/S0022-1694(01)00591-1

Jarvis, N., Koestel, J., Larsbo, M., 2016. Understanding Preferential Flow in the Vadose Zone: Recent Advances and Future Prospects. Vadose Zo. J. 15, 0. https://doi.org/10.2136/vzj2016.09.0075

Jarvis, N.J., 2007. A review of non-equilibrium water flow and solute transport in soil macropores: Principles, controlling factors and consequences for water quality. Eur. J. Soil Sci. 58, 523–546. https://doi.org/10.1111/j.1365-2389.2007.00915.x

Jarvis, N.J., Moeys, J., Koestel, J., Hollis, J.M., 2012. Preferential Flow in a Pedological Perspective, in: Hydropedology. Elsevier, pp. 75–120. https://doi.org/10.1016/B978-0-12-386941-8.00003-4

Jirků, V., Kodešová, R., Nikodem, A., Mühlhanselová, M., Žigová, A., 2013. Temporal variability of structure and hydraulic properties of topsoil of three soil types. Geoderma 204–205, 43–58. https://doi.org/10.1016/j.geoderma.2013.03.024

Jury, W.A., Roth, K., 1990. Transfer functions and solute movement through soil: theory and applications. Birkhäuser Verlag AG, Basel.

Kabat, P., Hutjes, R.W.A., Feddes, R.A., 1997. The scaling characteristics of soil parameters: From plot scale heterogeneity to subgrid parameterization. J. Hydrol. 190, 363–396. https://doi.org/10.1016/S0022-1694(96)03134-4

Klier, C., Grundmann, S., Gayler, S., Priesack, E., 2008. Modelling the environmental fate of the herbicide glyphosate in soil lysimeters. Water, Air, Soil Pollut. Focus 8, 187–207. https://doi.org/10.1007/s11267-007-9171-5

Krzeminska, D.M., Bogaard, T.A., Debieche, T.H., Cervi, F., Marc, V., Malet, J.P., 2014. Field investigation of preferential fissure flow paths with hydrochemical analysis of small-scale sprinkling experiments. Earth Surf. Dyn. 2, 181–195. https://doi.org/10.5194/esurf-2-181-2014

Kumahor, S.K., de Rooij, G.H., Schlüter, S., Vogel, H.-J., 2015. Water Flow and Solute

Transport in Unsaturated Sand—A Comprehensive Experimental Approach. Vadose Zo. J. 14, 0. https://doi.org/10.2136/vzj2014.08.0105

Kumahor, S K, De Rooij, G.H., Schlüter, S., Vogel, H.-J., 2015. Water Flow and Solute Transport in Unsaturated Sand—A Comprehensive Experimental Approach The investigation of solute transport during unsaturated water flow in soil 0–9. https://doi.org/10.2136/v14.08.0105

Larsbo, M., Koestel, J., Jarvis, N., 2014. Relations between macropore network characteristics and the degree of preferential solute transport. Hydrol. Earth Syst. Sci. 18, 5255–5269. https://doi.org/10.5194/hess-18-5255-2014

Leistra, M., Boesten, J.J.T.I., 2010. Measurement and computation of movement of bromide ions and carbofuran in ridged humic-sandy soil. Arch. Environ. Contam. Toxicol. 59, 39–48. https://doi.org/10.1007/s00244-009-9442-4

Lide, D.R., 2003. CRC Handbook of Chemistry and Physics. eBook 3485. https://doi.org/978-1466571143

Maher, K., 2010. The dependence of chemical weathering rates on fluid residence time. Earth Planet. Sci. Lett. 294, 101–110. https://doi.org/10.1016/j.epsl.2010.03.010

Maraqa, M.A., Wallace, R.B., Voice, T.C., 1997. Effects of degree of water saturation on dispersivity and immobile water in sandy soil columns. J. Contam. Hydrol. 25, 199–218. https://doi.org/10.1016/S0169-7722(96)00032-0

Masarik, K.C., Norman, J.M., Brye, K.R., Baker, J.M., 2004. Improvements to Measuring Water Flux in the Vadose Zone. J. Environ. Qual. 33, 1152. https://doi.org/10.2134/jeq2004.1152

Mitchell, A.R., Ellsworth, T.R., Meek, B.D., 1995. Effect of root systems on preferential flow in swelling soil. Commun. Soil Sci. Plant Anal. 26, 2655–2666. https://doi.org/10.1080/00103629509369475

Morari, F., 2006. Drainage Flux Measurement and Errors Associated with Automatic Tension-controlled Suction Plates. Soil Sci. Soc. Am. J. 70, 1860. https://doi.org/10.2136/sssaj2006.0009

Mualem Y., 1976. A New Model for Predicting the Hydraulic Conductivity of Unsaturated Porous Media. Water Resour. Res. 12, 513–522.

Otsu, N., 1979. A threshold selection method from gray-level histograms. IEEE Trans. Syst. Man Cybern. 9, 62–66.

Padilla, I.Y., Yeh, T.C.J., Conklin, M.H., 1999. The effect of water content on solute transport in unsaturated porous media. Water Resour. Res. 35, 3303–3313. https://doi.org/10.1029/1999WR900171

Pagliai, M., Pezzarossa, B., Zerbi, G., Alvino, A., Pini, R., Guidi, G.V., 1989. Soil Porosity in a Peach Orchard as Influenced by Water Table Depth. Agric. Water Manag. 16, 63–73.

Power, M., 1993. The predictive validation of ecological and environmental models. Ecol. Modell. 68, 33–50. https://doi.org/10.1016/0304-3800(93)90106-3

Pütz, T., Kiese, R., Wollschläger, U., Groh, J., Rupp, H., Zacharias, S., Priesack, E., Gerke, H.H., Gasche, R., Bens, O., Borg, E., Baessler, C., Kaiser, K., Herbrich, M., Munch, J.C., Sommer, M., Vogel, H.J., Vanderborght, J., Vereecken, H., 2016. TERENO-SOILCan: a lysimeter-network in Germany observing soil processes and plant diversity influenced by climate change. Environ. Earth Sci. 75. https://doi.org/10.1007/s12665-016-6031-5

Radcliffe, D.E., Simunek Jiri, J., 2010. Soil physics with HYDRUS: Modeling and applications, Soil Physics with HYDRUS: Modeling and Applications.

Rahman, A., 2008. A GIS based DRASTIC model for assessing groundwater vulnerability in shallow aquifer in Aligarh, India. Appl. Geogr. 28, 32–53. https://doi.org/10.1016/j.apgeog.2007.07.008

Remy, E., Thiel, E., 2002. Medial axis for chamfer distances: Computing look-up tables and neighbourhoods in 2D or 3D. Pattern Recognit. Lett. 23, 649–661. https://doi.org/10.1016/S0167-8655(01)00141-6

Sayem, H.M., Kong, L., 2016. Effects of Drying-Wetting Cycles on Soil-Water Characteristic Curve. DEStech Trans. Environ. Energy Earth Sci. https://doi.org/10.12783/dteees/peee2016/3881

Šimůnek, J., van Genuchten, M.T., 2008. Modeling Nonequilibrium Flow and Transport Processes Using HYDRUS. Vadose Zo. J. 7, 782. https://doi.org/10.2136/vzj2007.0074

Šimůnek, J., van Genuchten, M.T., Jacques, D., Hopmans, J.W., Inoue, M., Flury, M., 2001. 6 . 6 Solute Transport During Variably Saturated Flow — Inverse Methods. Inverse Methods 1435–1450.

Sprenger M., Seeger S., Blume T., W.M., 2016. Travel times in the vadose zone: Variability in space and time. Water Resour. Res. 52, 5727–5754. https://doi.org/10.1002/2015WR018077 Key

Thuyet, D.Q., Hien, T.Q., Watanabe, H., Saito, H., Phong, T.K., Nishimura, T., 2010. Micro paddy lysimeter for monitoring solute transport in paddy environment. Paddy Water Environ. 8, 235–245. https://doi.org/10.1007/s10333-010-0204-8

Toride, N., Inoue, M., 2003. Hydrodynamic Dispersion in an Unsaturated Dune Sand. https://doi.org/10.2136/sssaj2003.0703

Van Genuchten, M.T., P.J., W., 1976. Mass transfer studies in sorbing porous media I. Analytical solutions. Soil Sci. Soc. … 473–480.

van Genuchten, M.T., Wierenga, P.J., 1976. Mass Transfer Studies in Sorbing Porous Media I. Analytical Solutions1. Soil Sci. Soc. Am. J. 40, 473. https://doi.org/10.2136/sssaj1976.03615995004000040011x

Vervoort, R.W., Radcliffe, D.E., West, L.T., 1999. Soil structure development and preferential

solute flow. Water Resour. Res. 35, 913–928.

Vogel, H.J., Weller, U., Schlüter, S., 2010. Quantification of soil structure based on Minkowski functions. Comput. Geosci. 36, 1236–1245. https://doi.org/10.1016/j.cageo.2010.03.007

Vogel, T., Gerke, H.H., Zhang, R., Van Genuchten, M.T., 2000. Modeling flow and transport in a two-dimensional dual-permeability system with spatially variable hydraulic properties. J. Hydrol. 238, 78–89. https://doi.org/10.1016/S0022-1694(00)00327-9

Von Unold, G., Fank, J., 2008. Modular design of field lysimeters for specific application needs. Water, Air, Soil Pollut. Focus 8, 233–242. https://doi.org/10.1007/s11267-007-9172-4

Wossenyeleh, B.K., Verbeiren, B., Diels, J., Huysmans, M., 2020. Vadose zone lag time effect on groundwater drought in a temperate climate. Water (Switzerland) 12. https://doi.org/10.3390/W12082123

Wösten, J.H.M., van Genuchten, M.T., 1988. Using Texture and Other Soil Properties to Predict the Unsaturated Soil Hydraulic Functions. Soil Sci. Soc. Am. J. 52, 1762–1770. https://doi.org/10.2136/sssaj1988.03615995005200060045x

Wu, J., Sun, Z., 2016. Evaluation of Shallow Groundwater Contamination and Associated Human Health Risk in an Alluvial Plain Impacted by Agricultural and Industrial Activities, Mid-west China. Expo. Heal. 8, 311–329. https://doi.org/10.1007/s12403-015-0170-x

Zeng, W.Z., Xu, C., Wu, J.W., Huang, J.S., 2014. Soil salt leaching under different irrigation regimes: HYDRUS-1D modelling and analysis. J. Arid Land 6, 44–58. https://doi.org/10.1007/s40333-013-0176-9

Chapter 5. Overall conclusions

This Ph.D. thesis aimed to explore the environmental fate of glyphosate, focusing mainly on adsorption, dissipation and transport in different agroecosystems and soils of the Veneto region. The influence of preferential flow pathways has also been investigated as a key factor favouring solute leaching and enhancing groundwater vulnerability to contamination. Considering that glyphosate is still widely used in agricultural lands, the complexity of evaluating its fate in the environment under contrasting conditions was highlighted. The overall conclusions of the thesis are reported below differentiated for adsorption, dissipation, and transport.

Results on glyphosate adsorption showed that it was non-linear in all soils, resulting in a good fitting by applying the Freundlich equation, and was found to increase with the soil depth. Different soils resulted in different adsorption capacities: in the foothills, Conegliano soil (silty loam) showed greater affinity towards glyphosate – almost four times higher – than Valdobbiadene (sandy loam) and Legnaro (low Venetian plain, silty loam) soils. Soil texture, cation exchange capacity, electrical conductivity, Fe and Al complexed with the organic matter were identified as common factors that influence glyphosate adsorption in all soils. Additional factors were identified for the low Venetian plain soil, like soil organic carbon and available phosphorus. Regardless the investigated soil and agricultural system, the mineral composition was a key driver to modify the GLP adsorption. It must be noted that very few studies characterized herbicide adsorption and soil properties, including Fe and Al speciation, down to 70 and 110 cm as has been done in this thesis, highlighting that an in-depth investigation of the mineral composition is pivotal to better characterize the pesticide affinity to the soil phase. Results suggested that short-term conservation agriculture did not affect soil properties, and in turn herbicide adsorption.

Dissipation times (DT_{50}) were calculated for the 0-5 cm layer in foothills soils for glyphosate and AMPA. Both molecules had a faster dissipation in Conegliano soil than in Valdobbiadene, but slower for the metabolite than for the parent (28 and 42 days in Conegliano, 43 and 92 days in Valdobbiadene, for glyphosate and AMPA respectively). Differences in decay rates under field conditions are likely due to microbial degradation, soil moisture and temperature, as rainfall intensity. In the low Venetian plain soil, DT_{50} was not calculated but glyphosate residues in soil at different depths were detected, demonstrating rapid dissipation of the molecule in almost a month in surface soil (-99%). Below ground, concentrations of glyphosate

and AMPA were different according to soil management: short-term conservation agriculture reduced the herbicide content in soil being glyphosate never found down to 15 cm, while under conventional agriculture it was randomly found. Also AMPA was seldom found in soil compared to conventional practices and in significantly lower concentration. These results suggested that peculiar management conditions of conservation agriculture, such as the presence of surface residues and a faster degradation in soil, could have reduced the risk of groundwater contamination. Further studies conducted under long-term conservation agriculture are required to evaluate whether more significant changes in the soil structure might modify the flow field and in turn the groundwater contamination.

Glyphosate and AMPA transport in pore-water through the soil profile was investigated in all three soils. In the high foothills, glyphosate was randomly found in both soils, with concentrations that fluctuated with time. High concentrations of both the parent and metabolite were detected after heavy rainfall events, even after 150 days from the distribution. The herbicide was hardly detected in Conegliano soil, likely due to the high adsorption capacity found which kept the herbicide bonded to soil particles. Valdobbiadene soil showed a different dynamic compared to Conegliano, being glyphosate detected mostly at 30 and 70 cm depth, suggesting that a preferential flow could have occurred bypassing the porous matrix in the shallow layer. AMPA was mainly found in the shallower layer, while in Valdobbiadene it reached 70 cm depth, suggesting a different transport according to soil type. In contrast, in the low Venetian plain, under shallow groundwater conditions, high concentrations of glyphosate were detected mainly in the first five days of sampling, then decreasing to values around zero, highlighting a fast movement of the herbicide through the porous matrix. Here, conservation practices did not affect glyphosate mobility compared to conventional and neither different shallow water table depths. Despite the high adsorption of glyphosate in both the foothill and low plain areas, some vertical movement occurred that might be associated with preferential flow movements. This suggest that a groundwater vulnerability is a peculiar condition that might happen in different agroecosystems, such as the well-structured soils of the high foothills as well as the poorly structured ones that characterize the low Venetian plain. In this context, *Chapter 4* confirmed the occurrence of preferential flow under shallow water table conditions, that is a typical condition of the low-lying Venetian plain, by enhancing solute bypass and modifying the soil structure and

macropore domain in soil. This has been achieved by applying the mobile immobile physical non-equilibrium model (MIM) on solute transport. A good prediction of water flow was performed by applying the uniform flow model, which revealed no need to apply a Dual-Porosity or Dual-Permeability model for both water and solute. Therefore, these results confirmed the fast movement of the herbicide found in the lysimeters managed with different groundwater levels. It must be noted that, in this thesis, the soil structure of foothill soils was not analysed in terms of macropore frequency and connectivity, which could further explain the differences detected between soils.

To conclude, the fate of glyphosate and AMPA in the environment resulted to be site-specific, depending on soil type, properties, structure, climate conditions and soil-crop management. Conservation agriculture influenced the concentration of the herbicide found in soil, while shallow water table conditions increased the risk of fast solute leaching down to the water table by modifying the soil structure. Further studies are therefore needed to better understand the role of long- and short-term conservation agriculture on the herbicide fate and the factors that govern soil- and water-related dynamics under peculiar soil and climate conditions.